Process intensification of microwave assisted methane dry reforming

Gangurde, Lalit

DOI
10.4233/uuid:7372f079-4bb5-46eb-b203-315afb8781c8

Publication date
2018

Document Version
Final published version

Citation (APA)
Gangurde, L. (2018). *Process intensification of microwave assisted methane dry reforming*. [Dissertation (TU Delft), Delft University of Technology]. https://doi.org/10.4233/uuid:7372f079-4bb5-46eb-b203-315afb8781c8

Process Intensification of Microwave Assisted Methane Dry Reforming

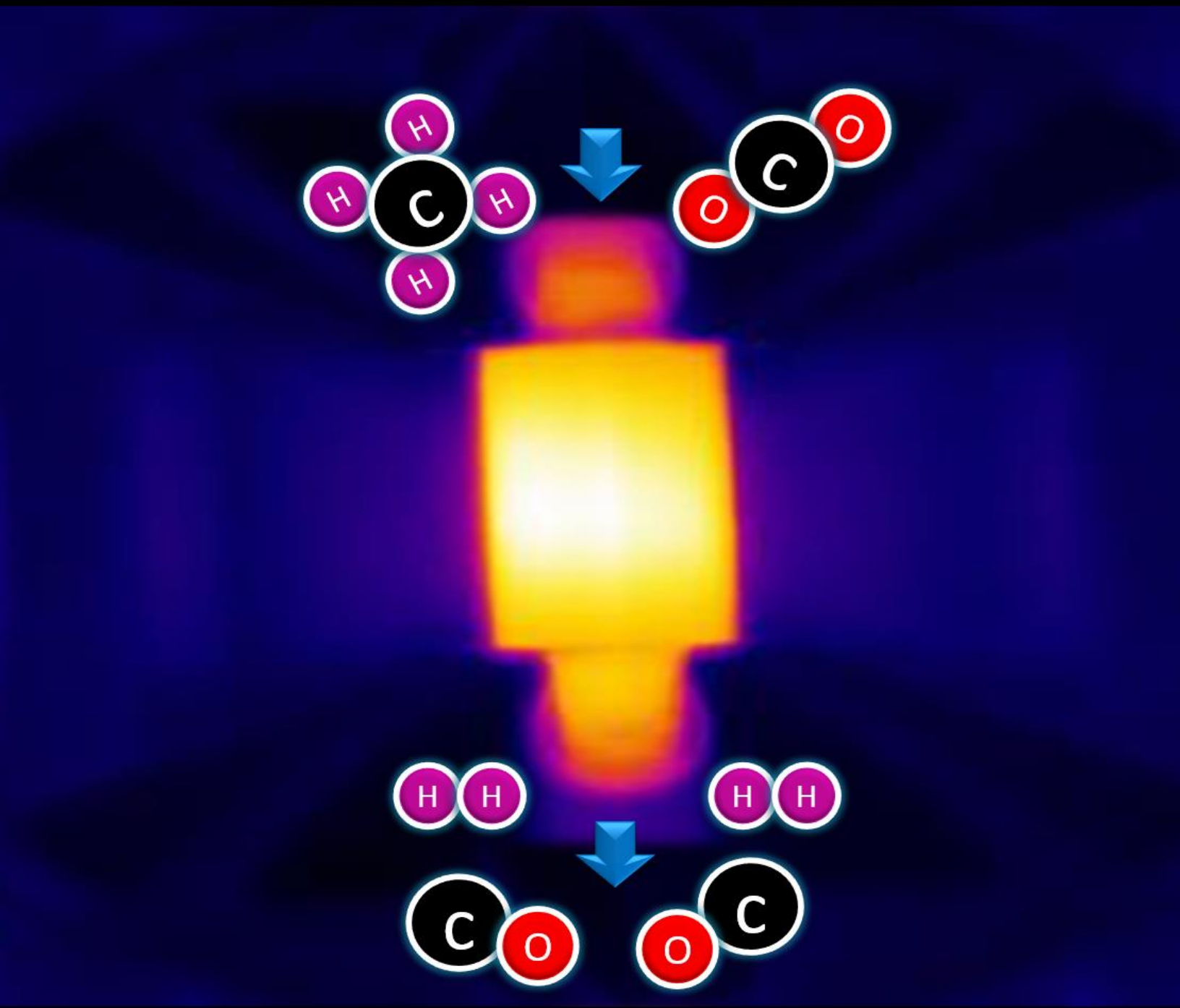

Lalit Sayaji Gangurde

Delft University of Technology, The Netherlands

Process Intensification of Microwave Assisted Methane Dry Reforming

Proefschrift

ter verkrijging van de graad van doctor
aan de Technische Universiteit Delft,
op gezag van de Rector Magnificus prof.dr.ir. T.H.J.J. van der Hagen,
voorzitter van het College voor Promoties,
in het openbaar te verdedigen op woensdag 12 December 2018 om 10:00 uur

door

Lalit Sayaji Gangurde

Masters in Inorganic Chemistry
University of Pune, Pune, India.
geboren te Ghodegaon, Maharashtra, India.

Process Intensification of Microwave Assisted Methane Dry Reforming

Dissertation

for the purpose of obtaining the degree of doctor
at Delft University of Technology
by the authority of the Rector Magnificus prof.dr.ir. T.H.J.J. van der Hagen,
chair of the Board for Doctorates
to be defended publicly on Wednesday 12 December 2018 at 10:00 o'clock

by

Lalit Sayaji Gangurde

Masters in Inorganic Chemistry
University of Pune, Pune, India.
Born in Ghodegaon, Maharashtra, India.

This dissertation has been approved by the promotors:
Prof.dr.ir. A.I. Stankiewicz and Prof.dr.ir. G.D. Stefanidis

Composition of the doctoral committee:

Rector Magnificus	Chairperson
Prof.dr.ir. A.I. Stankiewicz	Delft University of Technology, promotor
Prof.dr.ir. G.D. Stefanidis	Katholieke Universiteit Leuven, promotor

Independent Members:

Prof.dr.ir. K.M. Van Geem	Ghent University, Belgium
Dr.ir. T. Durka	Yara Sluiskil B.V, the Netherlands.
Prof.dr.ir. J.R. van Ommen	Delft University of Technology
Dr. P.V. Aravind	Delft University of Technology
Prof.dr. J. Santamaria	Zaragoza University, Spain
Prof.dr.ir. W. de Jong	Delft University of Technology, reserve member

ISBN: 978-94-6375-229-9

The research leading to this Ph.D. dissertation has received funding from the European Research Council under the European Union's Seventh Framework Programme (FP7/2007-2013) / ERC grant agreement no. 267348.

Cover designed by Lalit Sayaji Gangurde
Published by Lalit Sayaji Gangurde, TU Delft
Printed in the Netherlands by: Ridderprint BV | www.ridderprint.nl
[1]Author email address: lalitgangurde88@gmail.com

Dedicated to my family and friends who supported me during this Journey

Summary

Resource- and energy-efficient methane (CH_4) transformation to fuels and chemicals is a research topic with societal, environmental and industrial relevance owing to the great variety of methane sources, including existing gas networks, small natural gas fields, shale gas, coal beds, agricultural biogas, deep-sea methane hydrates and the pressing issue of methane flaring in remote locations. In addition, CH_4 and carbon dioxide (CO_2) are the two greenhouse gases contributing majorly to global warming and their effect is expected to increase in years to come due to the continuously increasing energy demand worldwide. In this frame, CH_4 reforming by CO_2 (dry methane reforming) by means of different catalytic materials and technologies has been investigated over the years as a potential route for valorisation of the two molecules.

In this doctoral work, dry methane reforming has been carried out in a custom designed microwave reactor to obtain syngas (H_2+CO), a building block for several fuels and chemicals. The aim of the research is to address certain challenges in process intensification of microwave-assisted heterogeneous catalytic reactions at high temperatures (>700 °C) in general and microwave-assisted methane dry reforming in particular. The thesis is divided into six chapters. In the first Chapter, a general introduction on the globally increasing energy demand is given and possibilities to meet this demand are discussed. Further, the motivation for the investigation of methane dry reforming is presented, and the challenges to improve the process under microwave heating are highlighted. The second Chapter describes the custom designed microwave reactor setup used for experiments in this work. The setup has been designed such that it provides concentrated microwave heating to the solid catalytic materials, maximizes the microwave energy utilization efficiency and enables measurement and monitoring of the spatiotemporal temperature distribution in the quartz tube fixed bed reactor where methane dry reforming is carried out.

Chapter 3 reports on the complexity and challenges in non-contact temperature measurements inside microwave-heated catalytic reactors. A methodology to monitor the temperature distribution inside a catalytic bed by using a thermal camera in combination with a thermocouple for a heterogeneous catalytic reaction (methane dry reforming) under microwave heating has been demonstrated. The effects of various variables that affect the accuracy of temperature recordings are discussed in detail. Coke formation and catalyst volume reduction are observed to be the major issues with carbon-based catalysts.

The limitations of carbon-based catalysts for microwave-assisted methane dry reforming have motivated the development of alternative catalysts that combine high activity, good microwave absorption capacity, thermal stability and resistance to coke. To that end, a series of ruthenium-doped strontium titanate ($SrTiO_3$) perovskite catalysts have been synthesized by conventional and microwave-assisted hydrothermal methods. Significant synthesis temperature and time reduction

from 220 °C for 24 h in conventional heating to 180 °C for 1 h under microwave heating were achieved. The synthesized catalysts were characterized with respect to their dielectric properties in a dual mode cylindrical cavity as well as their physicochemical properties by means of various analytical methods (XRD, BET, ICP-OES and high-angle annular dark-field scanning transmission electron microscopy (HAADF-STEM) coupled to energy dispersive X-ray (EDX) analysis). Based on the outcome of the characterization procedures, a 7 wt. % ruthenium-doped $SrTiO_3$ catalyst was selected for further testing of its catalytic activity for methane dry reforming under microwave heating in a custom fixed-bed quartz reactor. Microwave power, CH_4:CO_2 vol. % feed ratio and gas hourly space velocity (GHSV) were varied to determine the best operating conditions. Maximum conversions of ~99.5% and ~94% for CH_4 and CO_2, respectively, were achieved during a 3h stability test at 9000 $cm^3g^{-1}hr^{-1}$ GHSV, with the selected 7 wt. % Ru-doped $SrTiO_3$ catalyst, which was exposed at maximum temperatures in the vicinity of 940 °C. Scale-up calculations on the basis of 1 m^3h^{-1} CH_4 inlet flow rate on the perovskite catalyst show significant improvement in H_2 production capability compared to carbon-based catalysts.

Considering further scale-up and industrial implementation, the Ru-based catalyst might be expensive. Therefore, in Chapter 5, combinations of four commercial and relatively cheap nickel-supported metal oxide catalysts (Ni/Al_2O_3, $Ni/CaAl_2O_4$, Ni/Al_2MgO_4, and Ni/SiO_2-Al_2O_3) with a 7 wt. % Ruthenium (Ru)-doped $SrTiO_3$ perovskite catalyst were tested, as hybrid catalytic systems, for syngas production by microwave-assisted methane dry reforming. The experimental results showed that the introduction of the Ru-doped perovskite catalyst improves the microwave heating ability of the hybrid systems under typical dry reforming temperatures (up to 850 °C). The four catalytic systems were also evaluated under dry reforming reaction conditions in terms of CH_4 and CO_2 conversion and H_2/CO ratio as a function of MW power, gas hourly space velocity (GHSV) and time on stream. The combination of $Ru/SrTiO_3$ and Ni/Al_2O_3 was found to form the best hybrid catalyst system in terms of microwave absorption ability, syngas production capacity and catalytic stability. A comparative theoretical scale-up study showed improvement in H_2 production capacity in case of a combination of Ni/Al_2O_3 and $Ru/SrTiO_3$ as compared to the combination of Ni/Al_2O_3 and FY5.

Finally, the last chapter (Chapter 6) summarizes the findings of the entire research activity and provides recommendations for future work on the subject.

Samenvatting

Bron en energie-efficiënte methaan (CH_4) transformatie naar brandstoffen en chemicaliën is een onderzoeksthema met maatschappelijke, ecologische en industriële relevantie. Dit is vanwege de grote verscheidenheid aan methaanbronnen, waaronder bestaande gasnetwerken, kleine aardgasvelden, schaliegas, kolengoten, landbouwbiogas, diepzee methaanhydraten en de dringende kwestie van methaan verbranding op afgelegen locaties. Bovendien zijn CH_4 en koolstofdioxide (CO_2) de twee broeikasgassen die in belangrijke mate bijdragen tot het broeikaseffect en hun effect zal naar verwachting in de komende jaren toenemen als gevolg van de wereldwijd voortdurend toenemende vraag naar energie. Binnen deze kader is CH_4 hervorming met CO_2 (droge methaan hervorming) met behulp van verschillende katalytische materialen en technologieën door de jaren heen onderzocht als een mogelijke route voor valorisatie van de twee moleculen.

In dit promotieonderzoek is een droge methaan hervorming uitgevoerd in een speciaal ontworpen magnetron reactor om syngas (H_2+CO) te verkrijgen, een bouwsteen voor verschillende brandstoffen en chemicaliën. Het doel van het onderzoek is om bepaalde uitdagingen aan te pakken bij intensivering van het proces van microgolf-geassisteerde heterogene katalytische reacties bij hoge temperaturen (>700 °C) in het algemeen en in het bijzonder microgolf-geassisteerde methaan-droge hervorming. De scriptie is verdeeld in zes hoofdstukken. In het eerste hoofdstuk wordt een algemene inleiding gegeven over de wereldwijd stijgende energievraag en worden mogelijkheden besproken om aan deze vraag te voldoen. Verder wordt de motivatie voor het onderzoek naar methaan droog reformeren gepresenteerd en worden de uitdagingen om het proces onder microgolfverwarming te verbeteren benadrukt. Het tweede hoofdstuk beschrijft de op maat ontworpen opstelling van de magnetron reactor die voor experimenten in dit werk wordt gebruikt. De opstelling is zodanig ontworpen dat het geconcentreerde microgolfverwarming aan de vaste katalytische materialen verschaft, de efficiëntie van de microgolfenergiebenutting maximaliseert, met daarnaast meting en bewaking van de spatio-temporele temperatuurverdeling in de bed-reactor met kwartsbuizen mogelijk maakt, waar methaan droog wordt gereformeerd.

Hoofdstuk 3 omvat de complexiteit en uitdagingen in contactloze temperatuurmetingen in microgolfverwarmde katalytische reactoren. Een methode om de temperatuurverdeling in een katalytisch bed te bewaken met behulp van een thermische camera in combinatie met een thermokoppel voor een heterogene katalytische reactie (methaan droog reformeren) onder verwarming met microgolven, is aangetoond. De effecten van verschillende variabelen die de nauwkeurigheid van temperatuuropnames beïnvloeden, worden in detail besproken. Cokesvorming en afname van het katalysatorvolume zijn de belangrijkste problemen met katalysatoren op basis van koolstof.

De beperkingen van op koolstof gebaseerde katalysatoren voor microgolf-geassisteerd methaan droog reformeren hebben de ontwikkeling van alternatieve katalysatoren gemotiveerd die hoge activiteit, goede microgolfabsorptiecapaciteit, thermische stabiliteit en weerstand tegen cokes combineren. Daartoe is een reeks met ruthenium gedoteerde strontiumtitanaat ($SrTiO_3$) perovskietkatalysatoren gesynthetiseerd met behulp van conventionele en met microgolven

ondersteunde hydrothermische werkwijzen. Aanzienlijke synthese temperatuur en tijdverkorting van 220 °C gedurende 24 uur bij conventionele verwarming tot 180 °C gedurende 1 uur onder verwarming met microgolven werden bereikt. De gesynthetiseerde katalysatoren werden gekarakteriseerd met betrekking tot hun diëlektrische eigenschappen in een tweevoudige modus cilindrische holte evenals hun fysisch-chemische eigenschappen door middel van verschillende analytische werkwijzen (XRD, BET, ICP-OES en hooghoekige ringvormige donkerveldscanning transmissie-elektronenmicroscopie (HAADF-STEM) gekoppeld aan energie-dispersieve röntgen (EDX) analyse). Op basis van de uitkomst van de karakteriseringsprocedures, werd een 7 gew. % ruthenium-gedoteerde $SrTiO_3$ katalysator geselecteerd voor het verder testen van zijn katalytische activiteit voor methaan droog reformeren onder microgolfverwarming in een op maat gemaakte quartz reactor met een bed-reactor. Magnetronvermogen, CH_4: CO_2 vol. % voedingsverhouding en gasruimtesnelheid per uur (GHSV) werden gevarieerd om de beste omstandigheden te bepalen. Maximale omzettingen van ~ 99,5% en ~ 94% voor respectievelijk CH_4 en CO_2 werden bereikt tijdens een 3 uur stabiliteitstest bij 9000 $cm^3g^{-1}hr^{-1}$ GHSV, met het geselecteerde 7 gew. % Ru-gedoteerde $SrTiO_3$-katalysator, die werd blootgesteld aan maximale temperaturen in de buurt van 940 °C. Opschalingsberekeningen op basis van 1 m^3per uur van CH_4 inlaatstroomsnelheid op de perovskietkatalysator tonen, een significante verbetering in H_2-productievermogen vergeleken met op koolstof gebaseerde katalysatoren.

Rekening houdend met verdere schaalvergroting en industriële implementatie, kan de op Ru gebaseerde katalysator duur zijn. In hoofdstuk 5 wordt er daarom, combinaties van vier commerciële en relatief goedkope nikkel gedragen metaaloxide katalysatoren (Ni/Al_2O_3, $Ni/CaAl_2O_4$, Ni/Al_2MgO_4 en Ni/SiO_2-Al_2O_3) met een 7 gew. % Ruthenium (Ru) -gedoteerde $SrTiO_3$-perovskietkatalysator, getest als hybride katalytische systemen voor syngasproductie door microgolf-geassisteerde methaan-droge reformering. De experimentele resultaten toonden aan dat de introductie van de Ru-gedoteerde perovskietkatalysator het microgolfverwarmingsvermogen van de hybride systemen onder typische droge reformatietemperaturen (tot 850 °C) verbetert.

De vier katalytische systemen werden ook geëvalueerd onder droge reformerende reactieomstandigheden in termen van CH_4- en CO_2-omzetting en H_2/CO-verhouding als functie van MW-vermogen, gasruimtesnelheid per uur (GHSV) en tijd-in-stroom. De combinatie van $Ru/SrTiO_3$ en Ni/Al_2O_3 bleek het beste hybride katalysatorsysteem te zijn in termen van microgolfabsorptievermogen, syngas-productiecapaciteit en katalytische stabiliteit. Een vergelijkende theoretische opschalingsstudie toonde verbetering in de H_2-productiecapaciteit aan in het geval van een combinatie van Ni/Al_2O_3 en $Ru/SrTiO_3$ in vergelijking met de combinatie van Ni/Al_2O_3 en FY5

Ten slotte vat het laatste hoofdstuk (hoofdstuk 6) de bevindingen van de gehele onderzoeksactiviteit samen en geeft het aanbevelingen voor toekomstige werk met betrekking tot dit onderwerp.

Table of Contents

Contents

1

1. Introduction

This chapter aims to provide a brief overview on the subjects of globally increasing energy demand, the concern for CO_2 and CH_4 mitigation, the microwave technology and its applications. The motivation for developing an efficient microwave-driven methane dry reforming process is presented along with challenges that need to be addressed to achieve this goal. In this context, the scope of the doctoral work, the specific research questions addressed and the outline of the thesis along with a graphical abstract are presented at the end of the chapter.

1.1. Energy demand and feasible solutions

In years to come, the way we live, travel and communicate worldwide will change. The energy demand has been predicted to significantly increase due to the increase in population, industrialization and our dependence on energy demanding technologies [1][6]. International energy outlook 2017 reports that between 2015 and 2040, the world energy consumption will increase by 28% [2]. Global renewables status of 2013 reports that around 78% of the energy comes from fossil fuels (Petroleum, coal and natural gas)[3]. Despite the high rate at which the planet's resources have been exploited [4], oil, gas, and coal will constitute a large share of the global energy budget for several decades ahead.

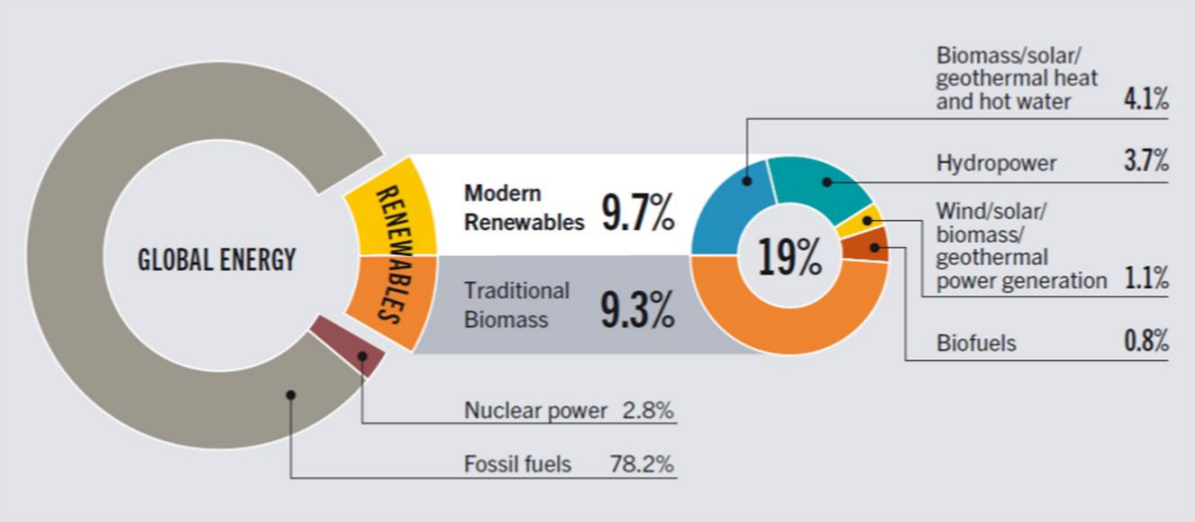

Figure 1.1 Estimated Renewable Energy Share of Global Final Energy Consumption [3]

Considering the negative impact of fossil fuels burning on the climate and the ongoing debate on the high rate of their utilization and their inevitable depletion in the short or long run, the transition from fossil fuels to sustainable and renewable energy resources is a global necessity. It is necessary for developing countries to realize the importance of efficient and clean technologies for the global goal of energy conservation and emissions reduction [5][6]. Alternative renewable energy sources such as solar, hydro and wind energy are contributing to meet the increasing global energy demand. However, as shown in **Fig. 1.1**, the renewable energy share of global energy consumption is only ~ 19% at present. Hence, the usage of renewable energy sources and fuels producing minimum carbon emissions needs to increase in every possible way worldwide. The annual energy outlook for 2018 by the U.S. Energy Information Administration reports that wind and solar generation lead the growth in renewable energy sources, accounting for 64% of the total electric generation growth in the reference case of 2050 projection [7]. In the European Union, renewables, mostly solar photovoltaics (PV) and wind power, account for almost 80% of the new additions to the global electric capacity. The World energy outlook 2017 reports that the wind power will become the leading source of electricity soon after 2030 due to its strong growth both onshore and offshore [8].

In this thesis, microwave technology has been explored, as a technology with the potential to be driven by renewable electricity, to convert two important greenhouse gases, CO_2 and CH_4, into syngas ($CO+H_2$), a building block for many fuels and chemicals.

1.2. Global concern for CO_2 and CH_4 mitigation

As shown in **Fig 1.2**, carbon dioxide (CO_2) release from burning fossil fuels, power generation, the transportation sector, and industries is a significant anthropogenic contributor to the greenhouse effect [9][10]. Greenhouse gases (GHGs) generated from the consumption of fossil fuels, and human activity have severe environmental implications [11][12]. CO_2 accounts for an estimated 77% of GHGs[13]. The concentration of carbon dioxide (CO_2) in the atmosphere has increased from approximately 277 parts per million (ppm) in 1750, the beginning of the Industrial Era, to 402.8 ± 0.1 ppm in 2016 [14]. The six largest emitting countries/regions (with their share in 2012 between brackets) were: China (29%), the United States (15%), the European Union (EU271) (11%), India (6%), the Russian Federation (5%) and Japan (4%). Remarkable trends were seen in the top three emitting countries/regions, which account for 55% of the total global CO_2 emissions [15].

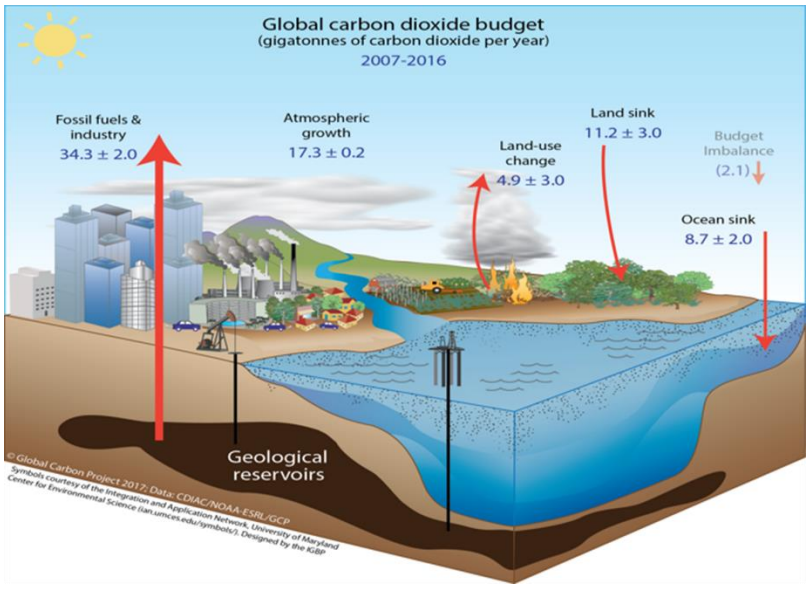

Figure 1.2 Schematic representation of the overall perturbation of the global carbon cycle caused by anthropogenic activities, averaged globally for the decade 2007-2016. The arrows represent emissions from fossil fuels and industry (EFF); emissions from deforestation and other land-use change (ELUC); the growth rate in atmospheric CO_2 concentration (GATM) and the uptake of carbon by the 'sinks' in the ocean (SOCEAN) and land (SLAND) reservoirs. The budget imbalance (BIM) is also shown. All fluxes are in units of GtC yr^{-1}, with uncertainties reported as ±1σ (68% confidence that the real value lies within the given interval) as described in the text. This figure is an update of one prepared by the International Geosphere-Biosphere Programme for the GCP, using diagrams created with symbols from the Integration and Application Network, University of Maryland Center for Environmental Science (ian.umces.edu/symbols/), first presented in Le Quéré (2009) [14].

Minimising CO_2 emissions is a very challenging multifaceted task that should be accomplished in a safe, reliable and affordable manner. The large storage capacity of the planet (1000-20000 Gt) in CO_2 can help neutralize the CO_2 emission budget for a few decades. However, CO_2 storage is limited by the energetic waste required for CO_2 capture and compression. In addition, CO_2 storage may become unsafe and risky in the long term due to potential leaks. Utilization of CO_2 as a raw material at large scale is, therefore, more attractive than CO_2 storage. However, its utilization involves thermodynamic barriers; CO_2 is a very stable molecule, and accordingly, energy must be supplied to drive the desired transformation. Therefore, potential renewable electricity-based energy sources may be exploited to carry out the carbon dioxide reactions.

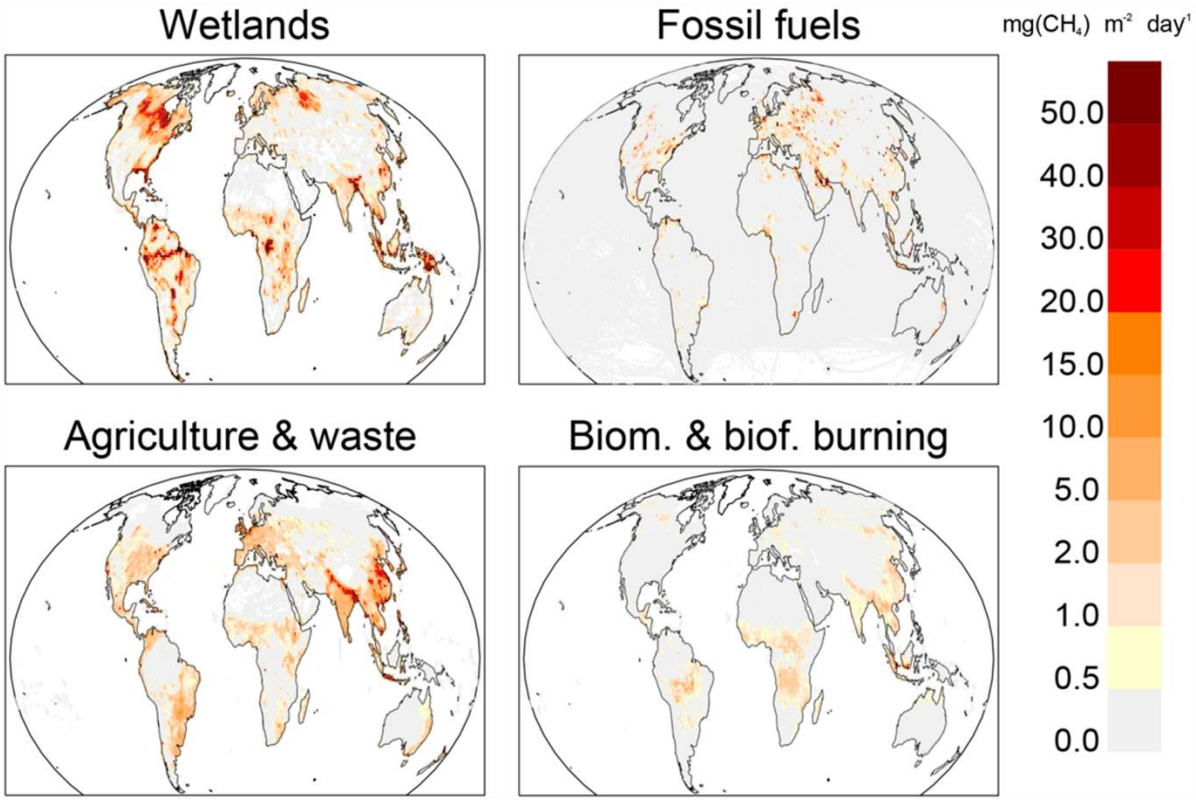

Figure. 1.3 Methane emissions from four source categories: natural wetlands, fossil fuels, agriculture and waste, and biomass and biofuel burning for the 2003–2012 decade in mgCH_4 $m^{-2}day^{-1}$. The wetland emission map represents the mean daily emission average over the 11 biogeochemical models listed in Table 1 of ref. [16] and over the 2003–2012 decade. Fossil fuel and agriculture and waste emission maps are derived from the mean estimates of EDGARv4.2FT2010 and GAINS models. The biomass and biofuel burning map results from the mean of the biomass burning inventories listed in Table 1 of Ref. [16] added to the mean of the biofuel estimate from EDGARv4.2FT2010 and GAINS models [16].

Atmospheric CH_4 is the second most impactful anthropogenic greenhouse gas after carbon dioxide (CO_2) in terms of radiative forcing. It is 21 times more potent than CO_2 in terms of increasing the atmospheric temperature [17]. There are five vital anthropogenic sources: agriculture, coal, landfills, oil and gas operations and wastewater together emit 68% of the total CH_4 emissions [11]. The vast quantities of methane available all over the world have a high potential value as a source

of clean fossil energy or as a raw material [18][19]. **Fig 1.3** highlights the areas of methane emissions worldwide from four source categories: natural wetlands, fossil fuels, agriculture and waste, and biomass and biofuel burning for the 2003–2012 decade in mg CH_4 $m^{-2}day^{-1}$. The large volume of methane resources available, as compared to petroleum, has driven considerable research efforts towards the conversion of methane into liquid fuels or high hydrocarbons [20]. Therefore, methane valorization has become a popular research topic in the chemical engineering field.

The correlation of mean global temperature rise due to the emission of CH_4 in the atmosphere from the source categories mentioned in **Fig 1.3** and the concentration of CO_2 in the atmosphere due to burning fossil fuels has resulted in drastic changes in the annual temperature cycle of the northern hemisphere and in increased volatility of the global weather patterns. There has been increased interest in better understanding of methane (CH_4) and carbon-dioxide (CO_2) removal, disposal, and utilization as well as their effect on the atmosphere [21]. The development of processes and reactor systems to valorise CH_4 by CO_2 reforming to value-added chemicals or liquid fuels at the local level will help avoid flaring, which will, in turn, contribute towards a decrease in the greenhouse effect. Recent developments in Power-to-X (chemicals) technologies utilizing CO_2 focus on the development of processes that use renewable electricity for the generation of chemical energy carriers, such as, hydrogen or methane (Power-to-Gas), liquid fuels (Power-to-Liquid), and base chemicals (Power-to-Chemicals) [22]. Electrification of chemical reactors using microwave heating as a process intensification tool can be one of the enabling approaches to the Power-to-X technologies.

1.3. Microwave technology and its applications

Microwave technology has had many application in different areas of chemical processing, such as organic synthesis, gas-solid heterogeneous catalytic reactions, polymerization, extraction, distillation, crystallization, and adsorbent regeneration/dehydration [23]. The non-contact, rapid, and selective heating are the main advantages of microwave energy as compared to conventional heating. Microwaves are electromagnetic radiation situated between radio waves and infrared frequencies. The wavelength lies between 1 mm and 1 m, corresponding to frequencies between 0.3 GHz and 300 GHz. The most common frequencies available for chemical processes are 915 MHz, 2.45 GHz, and 5.85 GHz [24][25]; they are selected to avert interferences with radar and telecommunication frequencies.

When the material is exposed to a microwave field, microwave radiation can either be absorbed causing heating (e.g., carbon), or can penetrate through the material (e.g., quartz glass), or can be reflected from the material surface (highly conductive materials, e.g., aluminum). Materials which absorb microwaves and dissipate them to heat are called microwave absorbers or dielectrics. In order to apply microwave energy to chemical process, one of the components must be a good

microwave absorber. It should be noted that only a few materials are either pure reflectors, pure absorbers or completely transparent to microwaves. Some materials are composites of materials with different lossiness, and thus partially absorb microwaves. The lossy dielectrics exhibit dielectric losses, which in turn result in heat generation in an oscillating electromagnetic field. The behavior of a material in a microwave field depends on its chemical composition and the physical shape and size.

Microwaves, as an energy source, produce heat through their interaction with materials at the molecular level without altering the molecular structure [26]. The capability of a material to be heated in the presence of a microwave field is expressed by its dielectric loss tangent $\tan\delta = \varepsilon''/\varepsilon'$ [27][28]. The dielectric loss tangent comprises two parameters: the dielectric constant, or the real permittivity ε', which signifies the ability to propagate microwaves into the material and the dielectric loss factor, or imaginary permittivity ε'', which represents the ability of the material to dissipate the energy in the form of heat.

Microwave heating in materials synthesis and heterogeneous catalytic processes is getting more attention due to their ability to reduce the processing time [25][29][30]. For example, Malghe et al. synthesized nanosized $SrTiO_3$ at low temperature from an oxalate precursor employing microwave heating. The $SrTiO_3$ precursor in combination with microwaves yielded pure cubic nanosized $SrTiO_3$ at temperatures as low as 500 °C within 30 min [31]. In [32], the authors prepared a $BaZnNbO_3$ phase through microwave heating (at 1000 °C) of a mixture of $BaCO_3$, ZnO, and Nb_2O_5 powders in 26 min; rather, the same process in an electric furnace had a holding time of 60 min at 1000 °C [32]. Further, Jhung et al. [33] synthesized $BaTiO_3$ crystals by hydrothermal and microwave. Similar morphologies were obtained with the two heating methods. However, smaller crystals were obtained under microwave heating while the crystallization time was reduced from hours to minutes [33].

Table 1.1 presents selected applications of microwave energy to different heterogeneous catalytic processes. Zhang et al. tested various catalysts for microwave-assisted methane dry reforming (DRM) and reported the following order of activity ½Pt-La_2O_3-Al_2O_3 > ½Pt-CeO_2-Al_2O_3 > ½Pt-Al_2O_3. Besides, higher reactants conversion and syngas selectivity were obtained under microwave heating; the effect was attributed to the formation of hot spots occurring at temperatures higher than the measured bulk one [34]. In [35], the authors demonstrated that selective microwave energy absorption by CuO in a ternary CuO/ZnO/Al_2O_3 oxide precursor for Cu/ZnO/Al_2O_3 catalysts over a short irradiation time (5-10 min) resulted in intensified catalytic activity for methanol steam reforming. The effect was attributed to microstructural modification at the Cu-ZnO interface and the creation of highly strained Cu crystals in the active catalyst[35]. Ferna et al. reported that constant removal of carbon deposits, which can be understood as an "in situ" regeneration of the catalyst, was favored under MW heating [36]. Fidalgo et al. reported that methane dry reforming using activated carbon as a catalyst is enhanced under microwave heating as compared to conventional heating due to the generation of microplasmas. The authors also remarked that in the

ideal temperature range of 700 – 800 °C, the active catalyst sites are continuously regenerated through gasification of the highly reactive carbon deposits by the CO_2 [37]. Chen et al. reported faster water gas shift reaction (WGSR) with microwave heating as compared to conventional heating due to the double-absorption of microwaves both by the catalyst and the water [38]. Further, microwave double absorption by microwave active metal oxide catalysts, such as CuO as well as reactants, e.g., water and methanol, were responsible for improving the overall reaction performance under microwave heating [39]. Finally, Deng et al. showed that faster methane decomposition under microwave heating is attained over a pyrolysis residue of sewage sludge (PRSS), compared to activated carbon, as PRSS is a better microwave receptor. In addition, the authors claim that the microwave heating performance of the two materials is affected by the composition of the gaseous environment (N_2, CH_4, or H_2) [40].

Table 1.1: Selected microwave-assisted heterogeneous catalytic processes

Reaction or process studied under MW heating	**Catalyst used**	**Study type/reactor used/temperature measurement technique**	**Dielectric properties reported (or not)/testing conditions**	**References**
CO_2 reforming of methane	Pt-alumina.	Cylindrical microwave cavity and conventional tubular furnace	No	[34]
Steam reforming of methanol	$Cu/ZnO/Al_2O_3$	Domestic microwave oven	No Power: 500W F: 2.45GHz	[35]
Dry reforming of methane	Rich potassium char	Electric furnace and single-mode microwave oven	No T: 800 °C	[36]
Decomposition of methane	Activated carbon (Filtracarb FY5), 0.5–2 mm	Electric furnace and single-mode microwave oven, quartz reactor (45cm ×2.2cm i.d.)	No T: 900 ˚C	[41]
Dry reforming of methane	Commercial activated carbon (Filtracarb FY5), 0.5- 2 mm	Single mode microwave oven, quartz reactor (45 cm × 2.2cm i.d.), thermocouple	No T: 700-800 °C	[37]
Water gas shift reaction	High-temperature Fe-Cr-based catalyst (3 mm)	K-type thermocouple (shielded by an alumina tube)	No F: 2.45 GHz, Power: 800 W T: 350-550 °C	[38]
Methanol steam reforming	$CuO/ZnO/Al_2O_3$	Quartz reactor tube (2.2 mm i.d.), K-type thermocouple (shielded by an alumina shell)	No F: 2.45 GHz Max Power: 800 W	[39]
Methane decomposition	Pyrolysis residue of sewage sludge (PRSS), 12 g	Quartz tube (40 cm × 2.2 cm i.d.), multimode microwave oven and electric furnace, IR sensor	No F: 2.450 GHz, Max power: 800 W	[40]
Dry reforming	Carbon catalyst	Tubular quartz reactor (15 mm O.D)	No F:2.450 MHz Total power: 10 kW P: 500 W	[42]
Accuracy and reproducibility of temperature measurements	CeO_2–ZrO_2 and Al_2O_3 particles	Fiber optic probes (FO) and infrared (IR) sensors	No	[43]
Methanol steam reforming	$CuZnO/Al_2O_3$ and $PdZnO/Al_2O_3$	Monomode microwave applicator (Discover, CEM Corporation), FO probes (FISO L-BA thermocouple)	No	[44]

Durka et al. studied the accuracy and reproducibility of fiber optic (FO) and infrared (IR) temperature sensors during microwave heating of solid materials [43]. For temperature measurement under MW heating, fiber optic (FO) measurements are reported to be realistic, but temperature variations were observed with respect to the location of the FO sensor. In contrast, IR sensors measure surface temperatures and consistently underestimated the real temperature inside the reactor [43]. Due to uneven heat distribution in solid materials, single-point temperature measurements may lead to incorrect conclusions concerning MW effects [44]. Therefore, development of a microwave reactor system that can provide concentrated MW field and allow for monitoring of temperature distribution over a catalytic bed are important challenges to address in the study of any microwave-assisted heterogeneous catalytic process.

1.4. The motivation for methane dry reforming process

The methane dry reforming reaction is important as it consumes two major greenhouse gases (CH_4 and CO_2), which can help reduce carbon footprint and limit global warming. In addition, the conversion of CH_4 and CO_2 to chemicals, such as syngas, methanol, and hydrogen, is an approach to store energy in chemical form. Reforming of methane with carbon dioxide has the potential for application at large scale as it produces syngas with a theoretical H_2/CO ratio of one. A brief overview of applications of syngas, being a building block for value-added commercial products, is illustrated in **Fig. 1.4.** Syngas with a rich CO content could be used as a direct feed for the synthesis of Dimethyl ether (DME), aldehydes, alcohols and olefin/gasoline by Fischer-Tropsch synthesis [45][46][47].

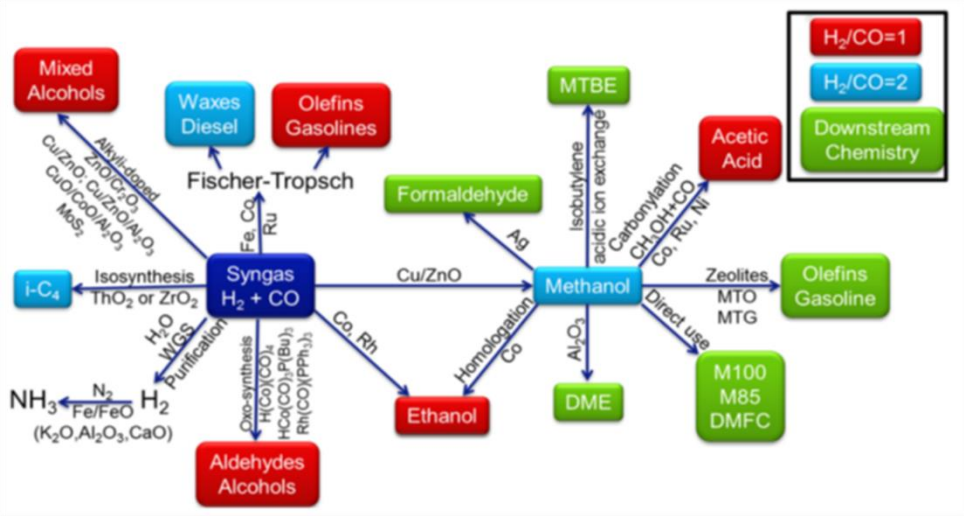

Figure 1.4 Use of syngas in the chemical industry (DME, DiMethyl Ether; DMFC, Direct-Methanol Fuel Cell; i-C4, isobutane; M85, a mixture of 15% methanol in benzine; M100, pure methanol; MTBE, MethylTertiary-Butyl Ether) [45].

Dry reforming of methane is an endothermic process. Thermodynamic analysis indicates that temperatures as high as 800 °C - 900 °C are required to achieve high syngas yields [46]. Both methane cracking and carbon dioxide gasification occur at high temperatures. The most common side reaction is the reverse water gas shift reaction (RWGS), which occurs at temperatures lower than 820 °C, and the Boudouard reaction, which occurs below 700 °C, and results in the formation of carbon deposits **(Table 1.2)**. A number of studies have been done on the dry reforming reaction, but the process has not yet implemented at commercial scale. The obstacles preventing commercialization is the high energy demand (247 kJ/mol**)** and catalyst deactivation due to coke formation.

Table 1.2: Upper and lower temperature limits of reactions involved in the global dry reforming reaction [48]

Reaction	Upper-temperature limit (ºC)	Lower-temperature limit (ºC)
Dry Reforming Reaction		640
Methane decomposition		557
Carbon Gasification		700
Reverse water gas shift reaction	820	
Boudouard Reaction	700	

Global DRM Reaction: $CH_4 + CO_2 \leftrightarrow 2CO + 2H_2 \quad \Delta H_{298K} = +247 \text{ kJ mol}^{-1}$ (**1.1**)

Intermediate Steps:

*Methane Cracking***:** $CH_4 \leftrightarrow C + 2H_2 \quad \Delta H_{298K} = +75.6 \text{ kJ mol}^{-1}$ (**1.2**)

Carbon Gasification: $C + CO_2 \leftrightarrow 2CO \quad \Delta H_{298K} = +172 \text{ kJ mol}^{-1}$ (**1.3**)
(*Reverse Boudouard reaction*)

Side Reactions:

RWGS reaction: $H_2 + CO_2 \leftrightarrow CO + H_2O \quad \Delta H_{298K} = +41.2 \text{ kJ mol}^{-1}$ (**1.4**)

Boudouard reaction: $2CO \leftrightarrow CO_2 + C \quad \Delta H_{298K} = -171 \text{ kJ mol}^{-1}$ (**1.5**)

The activation of CH_4 is the rate-limiting step in the methane dry reforming process. It primarily occurs on active metal sites and thus having a high dispersion of the metal in the catalytic materials is very important. Activation of CO_2 is a relatively faster process and occurs mainly on the support or the metal–support interface in case of acidic and basic supports of catalytic materials; hence, most catalysts with acidic or basic supports follow a bi-functional pathway where CH_4 and CO_2 are activated on different sites, and the reaction intermediates react at the metal–support interfacial sites. In case of inert supports, activation of CH_4 and CO_2 occurs on the metal alone (uni-functional pathway), and thus the inert support catalysts are more prone to deactivation by carbon deposition

than acidic or basic supports. Consequently, selecting an appropriate catalyst and operating temperature is vital in avoiding deactivation and stable catalytic performance [49]. Noble metals such as Pt, Ru, and Rh are highly active for methane dry reforming, do not suffer from sintering and are more resistant to carbon formation compared to common metals. On the downside, they significantly increase the catalyst cost.

1.5. Challenges for microwave-assisted dry reforming of methane

Microwave-assisted methane dry reforming has already been studied by several authors as shown in **Table 1.1.** However, there are still some challenges to be addressed for overall process intensification or improvement; these are discussed in this section.

Convective/conductive heat transfer heats up the whole catalytic reactor instead of the catalyst material only, resulting in excess of energy supply and wastage of energy. Energy consumption measurements of microwave heated processes have shown that lower energy consumption and higher heating rates can be attained in comparison to conventionally heated processes [50][51]. However, the available commercial microwave ovens are mostly general-purpose devices that cannot distribute the microwave field homogeneously over gas-solid catalytic reactors. This is due to the dependence of microwave heating on many factors, such as the dielectric properties, the chemical composition, the physical properties, the size and shape of the materials and the power range of the MW equipment. Therefore, ***the first challenge*** is the need for the development of a microwave reactor system that can provide a concentrated microwave field on the catalytic bed and high microwave utilization energy efficiency.

The second challenge concerns temperature measurement in heterogeneous catalytic beds under microwave heating. There are some available techniques or sensors, but they come with limitations. For instance, optical fibers can measure up to 300 °C - 350 °C and IR sensors or pyrometers can measure surface temperatures only. For the dry reforming process, the optimum temperature is rather high, above 800 °C [52], where optical fibers cannot be used. Even though sensors like optical fibers may be available to measure high temperatures in the future, a point temperature measurement will not be able to provide much insight into temperature distribution inside a catalyst bed under microwave heating [53]. Therefore, a provision for, at least, 2D temperature monitoring is necessary to rationalize reactor performance and avoid thermal runaway and reactor damage.

The third challenge is the development of a catalyst that can operate at high temperatures (> 800 ^{o}C) [52] without undergoing deactivation due to carbon deposition. Methane needs high temperatures to dissociate, and so a catalyst with high thermal stability, high catalytic activity, and excellent microwave absorption capacity to reach the optimum high reaction temperatures is necessary.

Not all catalysts active for steam reforming or dry reforming under conventional heating can directly be used for microwave-assisted methane dry reforming due to their different dielectric properties, some of which do not allow effective heating of the material up to reaction temperatures in a microwave field. Therefore, finding ways to increase the microwave absorption ability of commercial catalysts is imperative for their application to methane dry reforming under microwave heating. To this end, development of hybrid catalytic systems consisting of microwave inactive commercial catalysts mixed with microwave active catalysts could be the ***fourth challenge*** that needs to be addressed.

1.6. The scope of the thesis

The aim of this doctoral work is to study methane dry reforming using a customized microwave reactor and address the aforementioned challenges. The complex nature of microwave-catalyst interaction and its sensitivity to different variables render every microwave-heated process essentially unique. Therefore, insight into microwave and heat transport phenomena, the specific chemistry under consideration, catalysis and hardware of microwave equipment is necessary to ensure safe, stable and efficient operation of microwave heated catalytic processes. On the basis of the literature reviewed and past work of the group, the following specific research questions were formulated and tackled in the course of the Ph.D. study.

1.7. Research Questions

1. What are the most important challenges for application of the microwave technology to dry reforming of methane? (Chapter 1). How can concentrated microwave field be applied to heterogeneous catalytic systems? How can we monitor temperature distribution over a catalytic bed in 2D fashion and avoid overheating? (Chapter 2).

2. Which is the correct way to measure high temperatures in microwave-assisted heterogeneous catalytic processes? Why is it complex and challenging to reproduce temperature profiles in microwave-heated processes? (Chapter 3).

3. Can we develop new catalysts combining high microwave dissipation rates, high catalytic activity, and stability at high temperatures for microwave-assisted methane dry reforming? Can microwave heating be helpful to synthesize such catalytic materials? (Chapter 4).

4. Can common commercial catalytic materials for methane reforming processes be heated directly by microwave energy and how can we maximize their maximum absorption ability? (Chapter 5).

1.8. Outline of the thesis

The thesis is divided into six chapters including; a general introduction (Chapter 1), a description of the custom microwave reactor setup used (Chapter 2), a methodology for temperature monitoring in catalytic beds by means of temperature sensors and thermal camera (Chapter 3), reporting on synthesis, characterization and catalytic performance evaluation of a series of ruthenium-doped $SrTiO_3$ catalysts (Chapter 4), the application of hybrid catalytic systems, comprising microwave inactive commercial catalysts and highly active and microwave absorbing in-house catalysts, to methane dry reforming under microwave heating (Chapter 5), and, finally, conclusions and recommendations for future work in this field (Chapter 6). A brief description of the content of each chapter is given below.

In Chapter 1, a general introduction to the increasing societal energy demand and possibilities to meet the global energy challenge are discussed. The need for utilization of renewable energy sources and different possibilities to increase their contribution to the total energy budget are highlighted. The concept of electrification of chemical reactors and the motivation for CO_2 and CH_4 utilization to convert them into value-added chemicals, such as syngas, methanol, and hydrogen, are explained. The advantages of microwave technology in general and the challenges of microwave-assisted methane dry reforming, in particular, are presented. Finally, the research questions for overall improvement or intensification of microwave-assisted methane dry reforming are formulated.

Chapter 2 addresses the first challenge related to the need for a custom-designed microwave reactor system. A new microwave reactor assembly has been designed and developed in this work. It is able to provide concentrated microwave field onto the heterogeneous catalytic materials inside the microwave applicator. The overall setup design enables monitoring of the temperature distribution of the catalytic bed in 2D fashion with the help of non-contact temperature measurement by a thermal camera. The relevant theory and technical details of the microwave reactor setup are given. The standard experimental operating procedure to conduct microwave experiments are also provided.

Chapter 3 addresses the temperature measurement challenge in microwave heated heterogeneous catalytic reactors. A methodology to study the temperature distribution inside a catalytic bed under microwave heating by using a thermal camera in combination with a thermocouple is demonstrated. Methods for calibrating the thermal camera and the effects of various parameters on the accuracy of temperature recordings are discussed in detail.

Chapter 4 reports on the development of catalysts that are susceptible to microwave heating, stable at temperatures up to 1000 °C and catalytically active for methane dry reforming. The advantages of microwave heating compared to conventional heating for catalyst preparation are presented. A series of ruthenium-doped strontium titanate ($SrTiO_3$) perovskite catalysts were synthesized by

conventional and microwave-assisted hydrothermal methods. Characterization of the synthesized catalysts was done by X-ray powder diffraction (XRD), N_2 adsorption-desorption (BET Surface area), inductively coupled plasma optical emission spectrometry (ICP-OES), high-angle annular dark-field scanning transmission electron microscopy (HAADF-STEM) images, energy dispersive spectroscopy (EDX) elemental maps and particle size distribution. A 7 wt. % ruthenium-doped $SrTiO_3$ catalyst showed the best dielectric properties, and thus its catalytic activity was evaluated for the methane dry reforming reaction under microwave heating. Microwave power, CH_4:CO_2 feed ratio and the gas hourly space velocity (GHSV) were varied in order to determine the optimal conditions for high reactants conversions and H_2/CO ratio. Finally, a theoretical scale-up study was done to compare the H_2 production capacity of the perovskite catalyst with a carbon-based catalyst reported in the literature.

Chapter 5 is concerned with the challenge of enhancing the microwave heating ability of microwave-insensitive Ni-based commercial catalysts. Particularly, we tested the individual (pairwise) combinations of four commercial nickel-supported metal oxide catalysts (Ni/Al_2O_3, $Ni/CaAl_2O_4$, Ni/Al_2MgO_4 and Ni/SiO_2-Al_2O_3) with a 7 wt. % Ruthenium (Ru)-doped $SrTiO_3$ perovskite catalyst, developed in Chapter 4, as hybrid catalytic systems for methane dry reforming under microwave heating. First, the dielectric properties of the nickel-based commercial catalysts were investigated to determine their microwave absorption ability and potential for microwave heating. The experimental results showed that the introduction of the Ru-doped perovskite catalyst plays an essential role in improving the microwave heating ability of the hybrid systems under typical dry reforming temperatures (up to 850 °C). The four catalytic systems were also evaluated under dry reforming reaction conditions in terms of reactants conversion and H_2/CO ratio as a function of microwave power, gas hourly space velocity and time on stream. The combination of $Ru/SrTiO_3$ and Ni/Al_2O_3 was found to form the best hybrid catalyst system in terms of microwave absorption ability, syngas production capacity and catalytic stability.

Chapter 6 (last chapter) summarizes the findings of the research work done and provides recommendations for future research on the subject.

1.9. Graphical abstract of Ph.D. Thesis

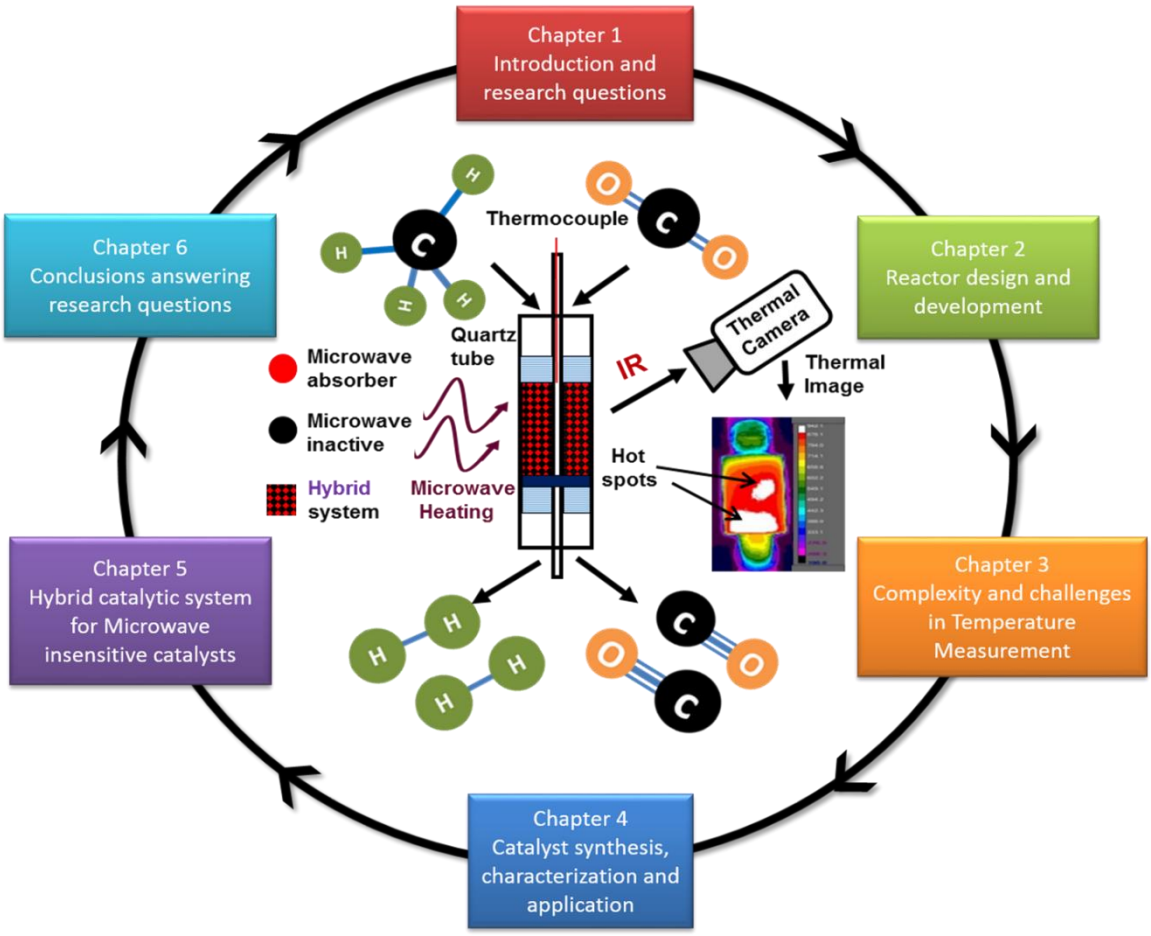

2

2. Design and development of the microwave reactor system

This chapter aims to explain the motivation behind the development of a custom-designed microwave reactor to be used for the study of methane dry reforming. It provides a description of the gas flow control system, the custom-designed microwave reactor assembly and the solid state microwave generator. It also gives a brief overview of the temperature measurement techniques used, the reactor control system, the reactor operating procedure, and safety considerations. A summary and recommendations for further improvements are given at the end.

2.1. Introduction

In this chapter, we discuss the details of the microwave reactor setup that was designed and developed to evaluate the application of the microwave technology to high temperature gas-solid catalytic reactions in general and methane dry reforming in particular, the latter being the reaction under study in this doctoral work. The microwave setup has been designed such that it can 1) provide concentrated microwave heating to the solid catalytic materials, 2) maximize the microwave energy utilization efficiency and 3) enable measurement and monitoring of the spatiotemporal temperature distribution in a quartz tube fixed bed reactor, where methane dry reforming takes place. The most important components and operation aspects of the entire microwave setup namely, gas flow control, microwave reactor assembly, solid state microwave generator, temperature measurement techniques, product gas analysis, reactor control and operating procedure, including start up and shut down, are discussed in different sections, which, together with a summary of the main features of the microwave reactor assembly and some recommendations for its further improvement, comprise this chapter.

2.2. Gas flow control

The overall setup configuration is composed of two reactors; a microwave catalytic reactor and a gas phase microwave plasma reactor that is not part of this work. The system has been designed in such a way that most gas lines and other components be used for both the reactors. **Fig. 2.1** shows the P&ID of the common gas supply for the two reactors. **Fig. 2.2a** and **b** show digital images of the main gas supply switches and gas supply control panel. As shown on the left side of **Fig. 2.1**, and in the digital image of the gas line control panel in **Fig. 2.2**, all the gases in use come from the main gas lines of the Process and Energy Department of TU Delft. These valves need to be opened manually as per gas requirements. As shown in **Fig. 2.1** and **Fig. 2b**, in order for better control of the gas flows (Air, Ar, N_2, H_2, CH_4, O_2, CO_2, and CO) towards the reactors, first ball valves and then pressure reducers and pneumatic ball valves are added. After the pneumatic valves, shared mass flow controllers (MFCs) are placed. MFC 152 is for air, Ar, and N_2; MFC 153 is for H_2 and CH_4. MFC 154 is for O_2 and CO_2 and MFC 155 is for CO gas only.

Table 2.1 shows the maximum flow rates of MFCs along with their calibration gases. **Fig. 2.1** shows that MFCs 152 to 154 are used for multiple gasses. The gas flow control is designed in such a way that only a selected gas line valve gets open while other lines connected to the MFCs are closed. The mass flow controllers are calibrated for one gas only as shown in **Table 2.1**. Therefore, a conversion factor is used to convert the mass flow rate of the calibrated gas to the mass flow rate of the process gas that flows through the particular MFC.

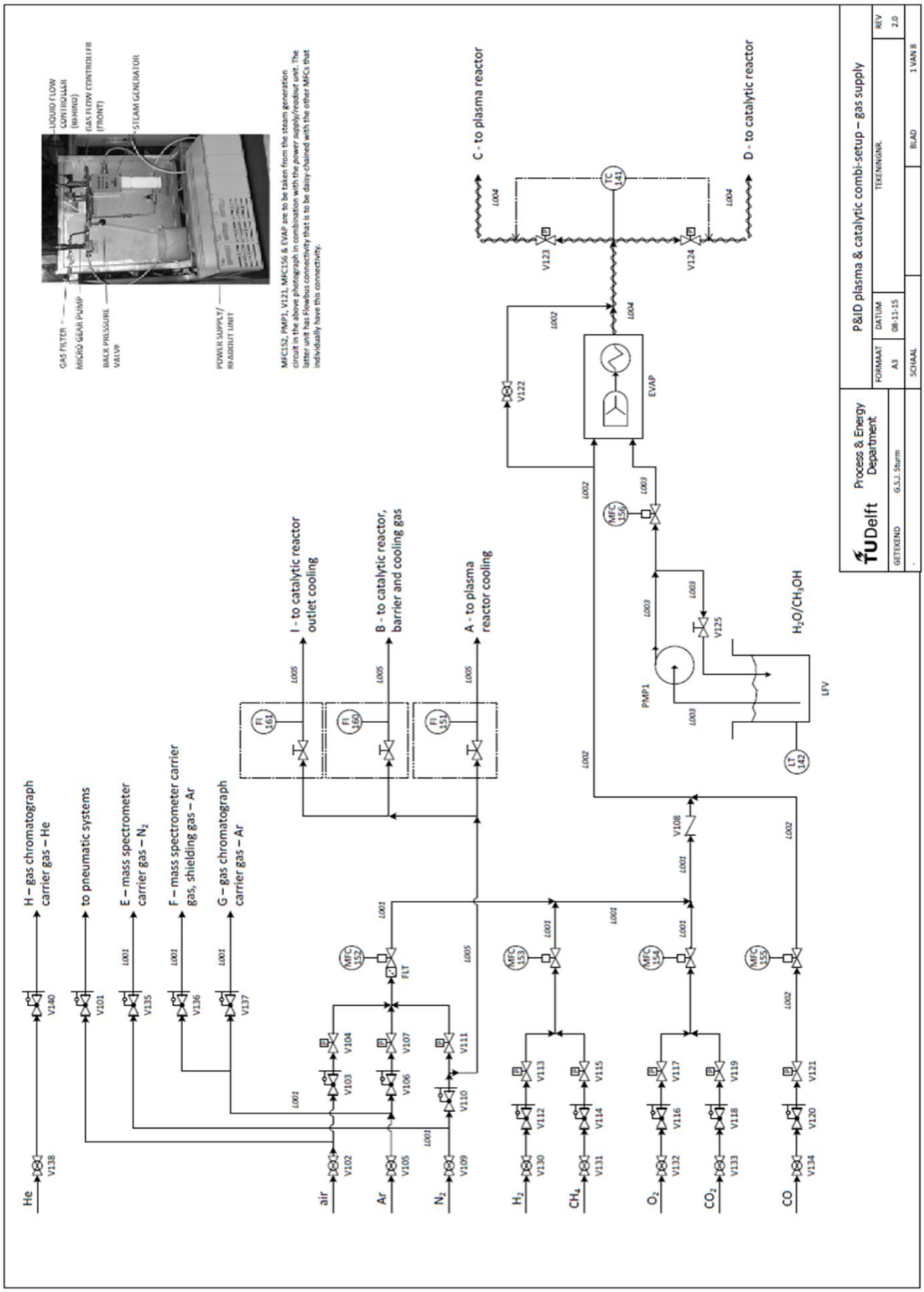

Figure 2.1 P&ID of gas supply control valves.

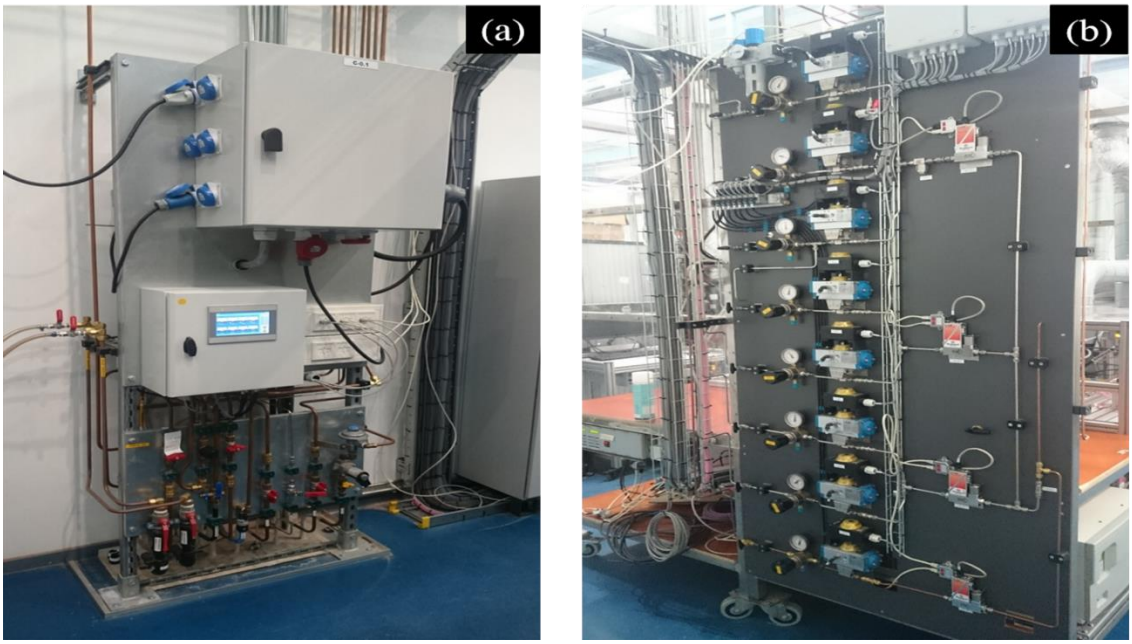

Figure 2.2 (a) Digital image of the main gas line controls and (b) control valves along with MFCs.

Table 2.1: Mass flow controllers and evaporator (Bronkhorst).

Tag	Address	Array position	Calibrated for	Gas 1	Gas 2	Gas 3	Max. Range	Unit	Type
MFC 152	3	0	Ar	Air	Ar	N_2	6.5	ln/min	F-201CV-5K0-AAD-22-V
MFC 153	4	1	H_2	H_2	CH_4	-	1000	mln/min	F-201CV-1K0-RAD-33-V
MFC 154	5	2	CO_2	O_2	CO_2	-	340	mln/min	F-201CV-1K0-RAD-33-V
MFC 155	6	3	CO	CO	-	-	500	mln/min	F-201-CV-1K0-RAD-33-V
MFC 156	7	4	Water	Water	-	-	100	g/h	L13-AAD-11-K-30S
EVAP	8	5	Temp.	-	-	-	200	°C	W-202A-122-K

Table 2.2: Used conversion factors, 20 °C, 1 atm.

Gas	Conversion factor	Used factors
Air	1	0.7143
Ar	1.4	1
N_2	1	0.7143
CH_4	1.01	1
O_2	0.98	1.3243
CO_2	0.74	1
CO	1	1

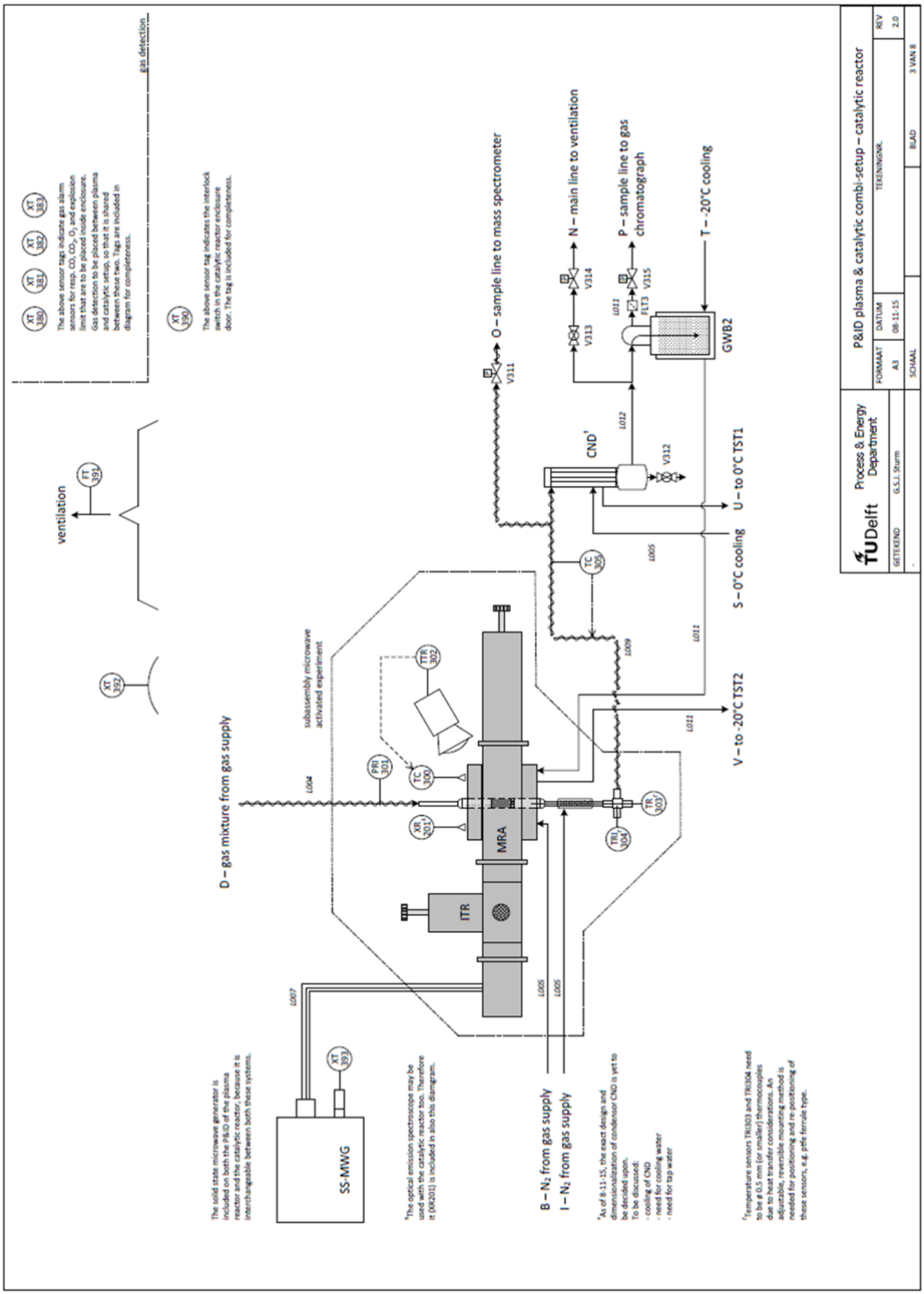

Figure 2.3 P&ID of the catalytic reactor setup.

Table 2.2 shows the conversion factors used, at 20 ºC and 1 atm (Source: Bronkhorst documentation). The 'Used factors' are obtained by dividing the conversion factor of the used gas by the conversion factor of the gas that the mass flow controller is calibrated for. The conversion is done in the software running on the Compact Rio. The conversion number is updated every time a valve is opened. The conversion numbers are stored in the subsystem 'ValveControl.'

As shown in **Fig. 2.1**, all the MFCs are connected to one common line L001 (Stainless steel, ⌀6mm or ⌀1/4"). For CO, only copper piping ⌀6mm, or ⌀1/4", is used. Along with the inlet gas line, some other parts like thermostats, a microwave generator, and the analysis instruments are shared between both the (microwave catalytic and plasma) reactors. The P&ID of the plasma setup is not included in this chapter as it is not relevant to our work. Therefore, in this chapter, we will discuss the details of the catalytic setup only. **Fig. 2.1** shows that valve V124 gets open when the catalytic setup is selected, and valve V123 remains closed.

Fig. 2.3 shows the P&ID of the catalytic setup. The catalytic reactor receives a gas mixture from line D once valve V124 is open. For the microwave heating and heterogeneous catalytic reaction experiments, a quartz tube with a length of 290 mm, 1 mm wall thickness, 10 mm outer diameter and 8 mm internal diameter is used. As our target reaction occurs at atmospheric pressure, a pressure sensor (PRI 301, range < 2000 mbar) is installed at the inlet line. At a pressure higher than 2000 mbar, the sensor gives an alarm and stops the inlet gas flow automatically to prevent breakage of the quartz reactor. Two N-type thermocouples, TRI 304 and TR 303 (temperature range,−200 to +1250 °C), with 0.5 mm diameter are used for high-temperature measurements. These thermocouples are placed at positions where thermocouple-microwave interaction, possibly leading to thermocouples failure, cannot occur.

2.3. Microwave reactor assembly

A custom-designed microwave reactor assembly (MRA) has been developed considering the process requirements with variable reflector and tuner possibilities. The objectives of the MRA design are: (1) to focus the electromagnetic field on the catalytic bed. The cavity geometry was optimized for this purpose; (2) to enable contact-free temperature measurements in the catalytic bed by means of a thermal camera. Therefore, the temperature distribution can be monitored in a 2D fashion, as opposed to temperature measurement at one position only. A germanium window (50 mm Dia. x 2 mm thick, 8−12μm range) is installed in the split shell waveguide (Sairem MW circuitry) as shown in **Fig. 2.4**. The purpose of adding an IR window is to allow infrared radiation to travel towards the thermal camera and avoid MW leakage on the window side. Two conical blocks are placed at the top and bottom part of the microwave cavity. These blocks consist of bushings with Teflon supports to hold a quartz tube inside the cavity. These bushings are very helpful to adjust the catalytic bed position up or down as per requirement.

Fig. 2.4 shows a digital image of the developed MRA. Three WR340 manual sliding short circuit - impedance tuners are included in the MRA to tune the MW field and concentrate it as much as possible on the catalytic bed only. The purpose of adding the sliding short circuit is to minimize the reflected power (RP) to ~ 0. During microwave heating, if RP >0 W, the manual sliding circuits need to be slid towards or outwards the reactor in order to get the minimum RP value. Once RP ~0 W is achieved, then the forwarded power, transferred from the microwave generator to the reactor, can be increased to the desired level. This exercise allows repeating the tuning until the lowest level of reflected power is obtained for the selected forwarded power. As shown in **Fig. 2.4**, tuners (WR340 sliding short circuit) have a readable scale to record the value at which matching is achieved. Once the required positions are reached, these particular locations can be locked by a blocking screw. Further, there are four cooling zones around the cavity, two on each side. Each zone has inlet and outlet lines, which are cooled by ethylene glycol and water at 2:1 ratio in order to remove the heat from the cavity and maintain a low temperature. The split-shell waveguide has an endplate on the opposite side of the germanum window. This endplate is replaceable and useful during loading and unloading of the catalytic quartz tube, as it allows for visual access to it and to check whether it has been adequately placed.

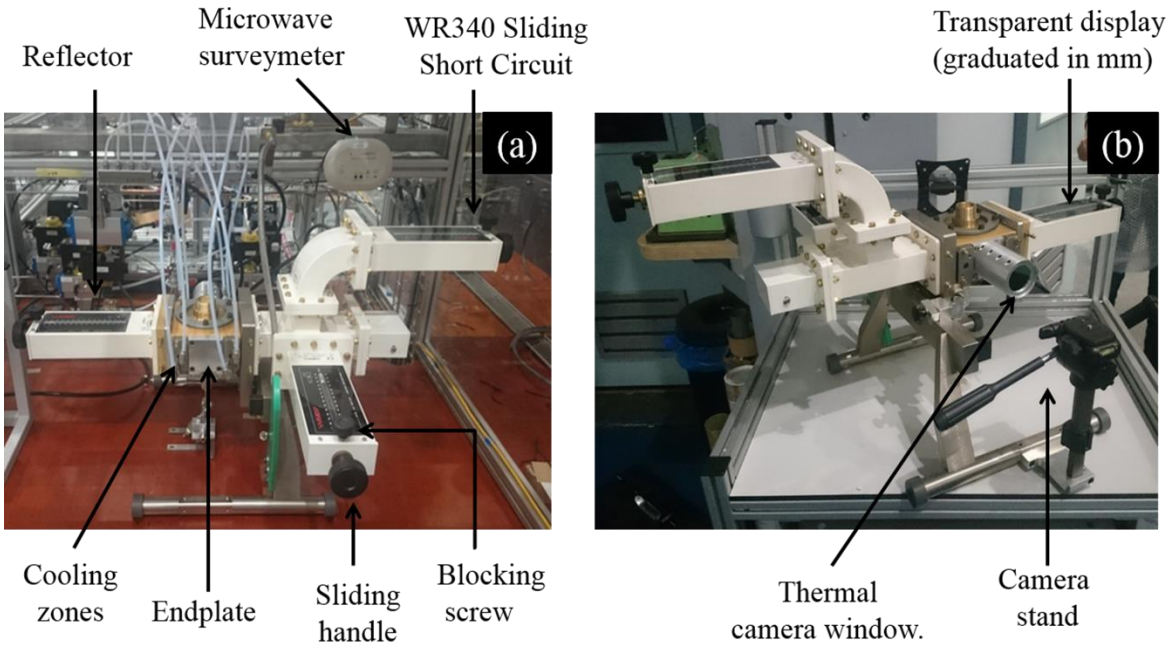

Figure 2.4 In-house custom designed Microwave Reactor Assembly (MRA).

2.4. Solid state microwave generator

The solid-state MW generator (SS-MWG) is shown in the P&ID of the catalytic reactor setup (**Fig. 2.3**). It is connected to MRA by a coaxial cable (Rigid coax, UT-250A-TP-M17) to transfer the microwave energy. **Fig. 2.5** shows a digital image of the Miniflow 200SS-MWG along with a wall mount microwave leak detector DFM and a microwave leak detector IFP 05C. The MW generator provides MW energy at 2.45 GHz at a maximum available power of 200 W. It is stable in operation from microwave power levels as low as 0.5 W. It has no magnetron and has excellent frequency spectrum even at low power. The frequency spectrum of magnetron-based generators has poor stability below 100-150 W. It has built-in internal protection against mismatching and reflected power interlock. It also has the possibility to adjust microwave frequency of 20 MHz, i.e., from 2430 MHz to 2470 MHz with 100 kHz increment. For any MW heated reactor, the microwave power absorbed by a reactor system to achieve a specific effect is a crucial parameter. The miniflow makes this measurement possible due to its solid state generator that provides an exact measurement and set-up of the microwave forward power and reflected power. In addition, the miniflow helps the operator to optimize the power consumed by the reaction by tuning the system, thereby minimizing the reflected power with the help of tuners as explained in an earlier section.

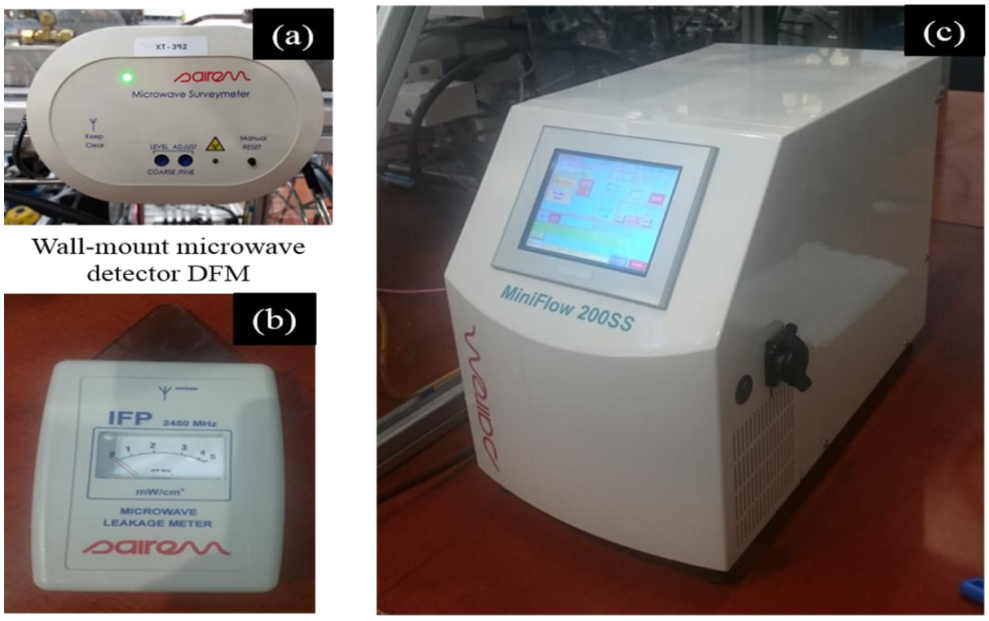

Figure 2.5 Solid state microwave generator along with a wall mount MW detector DFM and a microwave leak detector IFP 05C.

A microwave survey meter (wall-mount microwave detector DFM) has been placed near the cavity to detect any MW leakage during the experiments (**Fig. 2.5a**). It is a system designed to measure and alarm if microwave leakage is detected in the immediate vicinity of a microwave system. It can detect MW leakage up to 20 m from the MW system to be surveyed. Before performing a

reaction experiment, MW leak check at the different connection points is an indispensable requirement. These points can be in the miniflow where the coaxial cable is connected, in the microwave cavity where the coaxial cable is connected and around the split shell waveguide due to the improper top and bottom cone placements or endplate connections. **Fig. 2.5b** shows an IFP 05C microwave detector. It operates at 2.45 GHz and 915 MHz. It has been used for manual checking of MW leaks before starting any MW heating experiment. The IFP 05C is a conveniently shaped handheld meter made of a material transparent to MWs. It contains the antenna, the detection element, and linearization systems. Its galvanometer enables direct reading of the microwave leakage in mW/cm^2. The IFP works without power supply; the power required is directly taken from the MW leakage operation. It is necessary to hold the device behind the galvanometer while doing the MW leak test. The measurements will be wrong if the holding hand is around the galvanometer, as the presence of the hand alters the MW field. To perform the MW leak test, it is necessary to hold the measuring triangle against the checking points (door interval, joints, etc.). The IFP given measurement is a direct reading of the power density in mW/cm^2 at 5 cm from the leakage point (standard security regulations).

2.5. Temperature measurement techniques

Accurate temperature measurement in microwave heated catalytic reactors is essential. Due to the non-contact heating mechanism and the dependence of the MW absorption ability of the catalytic materials on their temperature-dependent dielectric properties, temperature measurements in this kind of systems are complex and challenging. Another problem is that MW interacts with standard thermocouples that, consequently, cannot be used directly inside the microwave field. Therefore, in our MW experiments, lower temperature measurements were done by optical fibers (< 250 °C). In particular, the relevant measurements have been done by two optical fibers, one directly connected to the solid-state miniflow 200SS generator and the other one connected to the NOMAD-Touch portable fiber-optic thermometer.

Fig. 2.6b shows a digital image of the Neoptix NOMAD-Touch optical thermometer. The reason to use this device is that it does not need any calibration when changing the optical fiber sensor, which makes it easy to get quick measurements of temperature changes during MW heating. It runs on a rechargeable battery and can be moved freely to measure temperatures at any point. It also measures temperature in the range −80 to 300 °C with an accuracy of ±1 °C. Finally, it has a large 240 x 320 pixels LCD display with an LED backlight to show temperature changes instantly.

The optimal temperature limit of an optical fiber is 250 or 300 °C, and thus it is not useful for high-temperature measurements under microwave heating. To monitor higher temperatures, a thermal camera model FLIR A655sc was used as shown in **Fig. 2.6d**. It is described as TTR302 in the P&ID of the catalytic setup shown in **Fig. 2.3**. The distance from the center of the quartz tube to the camera lens has been kept constant (0.3 m) in all experiments. The camera has been placed on

its stand in front of a germanium window as shown in **Fig. 2.4b**. It operates in the 7.5 –14 μm spectral range and measures temperature from −40 to 2000 °C. The FLIR ResearchIR Max software is used to record and collect thermal data during the experimental work. 2D monitoring of the catalytic bed temperature was done to track hotspot locations and control the MW power in order to avoid thermal runaway conditions. As the thermal camera-based temperature measurement is a non-contact technique, the critical factor for accurate measurements is the correct emissivity value. To correct the emissivity value and track temperature, N-type thermocouples were used during microwave heating. The full details on the combined use of the thermal camera and thermocouples for temperature monitoring can be found in [54].

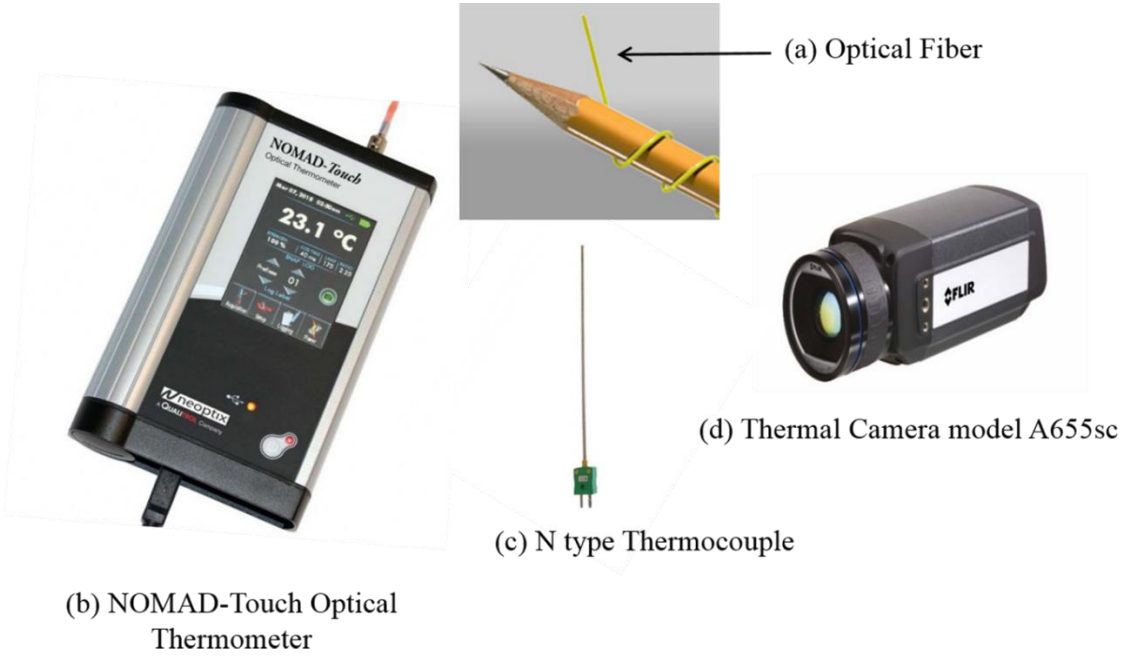

Figure 2.6 Temperature measurement techniques used: (a) optical fiber, (b) NOMAD-Touch optical thermometer, (c) N-type thermocouple and (d) thermal camera mode A655sc.

2.6. Product gas analysis

Due to the generation and migration of hotspots during MW heating, it is difficult to reproduce the temperature values, unlike the case of conventional heating experiments. Therefore, it is indispensable to continuously monitor the reaction progress or analyze the product gases with respect to MW power input while studying MW heated reactions. **Fig. 2.7** shows that two analytical instruments, a mass spectrometer, and a micro GC, are part of the P&ID for product gas analysis. In this project, we used only the Varian CP4900 micro-GC. It is equipped with a TCD detector and uses two columns, 20 m MS5A and 10 m PPU, for analysis.

During our reaction studies, there is the possibility of water generation due to reverse water gas shift reaction at low MW power inputs. Therefore, before analysis of the product gas, it is essential

first to cool it down to avoid moisture content in the μGC. To that end, a condenser (CND), as shown in **Fig. 2.3**, is placed at the exit of the reactor to avoid condensation in the line towards the μGC. Two thermostats are used to pump the coolant (a mixture of ethylene glycol and water in a 2:1 ratio). TST 1, a Lauda Thermostat RE 304 is used to maintain the MW cavity and condenser temperatures. TST 2, a Lauda RE 620 is used to maintain the gas wash bottle temperature. The gas wash bottle (GWB2), as shown in **Fig. 2.3**, is filled with calcium oxide (CaO), an adsorption agent, to dewater the remaining moisture present in the outlet gas line. A Whatman FP050/1 filter holder with 50 mm filter paper (FLT3), as shown in **Fig 2.3** and a genie membrane (GMB) as shown in **Fig. 2.7**, are placed after the gas wash bottle to avoid any impurities towards the μGC.

In order to do a comparative study of microwave heated reactions with their conventional counterparts, a tubular furnace, described as FNC in **Fig 2.8**, has also been installed. It is a Carbolite tubular furnace (FNC) MTF 10/15/130, 1000 °C, 15 mmØ x 130 mm heated length. In the present setup configuration, only the MRA is replaced by the tubular furnace while the other setup parts remain the same. Both the MRA and the tubular furnace are placed in the specially designed enclosure shown in **Fig. 2.3**. The enclosure has three holes with fringes on to adjust the reflector positions during the reaction. The enclosure has an interlock, which does not allow the flow of gases when the enclosure is open. On the top side of the enclosure, a ventilation system with a flow sensor (FT391) is placed to check the ventilation flow speed; if the flow is less than the set value, then the electric cabinet shows a red signal and does not allow operation of the reactor. The shared gas sensors (XT380, 381, 382 and 383) are placed inside the enclosure. These are gas alarm sensors for CO, CO_2, O_2 and explosion limit, respectively.

2.7. Reactor control system

The LabVIEW interface, the μGC software, and the thermal camera software are installed on separate computers and are connected to one screen using a KVM switch to control the various functions of the reactor. Aten CS1708A 8-Port PS/2-USB KVMP Switch is used for this purpose. A single CS1708A unit can control up to 8 computers. The LabVIEW interface along with an NI-9074 cRIO controller is used to control the setup and take care of data acquisition. The controller interfaces with; 1. valves and valve status readouts, 2. mass flow controllers (Bronkhorst) to regulate gas flows, 3. pressure sensors and 4. N-type thermocouples.

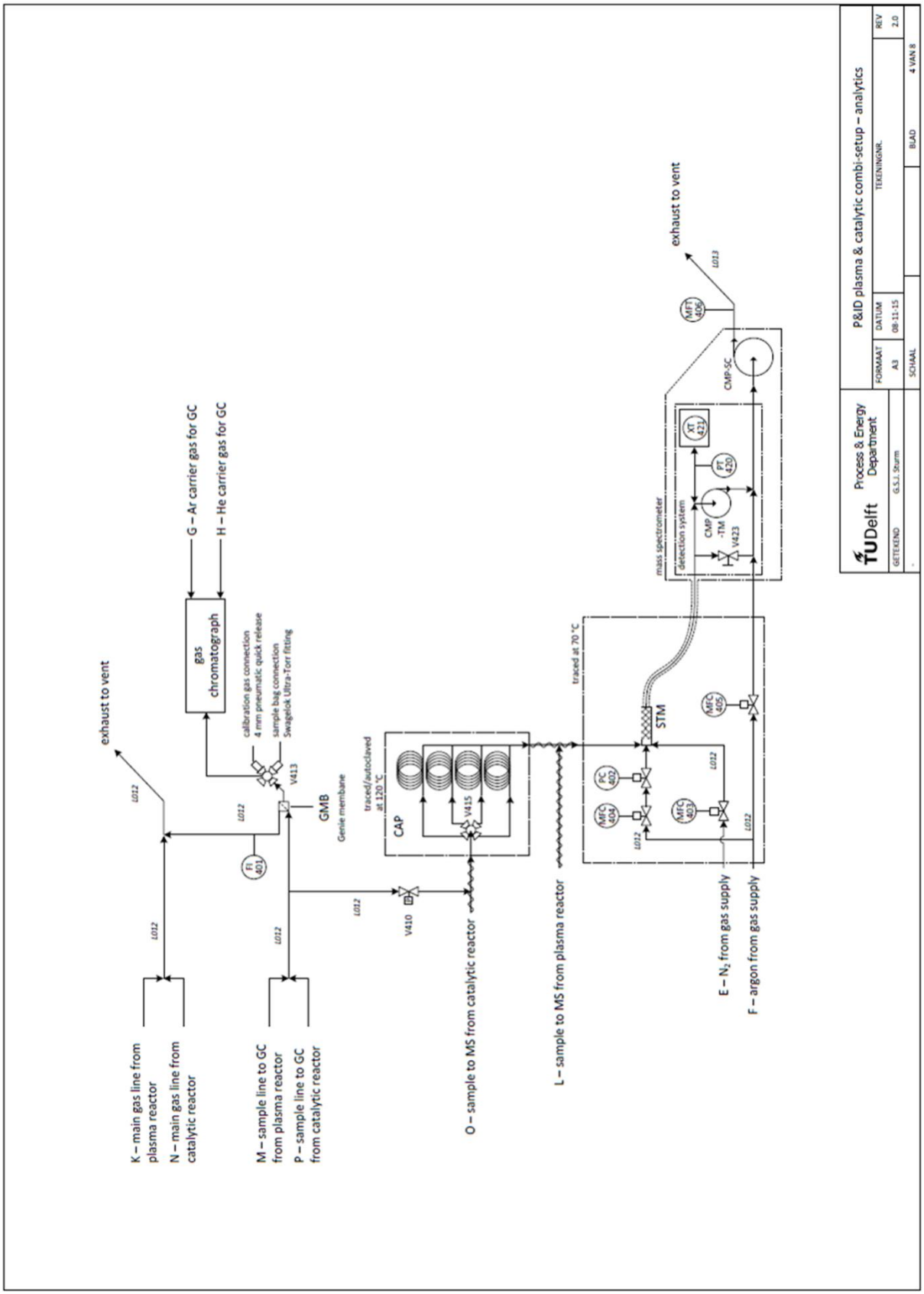

Figure 2.7 P&ID part with GC and mass spectrometer details

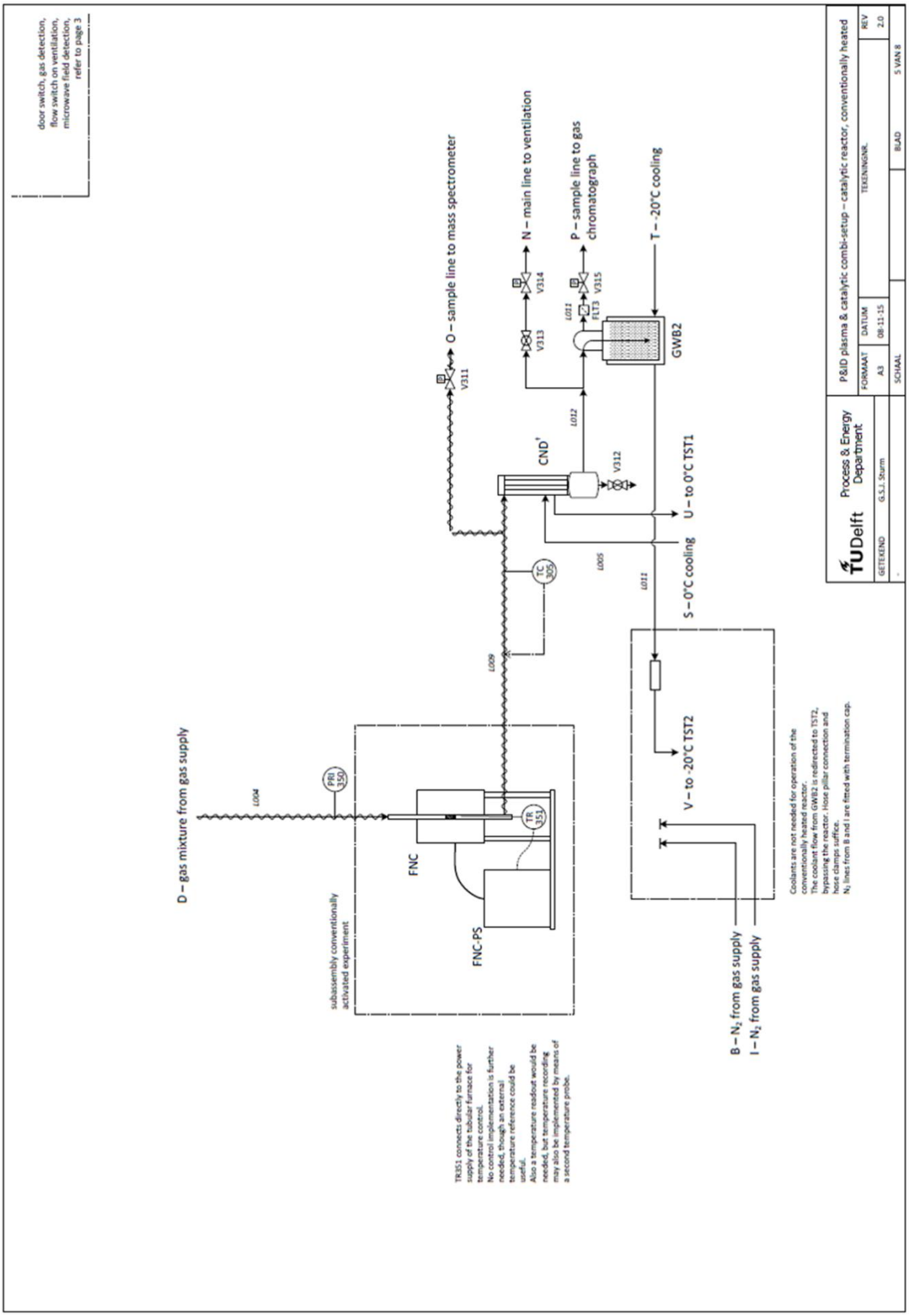

Figure 2.8 P&ID of the conventional setup employing a Carbolite tubular furnace.

Through the control interface, the valves on the gas supply lines can be opened. The valves that control the flow of gas to and from the different setups are controlled by the selector switch on the cabinet. The status (open or closed) of all valves is read out by the controller. The system for gas selection has a security system that prevents the different supply lines connected to one mass flow controller from opening at the same time. The system also inputs a new conversion factor to the mass flow controller interface when a valve is opened. The valve control subsystem communicates through three notifiers with other subsystems. It receives the digital inputs and system states through the notifier 'DI_Signals.' Commands are received through 'ValveControl,' and the conversion factors are sent through 'MFC_Conv.' The system uses five mass flow controllers and an evaporation system from Bronkhorst (**Table 2.1**). Commands to this system are sent over the flow bus through the chassis RS-232 port of the Compact Rio.

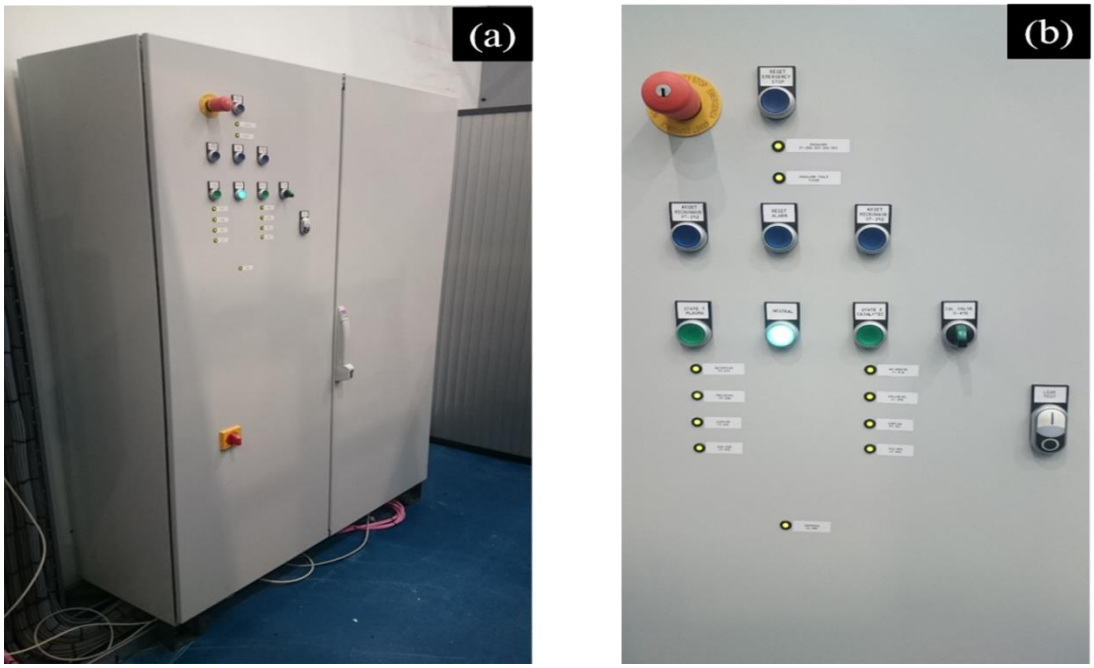

Figure 2.9 (a) cabinet of the control system and (b) manual buttons for reactor selection along with safety indicators

Fig. 2.9a shows the control cabinet for both microwave catalytic and plasma setups. **Fig 2.9b** shows the manual selection buttons for the reactors along with safety indicators. The top blue button is an emergency stop reset button. The three green buttons in the middle are for the plasma reactor, the neutral state, and the microwave catalytic reactor, respectively. The standard black and white color button allow for N_2 flow even when the enclosure is open, to perform the reactor leak test after reactor loading. Four green indicators are installed for each reactor to ensure that; 1st the coolant flow is ON or OFF, 2nd to indicate whether the enclosure is closed or open, 3rd to indicate whether the airflow of ventilation is ON or OFF and 4th to indicate the position of the microwave generator to plasma or catalytic reactor.

Digital inputs: Digital inputs are used to get the system status from the control cabinet and to read the valve state indicators. The signals are read out in the FPGA and then processed by the digital input subsystem. The result is transmitted through the notifier 'DI_Signals.' The system state is determined using the elements mentioned in **Table 2.3**. The inputs for 'Emergency stop' and 'Alarm' can overrule the other inputs. So if DI 0 switches to a low state then the state of the other inputs are ignored. In 'Emergency stop' and 'Alarm' states, all set points are set back to zero, and the gas supply valves are closed. It is essential to use the buttons on the control cabinet first, as shown in **Fig. 2.9**, to switch from the neutral state to the catalytic state. When this selection is made, the valves connecting the setup (V-124, V-314, V-315) get open.

Table 2.3: Digital input states and resulting system states.
L is a low signal, H high signal.

DI	0	1	2	3	State
	L				Emergency stop
				L	Alarm
		L	L		Alarm
		H	H		Neutral
		L	H		Plasma
		H	L		Catalytic

2.8. Reactor operating procedure and safety

2.8.1. Experimental start-up procedure

To work safely and avoid manual errors, a standard methodology to work with the reactor was developed. The methodology comprises the steps below that are carried out in the given order (i.e., stepping from the first to the last bullet point):

- Fill in the quartz tube reactor with the desired amount of catalyst and introduce it inside MRA.
- Connect inlet and outlet line Swagelok connections.
- Insert thermocouples to the top and bottom part of the catalytic bed (the thermocouples should not be placed inside the MRA to avoid interaction with MW).
- Set the thermal camera position such that it focuses on the catalytic bed inside the MRA for collecting thermal images during experiments.
- Check the ventilation flow switch indicator.
- Set the flow rates for thermostats 1 and 2 at the required temperatures and start both thermostat flows.
- Do leak tests at inlet and outlet connections under N_2 flow with a trace detector before sending reactant gases.
- Connect the MW generator to MRA using a coaxial cable. Open the source valves of the carrier and reactant gases lines from the main gas line supply.

- Turn on the control unit for mass flow controllers and pneumatic valves from the LabVIEW interface. Check whether all thermocouples and thermal camera are connected or not to the temperature control system and thermal camera software.
- Close the enclosure while performing the reaction experiment and switch on the microwave survey meter to check for microwave leakage during experiments.
- Start the Mini-Flow 200SS and first set the minimum power to check the heating behavior of the catalytic material. Increase MW power as per the temperature response of the material. Test the heating behavior of the catalyst up to 1000 °C. Bring back the temperature to the required level by tuning power and feed the reactant gases.
- Record gas-solid temperature differences when the reactant gases flow through the catalytic bed. Try to maintain temperature with varying power. Note down forward and reflected power for each temperature interval. Feed a small amount of sample to GWB2 and then to micro GC for product gas analysis. Maintain ~15-20 ml/min flow towards GC with the help of the manual ball valve V313 and direct the rest of the product gas to ventilation. Monitor pressure on PRI301; it will increase in the case of catalyst sintering or block of inlet flow due to excessive coke formation. If the reactor pressure reaches ~2 bar, then the reactant gas flow will be automatically stopped by the reactor control system in order to avoid quartz tube damage. Thermocouple values, gas flow values towards GC and forward and reflected MW powers should continuously be recorded in the log book while performing the MW experiments.

2.8.2. Shut down procedure

After finishing a MW experiment, it is imperative to shut off the entire MW reactor system properly. This comprises the following steps:

- The first essential thing is to shut down the microwave generator in case of MW heating and the furnace in case of conventional heating experiments and allow the reactors to cool down naturally under N_2 flow and coolant flow.
- Set the temperature of the furnace to ambient and allow it to cool down.
- Set the flow of reactant gases to zero and allow only N_2 to flow through the reactor until it reaches room temperature. Switch off both thermostats after the system is at room temperature.
- Save a) thermal videos to a self-viewing file format for post-processing; b) LabVIEW login data files to retrieve thermocouple temperature values; c) GC data in drive folder.
- Disconnect the camera from its software and then remove it.
- Set N_2 flow to zero and turn off the control system for the mass flow controller and evaporator. Keep GC for conditioning overnight to clean the GC columns. If all necessary experiments have been performed, then remove the quartz tube and unload the catalyst. Always keep the enclosure closed when the set up is not in use.

2.9. Summary and recommendations for further improvement

In this project, we have designed and developed a microwave reactor assembly (MRA) and built a new microwave reactor setup. We have successfully verified that the MRA can effectively heat several catalytic materials up to high temperatures (1000 ^{o}C) and be used to carry out relevant heterogeneous catalytic reactions, such as methane dry reforming that has experimentally been studied in this project. The MRA can provide concentrated microwave energy to the catalytic bed leading to >95% energy utilization efficiency and minimization of wasted MW energy. The provision to measure or monitor temperature with the help of a thermal camera provides a better understanding of the temperature changes inside the catalytic bed. In particular, the thermal camera helps detect hotspot formation during MW heating, or chemical reaction experiments in the static microwave-heated fixed bed quartz tube reactor. This approach allows for adjustment of the microwave power input to avoid reactor damage due to thermal runaway. However, it is sometimes difficult to manually control uneven heat or temperature distribution inside the catalytic bed. Therefore, devising an automated temperature-to-power control system for the existing reactor is recommended for future projects. It will also be useful to develop a parallel technique, which will record thermocouple temperatures and input them to the thermal camera calculator that will instantly update the emissivity value according to the actual thermocouple temperature; this will, in turn, enable the immediate update of the 2D temperature distribution inside the reactor in the course of the experiment. Finally, during the experimental work, it was observed that not all materials could be effectively heated in this reactor, as different materials have different dielectric properties. Therefore replacing the existing MW generator with a higher power MW generator could be helpful to heat up the weakly MW absorbing materials.

3

3. Complexity and challenges in non-contact high-temperature measurements in microwave-assisted catalytic reactors

This Chapter is published as:

Lalit S. Gangurde, Guido S.J. Sturm, Tushar J. Devadiga, A. I. Stankiewicz, Georgios Stefanidis, Complexity and challenges in non-contact high-temperature measurements in microwave-assisted catalytic reactors, Industrial and Engineering Chemistry Research, 56 (45), 13379–13391, 2017.

Abstract

The complexity and challenges in non-contact temperature measurements inside microwave-heated catalytic reactors are presented in this chapter. A custom-designed microwave cavity has been used to focus the microwave field on the catalyst and enable monitoring of the temperature field in 2D. A methodology to study the temperature distribution in the catalytic bed by using a thermal camera in combination with a thermocouple for a heterogeneous catalytic reaction (methane dry reforming) under microwave heating has been demonstrated. The effect of various variables that affect the accuracy of temperature recordings are discussed in detail. The necessity of having at least one contact sensor, such as a thermocouple, or some other microwave transparent sensor, is recommended to keep track of the temperature changes occurring in the catalytic bed during the reaction under microwave heating.

Graphical Abstract:

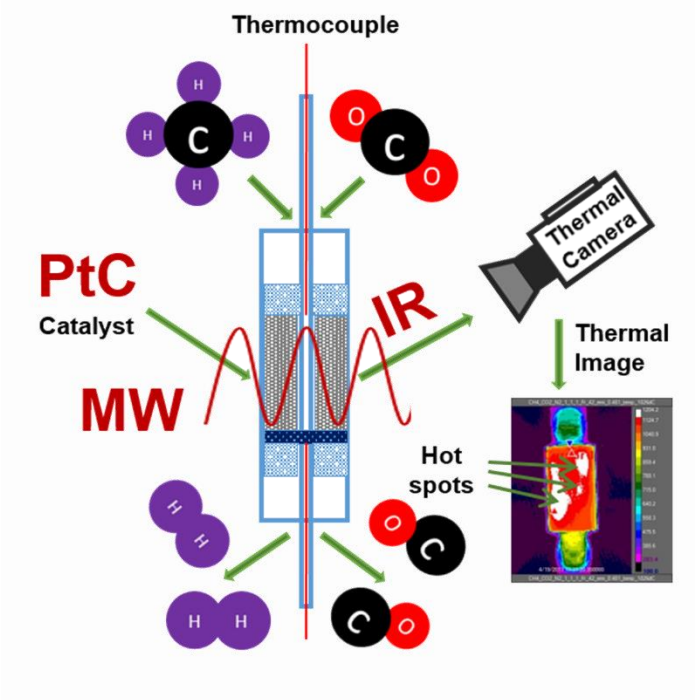

3.1. Introduction

The history of microwave (MW) technology confirms its rapid development after the thermal effects of microwave heating were discovered in the 1940s [55][56]. Since then microwave heating has been applied to food processing, polymer processing, plasma processing, organic chemistry, sintering of metals, inorganic material synthesis and various industrial and research applications. Microwave heating in catalytic material synthesis, multiphase catalysis like gas-solid and solid-liquid reactions, has shown performance improvements as compared to conventional heating mode, due to its rapid, selective and volumetric nature [23][29][30]. Along with its thermal effects, non-thermal microwave effects have also been reported to be responsible for increased catalytic activities resulting in overall improved process performance [30]. In some works, energy consumption measurements of microwave heated processes have shown that lower energy consumption and higher heating rates are obtained compared to conventionally heated processes [57][58]. Recent developments in the wind, solar, plasma and microwave technologies have shown the importance of microwave energy as a renewable, clean and exergetically efficient form of energy [59][60].

To use microwave energy efficiently for any chemical process requires a good understanding of process parameters and knowledge of materials response under their exposure to microwaves. Dielectric properties measurements provide insight into the heating ability of any material under microwave exposure [61][62]. The dielectric properties of any material or fluid are described by their complex permittivity (ε*). The complex permittivity (ε*) is divided into two parts; a) the dielectric constant (ε'), or real part of the dielectric permittivity, represents the ability of the material to store electric energy in its structure; b) the loss factor (ε''), or imaginary part of the dielectric permittivity, indicates the ability of the material to dissipate the stored electric energy in the form of heat. The ratio of the loss factor to the dielectric constant is called loss tangent (tan δ). Along with dielectric properties, the physics of electromagnetism involved during MW heating, the wave nature of microwave field and its high degree of control are also essential to consider [63]. Therefore, it is important to know the dielectric properties of catalytic materials, preferably in the real reaction conditions, or at least in the expected temperature range of the catalytic application.

Horikoshi et al. reported generation of hot spots (electric discharges) and their impact on heterogeneous Suzuki-Miyaura coupling reaction for the synthesis of 4-methylbiphenyl in toluene solvent in the presence of Pd/AC catalyst [64]. Zhang et al. studied microwave assisted sulfur dioxide reduction using methane over MoS_2 catalyst and reported that the enhanced reaction performance was a result of hotspot generation within the catalyst itself [65]. To generalize, non-uniform microwave and hot spots formation at particle or reactor scale frequently determine reactor performance. Hence, it is important to track these temperature patterns experimentally.

The major technical challenge for a detailed investigation of temperature distribution is the unsuitability of conventional methods and their limitations in measuring temperature under microwave heating. The tutorial review on temperature measurement in microwave-heated transformations, by Kappe, reports that accurate temperature measurement in microwave heated system is a complex and non-trivial affair [66]. The review is concerned with external temperature measurements and reports that surface measurements will always be problematic and will not adequately record temperature variations inside the reactor, although proper calibration for non-contact methods might provide realistic approximate temperature values. In the earlier work of our group, fiber optic sensors were used to record temperature non-uniformities in solid catalytic beds in the axial and radial directions [43][44]. Significant temperature gradients were found in a small amount of sample heated in a mono-mode cavity. Recently, in the Ramirez group, a dual temperature measurement method of thermography combined with optical fiber was developed to investigate gas-solid temperature differences in a low-temperature range (100 to 250 °C), under microwave heating [67][68]. In this method, the importance of corrected emissivity values to get accurate thermographic temperature readings from a thermal camera was demonstrated. These findings, however, were obtained in the low-temperature range (0 to 300 °C), where common optical fibers can be used. As optical fibers cannot be used above 300 °C, reliable temperature measurements under microwave heating above 300 °C becomes a major technical challenge to resolve.

A literature study reveals a confusion regarding the direct use of metallic thermocouples in microwave reactions. Pert et al. reported that the presence of thermocouples in microwave reactors can locally distort the electromagnetic field, induce thermal instabilities and lead to serious measurement errors [69]. Will et al. quickly inserted a thermocouple inside the catalytic bed when MW was turned off, to avoid thermocouple-microwave interaction resulting in sparks [70]. In contrast, Li et al. directly used a thermocouple under microwave heating for methane mixed reforming [71]. They reported that the interaction of the thermocouple with microwaves could be avoided by placing it in a 1-mm-thick quartz tube. Quartz, however, would theoretically not be expected to shield a microwave field in this case, since its relative permittivity is 3.78–0.001i, which is not nearly sufficient to attenuate a microwave field over 1 mm distance.

Overall, direct use of a thermocouple inside a microwave reactor is risky, but its placement at the position where it would not come in contact with microwaves is a better experimental approach. Nonetheless, detection of hot spots and thermal gradients inside catalytic reactors are difficult to measure with this approach. Previous simulation studies done in our group show that local geometric and/or operating parameter variation at one point affects the microwave field over the entire volume in a microwave coupled system [72]. Temperature measurement at one point inside the reactor is insufficient in heterogeneous catalytic processes [43]. Therefore, an approach for simultaneous temperature measurements inside a reactor and on the reactor wall needs to be developed for high-temperature microwave-heated reactors.

The aim in this work is to develop such an approach for heterogeneous catalytic reactions occurring under microwave heating in the range 300 to 1000 °C. The methane dry reforming ($CH_4 + CO_2 \leftrightarrow 2H_2 + 2CO$) reaction is taken as an illustrative example to study temperature distribution in the catalytic bed under microwave heating. First, dielectric properties of 10 wt. % loading of platinum on an activated carbon support (PtC) from room temperature to 850 °C are measured. A tailored microwave cavity has been constructed and used to focus the microwave field on the loaded reactor and collect thermal data in a 2D fashion. The factors affecting the thermal measurements are explained and demonstrated by means of an approach combining the use of a thermal camera and simultaneous thermocouple measurements. The existence of hot spots and their dislocations due to different gas environments under MW heating are shown. Thermal gradient differences in axial and radial positions in the catalytic bed are explained using thermal data post-processing.

3.2. Experimental Section

3.2.1. Schematic diagram of the microwave reactor

A schematic diagram of the microwave reactor system is shown in **Fig. 3.1**. The most important parts of this schematic are the custom-designed microwave reactor and quartz tube for the catalyst loading. The LabVIEW interface along with an NI-9074 cRIO controller is used to control the setup operation and perform data acquisition. The controller interfaces with valve status readouts, mass-flow controllers (Bronkhorst) to regulate gas flows, pressure sensor, and N-type thermocouples. For non-contact temperature measurements, the thermal camera model FLIR A655sc is used. It operates in the 7.5 – 14 μm spectral range and measures temperature from –40 to 2000 °C. Thermal data from the experiments was collected via a PC using the FLIR ResearchIR Max software. A solid-state microwave generator (SAIREM Miniflow 200 SS) is used to supply the MW energy at 2.45 GHz. The maximum available power is 200W.

A condenser is added at the exit of the reactor to avoid condensation in the ventilation line and the line towards the GC. Two thermostats are used to pump the coolant as a mixture of ethylene glycol and water at a ratio of 2:1 (EG: H_2O). One is used to maintain the gas wash bottle temperature at –8 °C. The second one maintains the MW cavity and condenser temperature at +8 °C. The gas wash bottle is filled with CaO, as adsorption agent, to dewater the remaining moisture in the outlet gas line. A Whatman FP050/1 filter holder with 50 mm filter paper and Genie membrane are placed after the gas wash bottle to avoid any impurities towards the chromatogram. A Varian CP4900 micro-GC is used for product gas analysis. It is equipped with a TCD detector. It uses two columns, 20 m MS5A and 10 m PPU, for analysis. The LabVIEW interface, the μGC software, and the thermal camera software were controlled by separate computers connected to one screen using a KVM switch.

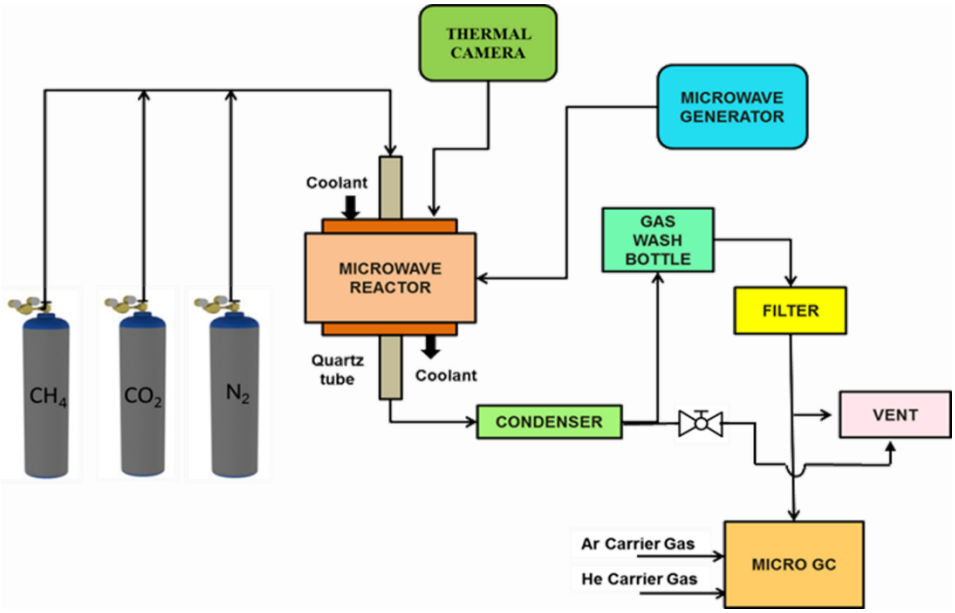

Figure 3.1 Schematic diagram of the microwave reactor setup

3.2.2. Catalyst loading for microwave heating

A quartz tube with a length of 290 mm, 1 mm wall thickness, 10 mm outer diameter and 8 mm internal diameter was used for all heating and reaction experiments. Neoptix optical fibers (–80 to 250 °C) were used for low temperature (<150 °C) calibration and for verification of the temperature distribution from the center to the inner wall of the catalytic reactor up to 150 °C, as thermocouples cannot be inserted inside the catalytic bed under microwave exposure. Two N-type thermocouples (–200 to +1250 °C) with a 0.5 mm diameter were used for high-temperature measurements. Specifically, the thermocouples were placed at the top and bottom part of the catalytic bed (**Fig. 3.2a**) to avoid MW-thermocouple interaction during MW heating.

Fig 3.2a shows a schematic diagram of catalyst and thermocouple positions in a quartz tube. Initially, ~1000 mg of powdered PtC catalyst was pressed at 20 kg/cm^2 to make a pellet. The pellet was broken again to make sieves in a size range of 75-112 µm. The sieved powder was heated in an electric oven at 140 °C for 3 h to remove its moisture content. As shown in **Fig 3.2a**, first a quartz wool plug was fixed in the quartz tube. Then, a quartz P3 frit (thickness 1.5 mm, diameter 7.9 mm and pore size 40-60µm) was placed on top of it. The purpose of adding the frit is to keep the ceramic well (99.8% dense alumina, o.d.= 3 mm and i.d.= 2 mm) position at the center of the quartz tube. The ceramic well was used to protect the thermocouple and to prevent its interaction with the microwave field. As shown in **Fig 3.2a**, 500 mg catalyst was loaded above the frit and equally distributed around the ceramic well. It was then tapped to maintain the bed compactness, and another quartz wool layer was added on the top to retain bed compactness. The reactor tube was then placed in the microwave cavity. The required thermocouple lengths to monitor the top

and bottom position of the catalytic bed were already measured and then inserted into the ceramic well to avoid microwave–thermocouple interaction.

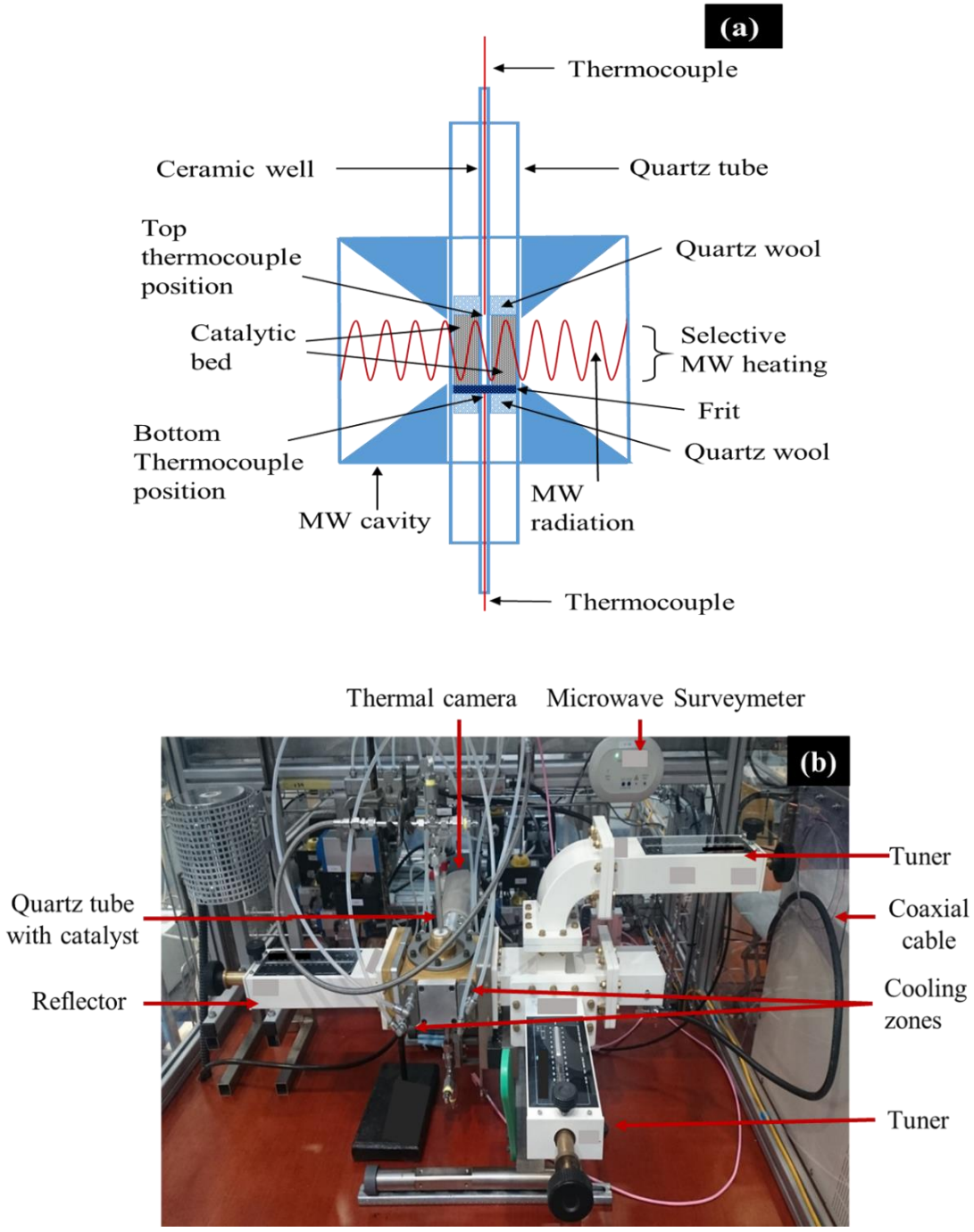

Figure 3.2 (a) Schematic diagram of catalyst and thermocouple positions in the quartz tube, (b) Digital image of the custom-designed MW reactor with a quartz tube inside.

3.2.3. Thermal camera working principle

The main advantages of non-contact infrared thermal cameras are their speed and their ability to measure in broad temperature ranges. As a non-contact measurement technique, the thermal camera detector does not measure temperature directly; it calculates the temperature using the Stefan-Boltzmann law and the emissivity value of the object or area of interest. The emissivity (ε) is a measure of an objects ability to emit infrared radiation. **Eq. 3.1** describes the relation between irradiation flux, temperature and emissivity value [67].

$$J = \varepsilon.\sigma.T^4 \qquad (\mathbf{3.1})$$

Where, J is the irradiance flux,
ε is the emissivity,
σ is Stefan-Boltzmann constant ($5.6\times10^{-8}m^{-2}K^{-4}$).

The emissivity change with temperature is a primary source of error in temperature measurements [73]. The emissivity also gets affected by structural or physical changes in the materials [74]. Inaccurate estimation of emissivity using table values incorrectly can also result in significant temperature measurement errors [75]. The emissivity of quartz glass has been reported to decrease with increasing temperature [76], and the emissivity of metals or metallic powders increases parabolically with temperature [73]. The extraction of accurate temperatures using a thermal camera is not possible without corrected emissivity of the heated load [75].

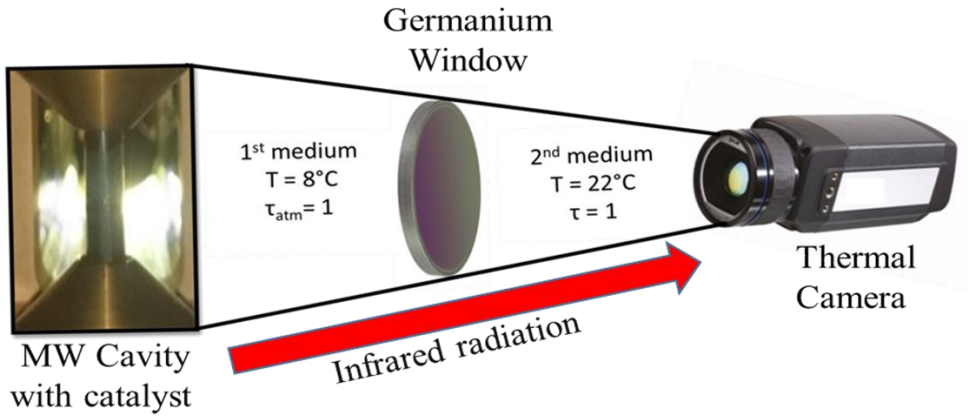

Figure 3.3 Schematic representation of the different media affecting the irradiance flux before reaching to the thermal camera (where T is the temperature and τ is the transmittance)

In our case, the heated load (catalytic reactor) is a combination of Pt, carbon and quartz tube of 1 mm thickness. As shown in **Fig. 3.3**, the infrared radiation of the catalytic bed has to travel through different mediums and through the germanium window from the microwave cavity to the camera detector. Therefore, it is imperative to consider medium changes during the emissivity calculation

procedure to ensure its correct value. Overall, in our case, infrared radiation received by the thermal camera gets affected by (1) the microwave field distribution in the catalyst bed, (2) changes in transmittance of the quartz tube, (3) the microwave cavity wall temperature (8 °C) as a first medium, (4) the anti-reflected coated germanium window and (5) the conditions of external atmospheric (22 °C), as a second medium. As the cavity wall to quartz tube distance is ~70 mm, the average temperature inside the cavity during microwave heating is expected to be higher than its wall temperature (8 °C) even with the application of cooling. However, in our case, the actual target temperature, as measured by the inside thermocouple, is provided to the camera software, which then automatically adjusts the apparent emissivity value according to the actual temperature given; therefore, the apparent emissivity value calculated is not affected by the temperature gradient outside the reactor.

3.2.4. Dry reforming reaction testing procedure under microwave heating

It is difficult to control and provide MW energy when the selective heating behavior of a complex catalytic system is unknown. Hence, first, a MW heating test under real reaction conditions was performed by increasing power from 0 to 200 W. From this heating test and reaction performance evaluation, 150 W of MW power was found to give the maximum reactants conversions for the PtC catalyst used. Therefore, we performed methane dry reforming at 150 W, 34 ml/min total reactant gas flow at 1:1 volume ratio of CH_4:CO_2 and atmospheric pressure. Once the catalyst reached a stable temperature under N_2 flow with 150 W, methane and carbon dioxide reactant gases were fed to the reactor. After 1000 s of MW heating time, the product gases were repetitively analyzed by the chromatogram (GC) every 400 s of reaction time intervals to evaluate the reaction progress.

3.3. Results and Discussion

3.3.1. Dielectric properties of catalyst measured at high temperature

Dielectric properties of 10 wt. % Platinum on carbon (PtC) were measured in specially designed equipment at the ITACA Institute of Valencia University, Spain. The methodologies mentioned in the refs [77] and [78] have been followed for the measurements. The PtC sample was placed in a quartz tube, which was located inside the specially designed setup. The dielectric properties were measured while simultaneously the sample was heated at 20 °C/min under N_2 atmosphere. The used methodology is based on the shift of the center resonant frequency and the alteration of the quality factor of the microwave cavity in the presence of PtC catalyst as compared to the empty cavity. The measurements were done in the range 20–850 °C. The accuracy of dielectric measurements was estimated as 3% for the dielectric constant and 10% for the loss factor in the entire measured range.

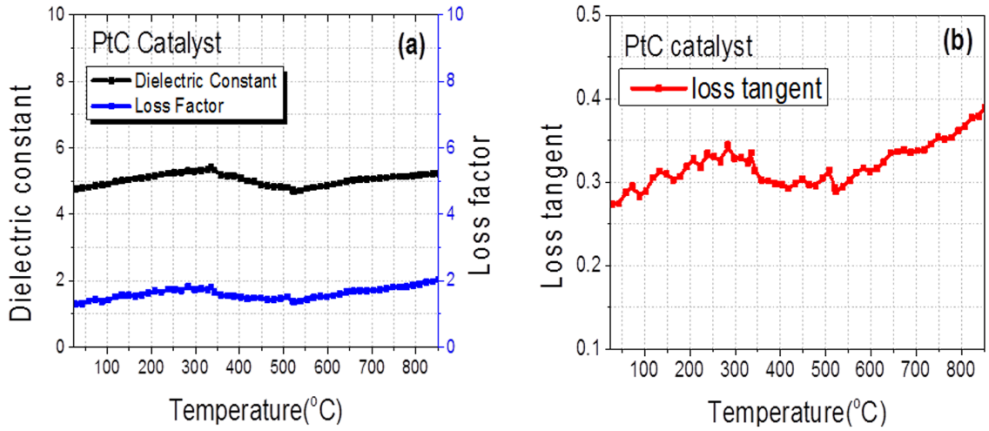

Figure 3.4 (a) Dielectric constant (ε') and loss factor (ε'') vs temperature. (b) Loss tangent (δ) vs temperature.

Three cycles of heating up to 850 °C with a heating rate of 20 °C/min followed by natural cooling using 0.507 g of PtC catalyst were performed. The evolution of the dielectric properties of the catalyst with temperature in the third cycle is shown in **Fig. 3.4**. **Fig. 3.4a** and **b** show that the materials dielectric properties have an overall increasing trend in the examined temperature range, but this trend is not monotonic.

The pre-processing or pre-heating of some materials may result in a change of their physical or chemical properties, e.g., density, which can also affect their dielectric properties. The observed decrease in the dielectric properties values at 360–375 °C is due to sample volume reduction as shown in **Fig. 3.13**(supporting information). This volume reduction could be attributed to moisture removal, and the shrinking of the material occurred during the heating up to 850 °C. The possibility of sample reduction due to moisture removal was not expected to happen after the first measurement cycle, as the sample tube was not open to absorb water before the second and third cycles. Therefore, volume reduction in the second and third cycles was majorly due to shrinking of the sample, which is responsible for the density change of the material and hence of the dielectric properties in the temperature range 360–375 °C. However, the effect of platinum might be predominant at temperatures higher than 600 °C, which results in increasing dielectric property values at temperatures above 600 ºC.

3.3.2. Radial temperature and emissivity differences by optical fibers

As thermocouples cannot be inserted directly inside the microwave field, we performed low temperature heating tests using optical fibers to calculate emissivities at the center and inner wall optical fiber positions. **Fig. 3.5a** shows the catalyst loaded quartz tube that is placed inside the microwave cavity along with two optical fibers kept in glass capillaries. The first sensor is placed at the center of the reactor and the second one at the inner wall of the quartz tube. Optical fiber 1

was directly connected to a microwave generator to limit the microwave heating in the workable temperature range of the optical fibers. Optical fiber 2 was connected to a nomad touch optical thermometer to record its thermal response.

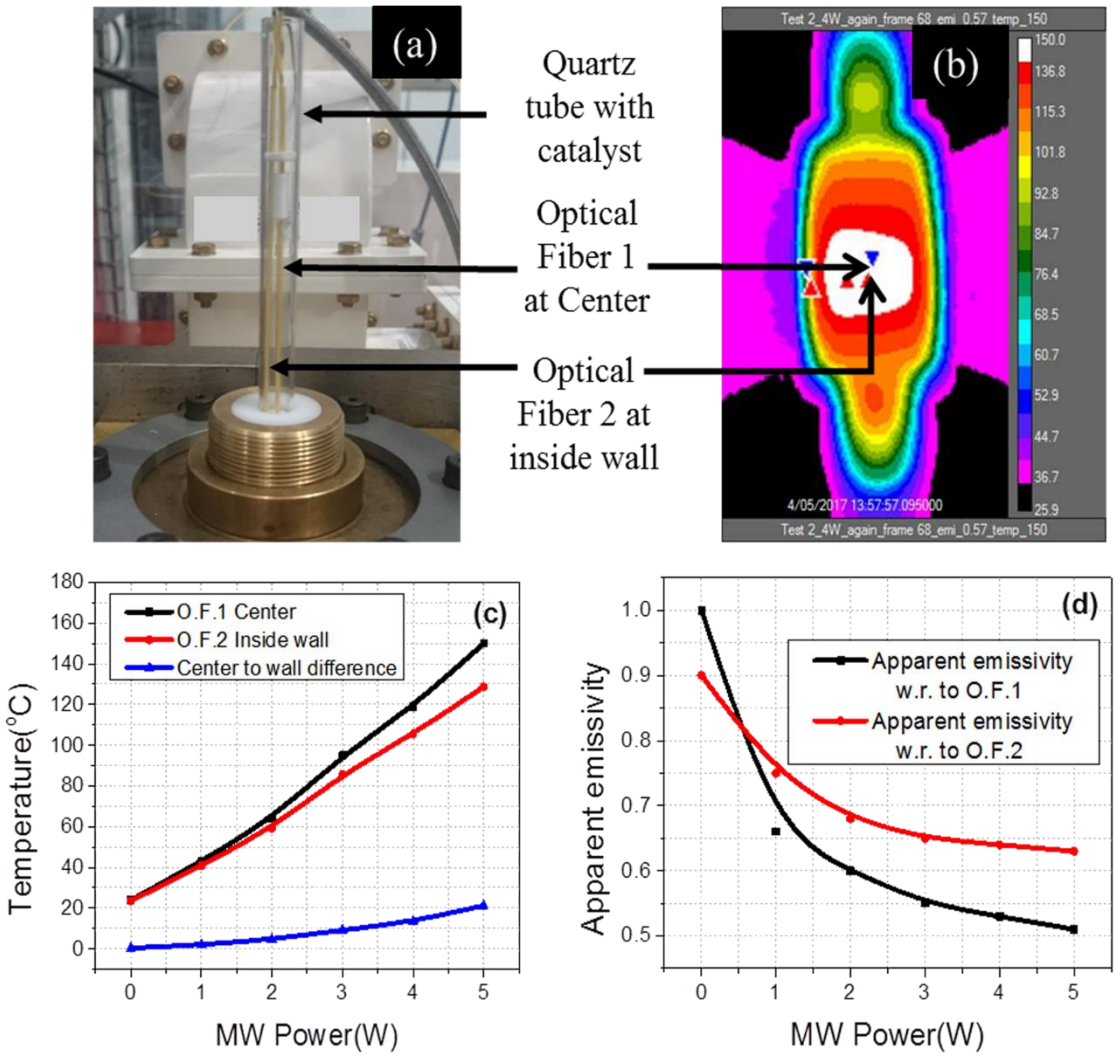

Figure 3.5 (a) Digital image of a quartz tube inserted in MW cavity along with two optical fibers. (b) Thermal image showing the points where emissivity was calculated with reference to optical fibers. (c) Temperatures and temperature difference measured by the two optical fibers. (d) Emissivity calculated with reference to optical fibers' temperature.

The catalytic bed was heated from 1 to 5 W of MW power without any gas flow as shown in **Fig. 3.5c**. The thermal videos were recorded for 120 s with a recording rate of 1 frame per second after a stable temperature was achieved at the supplied power. The emissivity at the optical fiber positions at the inner side of the wall and at the center was calculated with an inbuilt calculator of camera software. The cursor of the 3×3 pixel was placed at the locations shown in the thermal image of **Fig. 3.5b**. A quartz tube to camera distance of 0.3 m was considered along with actual temperature values to calculate the emissivity. Other settings, shown in **Fig. 3.3**, for the first

medium cavity environment; (temperature 8 °C, 100% transmittance), second medium (air at temperature 22 °C, 100% transmittance) and germanium window (temperature of 22 °C, 96% transmittance) were also adjusted in the camera software aside from the calculation of emissivity.

As shown in the emissivity graphs of **Fig. 3.5c** and **d**, the emissivity values at the center optical fiber 1 and at the inside wall optical fiber 2 can help obtain the direct center-to-inner surface temperature differences at the same quartz surface location. **Fig. 3.5d** clearly shows a decreasing trend of emissivity with an increase in temperature in both the center and surface cases. The emissivity value at the center is observed to be lower than the inside wall emissivity as temperature increases. These low-temperature heating experiments showed that center temperature emissivity and inside wall emissivity are very helpful to finding the radial temperature differences. **Fig. 3.5c** clearly shows that as the temperature inside the catalytic bed increases, the center-to-inner wall temperature difference also increases. The temperature measurement just at the surface of the catalytic bed will provide a lower temperature value than the actual center temperature value. Therefore, a thermal camera or any other IR measuring system should be directly calibrated with respect to a center temperature sensor, or a surface temperature sensor, to ensure the accuracy of the apparent emissivity at the respective point.

3.3.3. Effect of camera range and heating system used

The thermal camera has three different ranges to measure temperature. These temperature ranges have shown some influence on the emissivity calculations. Therefore, a separate heating experiment for each range was performed, and the emissivity was calculated accordingly. To ensure the accuracy of thermocouple temperature measurement, a heating test was done by placing a thermocouple and an optical fiber together at the top part of the catalytic bed. Heating was performed without N_2 gas flow. The temperatures shown by both sensors were very close to each other as shown in **Table 3.1**(supporting information). This test also confirmed that microwaves do not interact with the thermocouple during heating. To study the effect of camera range, the catalytic material was microwave-heated in the temperature range 120-140 °C for 60 min under a N_2 flow of 34 ml/min to remove the moisture absorbed during the loading procedure. After this initial heating for 60 min, the MW generator was switched OFF, and the system was allowed to cool down to room temperature. Once the system reached a stable room temperature, temperature measurement with the thermocouple and thermal frame capturing were started, and recording was done every 120 s to collect data simultaneously after MW was ON until the end of the MW heating experiment. The MW generator was switched ON with a power of 1 W increase per 120 s for the first (–40 to 150 °C) range of data collection and increased 5 W per 120 s for the second (100 to 650 °C) and third (300 to 2000 °C) ranges of data collection. During post-processing of thermal data, the emissivity was calculated for each range with reference to the actual inside temperature shown by a thermocouple.

Fig. 3.6 compares the effect of camera range on emissivity values in microwave heating. **Fig. 3. 6a** shows that in the first range of –40 to 150 °C, emissivity changes from 0.97 at 25 °C to 0.41 at 140 °C. **Fig. 3.6b** shows that in the second range 100 to 650 °C, emissivity decreases from 0.41 at 134 °C to 0.24 at 630 °C. In the third temperature range of 300 to 2000 °C, emissivity starts from a very low value of 0.16 at 390 °C and reaches a local maximum of ~0.22 at ~575 °C; then it remains ~0.2 up to 850 °C and finally increases monotonically up to 0.29 at 1000 °C.

As thermal cameras are factory calibrated for particular ranges, it is imperative to use them in their specified ranges only. The selection of suitable camera range as per temperature of interest, e.g., 600 to 1000 °C for dry reforming of methane, suggests that the third camera range is suitable. Therefore, while comparing experimental results, use of the same camera range can minimize the error due to different camera ranges as shown in **Fig. 3.6e** in 300–600 °C common scale. Two different ranges have different color or scale bars, which again creates a problem for visual comparison. In addition, hot spots that may be occurring at higher temperatures than the maximum limit of the camera range, during MW heating, may form another reason for inaccuracies in temperature calculation.

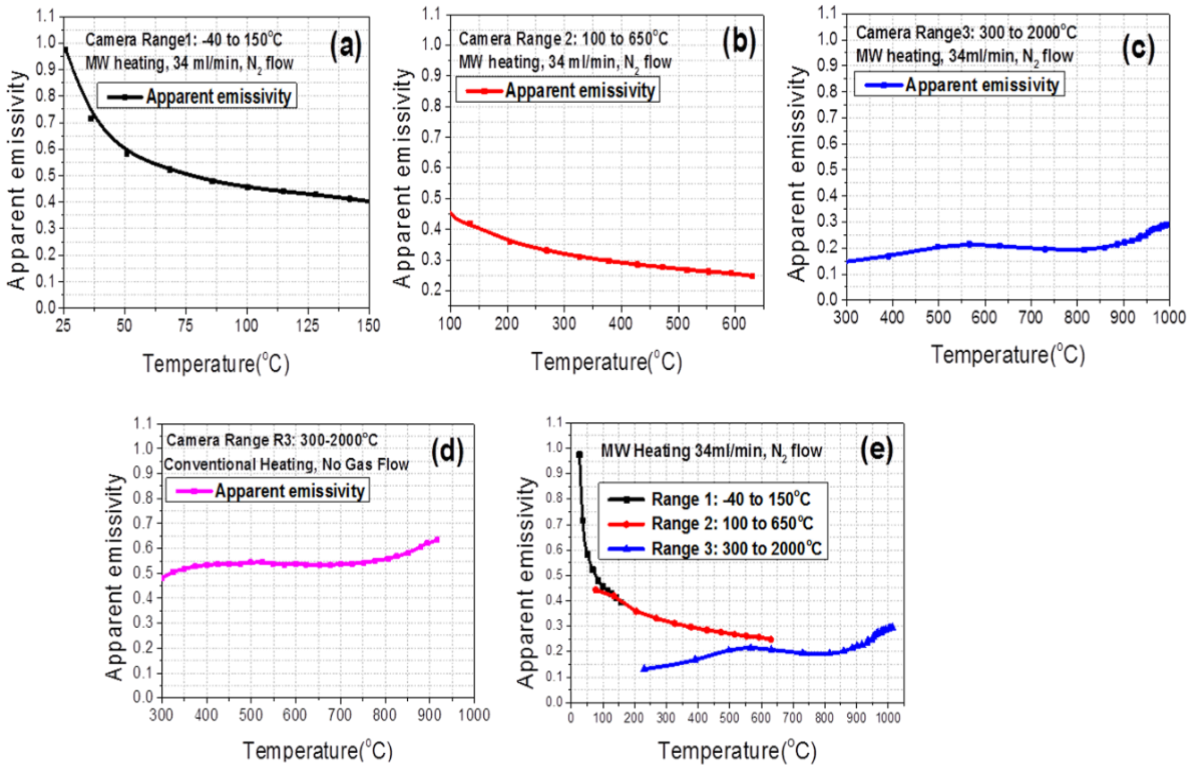

Figure 3.6 Effect of camera range and heating mode on emissivity. (a) First camera range (–40 to 150°C), (b) second camera range (100–650 °C), (c) Third camera range (300–2000 °C) (d) Emissivity calculated in conventional heating with the third camera range (300–2000 °C) and (e) Three camera ranges together.

Comparison of **Fig. 3.6b** and **c** on a common temperature interval 300–650 °C shows a clear effect of the camera range on the emissivity and temperature values. For example, the emissivity values

of 0.24 and 0.21 at 630 °C in the second (**Fig. 3.6b**) and third (**Fig. 3.6c**) range, respectively, show the clear effect of different camera range settings used on the temperature recordings. Specifically, if an emissivity value of 0.24 from the second range is used in the third temperature measurement range, then it matches with a thermocouple reading only at 948 °C. Therefore, use of a suitable thermal camera range for the required working temperature is necessary in order to have a fair comparison of heating patterns, or to study the influence of other parameters on temperature or heating patterns.

Another interesting aspect is the influence of the heating system on emissivity values. **Fig. 3.6d** shows the graph of emissivity measurements done in conventional heating using the tubular furnace (digital image shown in supporting information, **Fig. 3.14**) without N_2 flow. In this heating experiment, a quartz tube, with catalyst sandwiched between quartz wool plugs, along with a thermocouple at the center of the catalytic bed was placed in a tubular furnace. The loaded tube was heated up to 970 °C (the upper-temperature limit of the furnace is 1000 °C). After getting stable temperature values, the thermocouple and thermal camera recording were started. The tube along with the thermocouple was pulled out from the bottom side of the furnace until the catalytic bed was visible to record the thermal video (see **Fig. 3.14**). The quartz tube to thermal camera distance was also kept at 0.3 m in the conventional heating experiment. The emissivity values were calculated in the same manner as mentioned before from 300 to 900 °C.

It is clear in the case of conventional heating (**Fig. 3.6d**) that emissivity varies with an increase in temperature and stays in the range from 0.48 to 0.63 for the 300–900 °C temperature range. In the case of microwave heating, it stays with its lower value of 0.16 to 0.22 only for the 300 to 900 °C range and shows a fast increasing trend up to 1000 °C, where it becomes 0.29. The increased value of emissivity obtained by the conventional heating system explains the reasons behind the decreased emissivity in the microwave heating system. The first reason is the N_2 flow that removes heat from the catalytic bed, and the second reason is the medium through which the irradiance has to pass to reach the thermal camera.

This comparative study has also suggested that if the emissivity calibration is done in conventional heating with different conditions and the values obtained are used for microwave heating experiments, then these values will be unable to provide accurate temperature values during microwave heating experiments. Therefore, in-situ emissivity calculations under microwave heating are necessary for non-contact temperature measurement techniques using IR cameras.

3.3.4. Effect of gases on emissivity and detection of hot spots

It has been reported that the presence of different gases and reactions in the catalytic material influences the emitted infrared radiation [67], and eventually affects the apparent emissivity. Gases

such as CO, CO_2, CH_4, H_2, N_2 and other hydrocarbons have significant absorption bands due to their vibrational and rotational motions in the infrared range. As methane dry reforming involves most of the gases mentioned above, the emissivity calculated in N_2 flow is not applicable to detect the temperature changes occurring during the reaction. Therefore, we studied the influence of separate reactants and their possible combinations on emissivity under actual reaction conditions until 1000 °C.

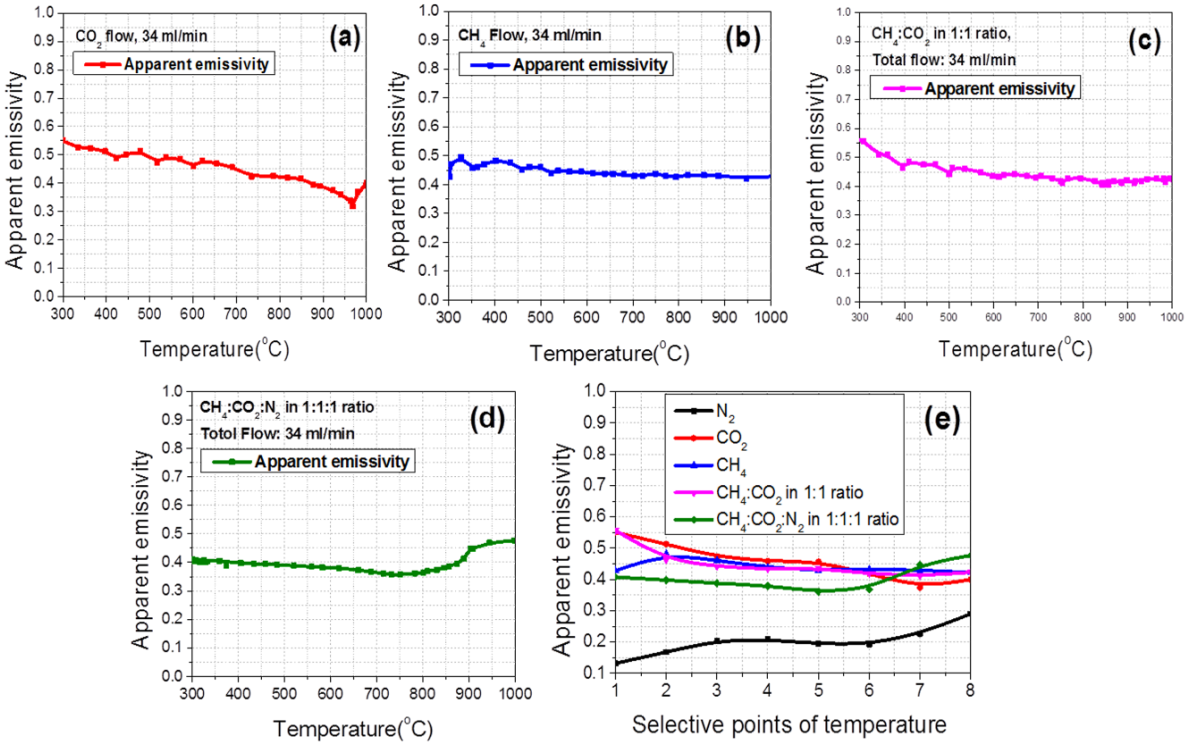

Figure 3.7 Effect of different gases on emissivity. (a) CO_2, (b) CH_4, (c) CH_4:CO_2 at 1:1 flow ratio, (d) CH_4:CO_2:N_2 in 1:1:1 flow ratio, and (e) comparison of emissivities under different gas flows (see Table 3.2).

Fig. 3.7 shows the effect of different gas flows on emissivity values. **Fig. 3.7a** shows the apparent emissivity in CO_2 gas flow. It shows that the emissivity value is 0.55 at 300 °C and gradually decreases with increasing temperature. **Fig. 3.7b** shows a lower emissivity value of 0.42 in CH_4 flow as compared to CO_2 flow at 300 °C. The emissivity under CH_4 flow shows some fluctuations up to 562 °C, and then it slightly decreases and remains 0.42 up to 946 °C. **Fig. 3.7c** shows the emissivity for a combination of CO_2 and CH_4 at 1:1 ratio in total flow. Emissivity is 0.55 at 300 °C; then it decreases to 0.44 at 571 °C with some fluctuations, and eventually reaches a seemingly plateau value of 0.42 at 1000 °C. **Fig. 3.7d** shows the effect of the combination of CO_2: CH_4: N_2 flow, at a 1:1:1 ratio, on the emissivity. The emissivity in this case is 0.4 at 300 °C; it decreases gradually up to 0.35 around 731 °C and then increases up to 0.47 at 998 °C. **Fig. 3.7e** shows a direct comparison of the emissivity calculated under different gas flows. As a comparison at precise temperatures is not possible in our case, some selective points from each test are taken to show

direct comparison (values are given in **Table 3.2** of supporting information). This comparison reveals that there are no big differences in the apparent emissivities under CO_2 and CH_4 flow. However, the emissivity under CO_2 flow has higher values among all tested gases up to 690.35 °C. The decrease in the emissivity of CO_2 past 690.35 °C is due to migration of hot spots in the catalytic bed. A continuous fluctuation in the apparent emissivities is observed due to the continuous migration of the hot spots during the experiments shown in **Fig. 3.7e**. Aside from the different heat removal properties of different gases, another possible reason for the different emissivity values under pure and combined gas conditions could be the change in the total dielectric properties of the catalytic material due to pyrolytic carbon formation or direct structural changes in catalytic materials.

The different trends of the gas emissivity lines at high temperatures, past point 6 in **Fig. 3.7e**, may be due to dissociation of reactant gases and the formation of product gases, which would affect the resultant irradiation flux. This comparison confirms that using only N_2 flow values will provide inaccurate information on temperature changes inside the bed.

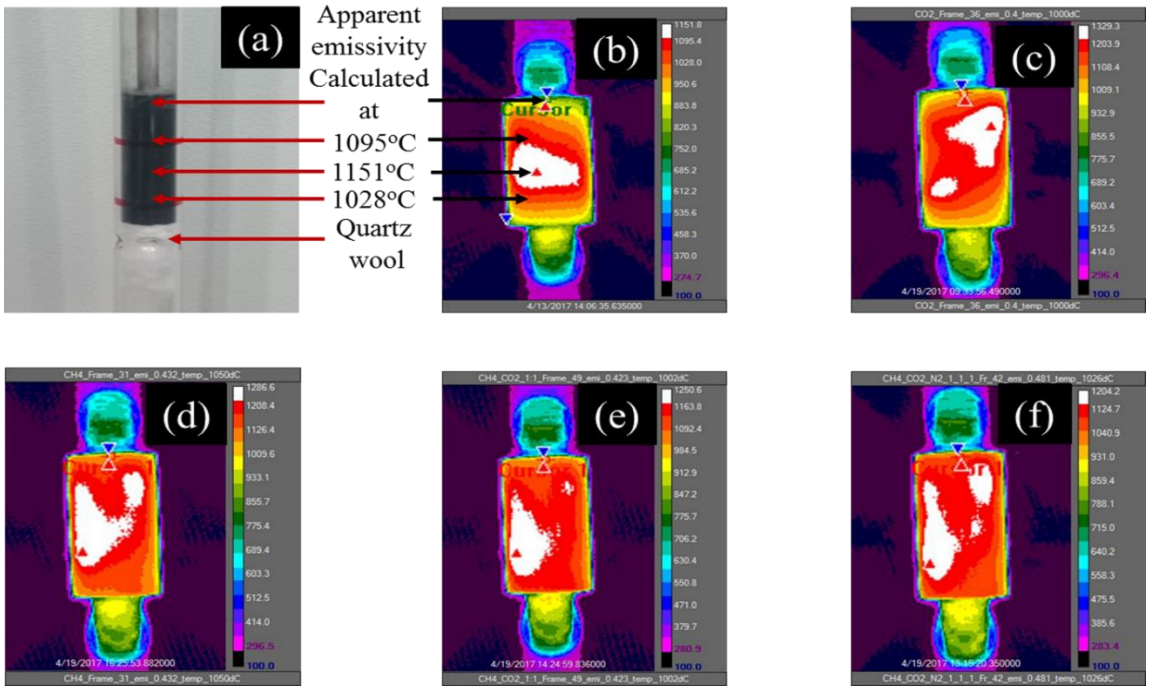

Figure 3.8. (a) Catalyst loaded quartz tube and detection of hot spots in the catalytic bed under different gas flows shown by thermal images in (b) N_2, (c) CO_2, (d) CH_4, (e) CH_4: CO_2 at a 1:1 ratio, and (f) CH_4:CO_2:N_2 in 1:1:1 ratio.

Along with finding emissivities for different gases, it is necessary to study 2D heat distribution in the catalytic bed in order to get insight into possible hotspots generation and non-uniform heating under MW exposure. The existence of hot spots in solid-liquid reactions has already been shown by high-speed cameras [64]. Studies done by Chen et al. for methane thermocatalytic decomposition showed that there was a 125 °C difference between the reactor inside and outside

temperatures in microwave-heated heterogeneous catalytic systems [79]. Zhang et al. have also reported that hot-spots temperatures were found to be 100–200 °C higher than the temperatures measured by optical thermometer [34]. Therefore, getting precise information on hot spot formation under microwave heating can support the discussion on possible factors determining process intensification. The thermal camera gives the advantage of finding out the exact locations of these hot spots in the catalytic bed, thanks to its rainbow pellet option to show hot spot positions inside the catalytic bed. **Fig. 3.8a** and **b** show the loaded quartz tube along with the N_2 flow thermal image. This thermal image shows that, in the case of the N_2 flow test, the temperature is higher at the center of the catalytic bed. It also reveals that the temperature where the emissivity has been calculated is lower than the center temperature of the catalytic bed (see the scale bar of the thermal image in **Fig. 3.8b**). The camera does not only provide a range of hot zones but also gives the highest temperature point present in the catalytic bed which is 1151 °C under N_2 flow.

The thermal images shown in **Fig. 3.8** confirm the presence of hot spots or zones and their shift or dislocation inside the catalytic bed with different gas flows. In addition, the thermal images in **Fig 3.8** can explain the fluctuations of emissivity values observed under different gas flows. It is clear in the thermal images that hot spots can migrate or split with respect to different gases present in the bed and with the duration of heating. Indeed hotspot locations change during MW heating due to the interaction of these gases with the catalyst, or homo-heterogeneous reactions.

The live streaming and recording option of the thermal camera allows for monitoring, in real time, changes in the heating patterns inside the catalytic bed. In most of the literature on heterogeneous catalysis in the temperature range 700–1000 °C under microwave heating, clear evidence on temperature differences between hot spots and average temperature is missing. This dual approach of matching internal and external temperature values with the help of thermal camera provides the most accurate values for temperature differences.

3.3.5. Catalyst performance evaluation and microwave absorption efficiency

The dry reforming of methane is a highly endothermic reaction (**Eq. 1.1,** chapter 1). It involves a combination of the two intermediate reactions; catalytic CH_4 cracking or decomposition (**Eq. 1.2**) and CO_2 gasification (**Eq. 1.3**)[36]. **Fig. 3.9a** shows CH_4 and CO_2 conversion over the PtC catalyst with 150 W of microwave power for 270 min of total reaction run. The conversion of methane and carbon dioxide were calculated by using the following equations.

$$CH_4 \text{ Conversion, \%} = 100 \times \left[\frac{(H_2)Out}{2}\right] / \left[(CH_4)_{out} + \frac{(H_2)out}{2}\right] \quad \textbf{(3.2)}$$

$$CO_2 \text{ Conversion, \%} = 100 \times \left[\frac{(CO)_{out}}{2}\right] / \left[(CO_2)_{out} + \frac{(CO)_{Out}}{2}\right] \quad \textbf{(3.3)}$$

Where $(CH_4)_{Out}$, $(H_2)_{out}$, $(CO_2)_{out,}$ and $(CO)_{out}$ are methane, hydrogen, carbon dioxide and carbon monoxide concentrations in the effluent gas (% by volume), as determined by gas chromatography. The microwave energy utilization efficiency was calculated by the following formula.

$$\text{MW Energy utilization Efficiency} = \left[\frac{(Forwarded\ Power(W) - Reflected\ Power(W))}{Forwarded\ Power\ (W)}\right] \times 100 \qquad \textbf{(3.4)}$$

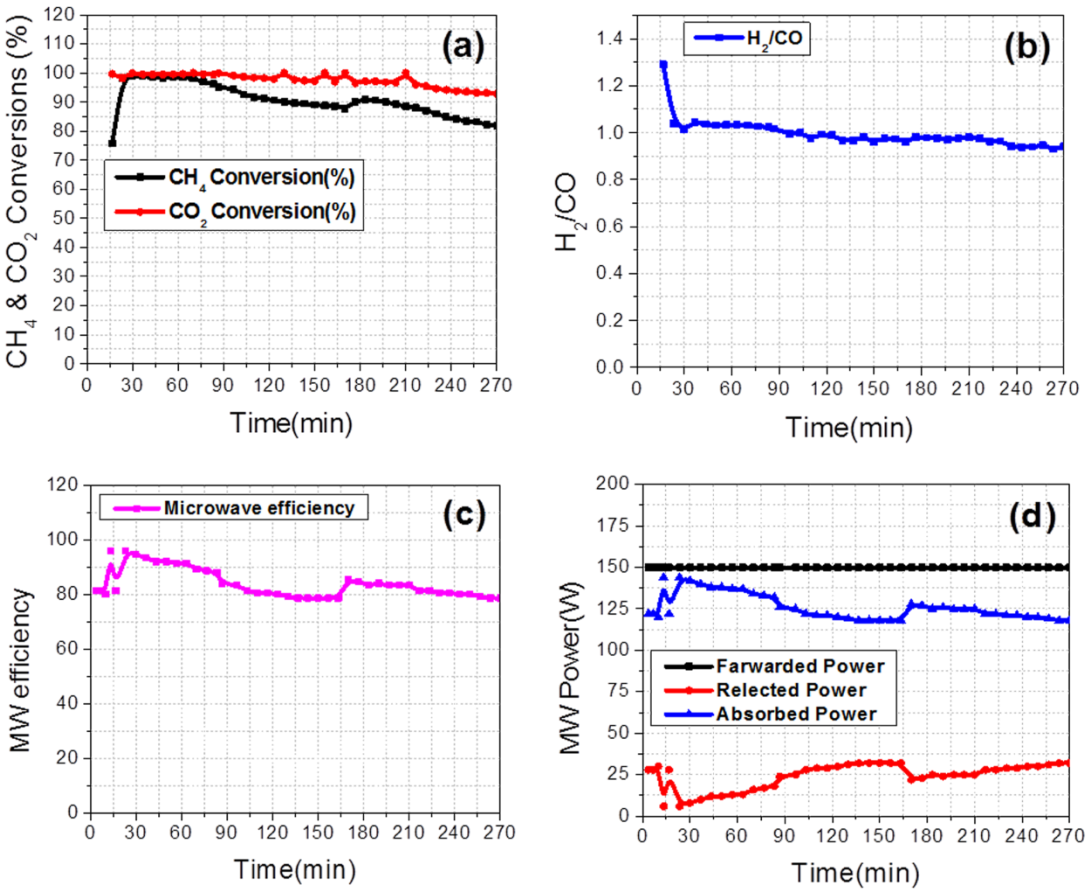

Figure 3.9 Methane dry reforming results. Temporal profiles of (a) CH_4 and CO_2 conversion, (b) H_2/CO ratio, (c) microwave energy absorption efficiency and (d) forwarded, absorbed and reflected microwave powers.

The conversion graph in **Fig. 3.9a** shows that CO_2 conversion is always higher than CH_4 conversion. As reaction time increases, CH_4 conversion decreases from 99 to 80% and CO_2 conversion decreases from 99 to 92%, while the H_2/CO ratio remains ~1 (**Fig. 3.9b**), during the complete run of 270 min. Zhang et al. have carried out dry reforming experiments and observed that, at temperatures higher than 700 °C, the heating efficiency was markedly reduced and a high power level was needed to increase temperature [34]. This observation is qualitatively consistent with the lower MW power absorption and the reduction in MW energy efficiency with time in our

case too. **Fig. 3.9c** shows that the microwave absorption efficiency at 30 min is ~94%; it decreases to ~78% after 270 min of reaction time. The main reason for the decrease in conversion with time is the deactivation of the catalyst. As the reaction runs for a long time, the formation of a pyrolytic carbon layer becomes significant on the inside wall of the quartz tube. The graphitic character of this deposited layer is responsible for the increase in the reflected power and hence compromises the overall microwave absorption ability of the catalytic bed [37]. As less MW energy is getting absorbed by the catalytic bed, the temperature in the catalytic bed decreases and results in a decrease in conversion with time.

3.3.6. Emissivity matching during the reaction

Fig. 3.10a shows the emissivity matching with thermocouple reading during the dry reforming process and its sensitivity to changes occurring in the catalytic system. First, the already calibrated emissivity value of 0.421 for a 1:1 ratio of CH_4:CO_2 was used. However, this emissivity was not matching with the actual temperature changes shown by the thermocouple. To get more realistic temperature values, we took actual temperature values shown by the thermocouple as a reference and recalculated the emissivity. After several trial-and-error attempts, a value of 0.737 was found to be the correct match for the stable temperature of ~800 °C in the time interval of 100 to 166 min. At 166 min, due to a technical reason, the MW generator turned OFF, and then the reactor did not receive MW supply for 30 s until the generator was restarted again. Once the MW was ON again, we observed that the emissivity value was changed and decreased to 0.687, which was matching with the thermocouple temperature values. In continuous MW heating experiments, if the dielectric properties of the catalytic bed change due to physical or chemical properties changes in the catalytic bed itself (resulting from high processing temperatures), then migration or shift of hot spots will also happen.

3.3.7. Factors affecting the emissivity and overall temperature distribution during the reaction

Fig. 3.11a shows the graph of temperature profiles with factors affecting the emissivity and temperature fluctuations during the reaction. As the reaction proceeds and reactant gases get converted to product gases, fluctuations in the intensity of emitted irradiation occur. A thermocouple remains unaffected by these changes and becomes the reference for emissivity correction at any time during the reaction. In **Fig. 3.11a**, the black line represents the temperature shown by the thermocouple. As it is not possible to change emissivity manually at every point, we selected the emissivity value of 0.737 after the emissivity match test reported earlier (see **Fig. 3.10a**).

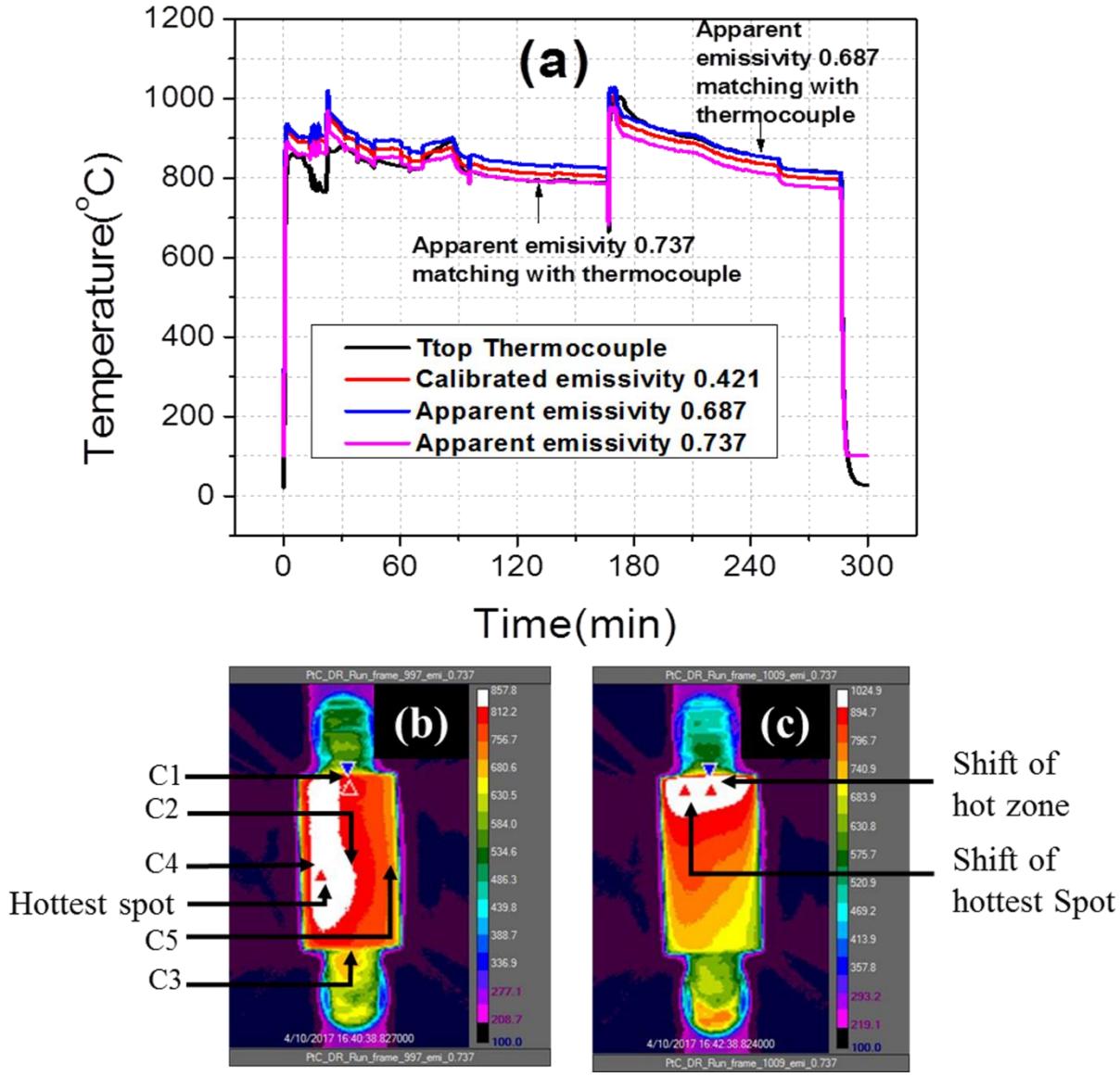

Figure 3.10. (a) Emissivity matching with actual temperature shown by a thermocouple during the methane dry reforming reaction. (b) The thermal image at 166 min; temperature values are extracted from the thermal video at C1(top), C2(center), C3(bottom), C4(Left), and C5(right) positions to study temperature distribution at these points. (c) The shift of hot spot or zone due to MW supply discontinuity.

Fig. 3.11a shows that after switching on the microwave generator, the catalyst reaches a temperature above 700 °C in 70 s under a N_2 gas flow. After 600 s, CH_4 and CO_2 were fed to the reactor at a flow rate of 17 ml/min for each gas. MW tuning was done to minimize the reflected power and to focus all forward power to catalyst only. After reactant feeding, a decrease in temperature is observed (see black line in **Fig. 3.11a**). This decrease in temperature could be due to an increase in the reflected power, which means that lower microwave energy is absorbed, and due to the endothermic nature of the reaction. As the reaction proceeds, more energy is utilized due

to the endothermic nature of reaction; this lowers the overall temperature of the catalytic bed and hence emits less infrared radiation that reaches the camera detector.

At 13, 16 and 23 min interval, reflector tuning was done to maximize utilization of MW energy. Therefore, sudden high peaks at the surface temperatures are shown by the thermal camera values, but the thermocouple shows a decrease in temperature until 16 min (**Fig. 3.11a**). This mismatch is a result of two reasons: (1) the change in infrared radiation occurring due to reaction progress and (2) the emissivity value used for this analysis is not applicable for these initial temperature changes.

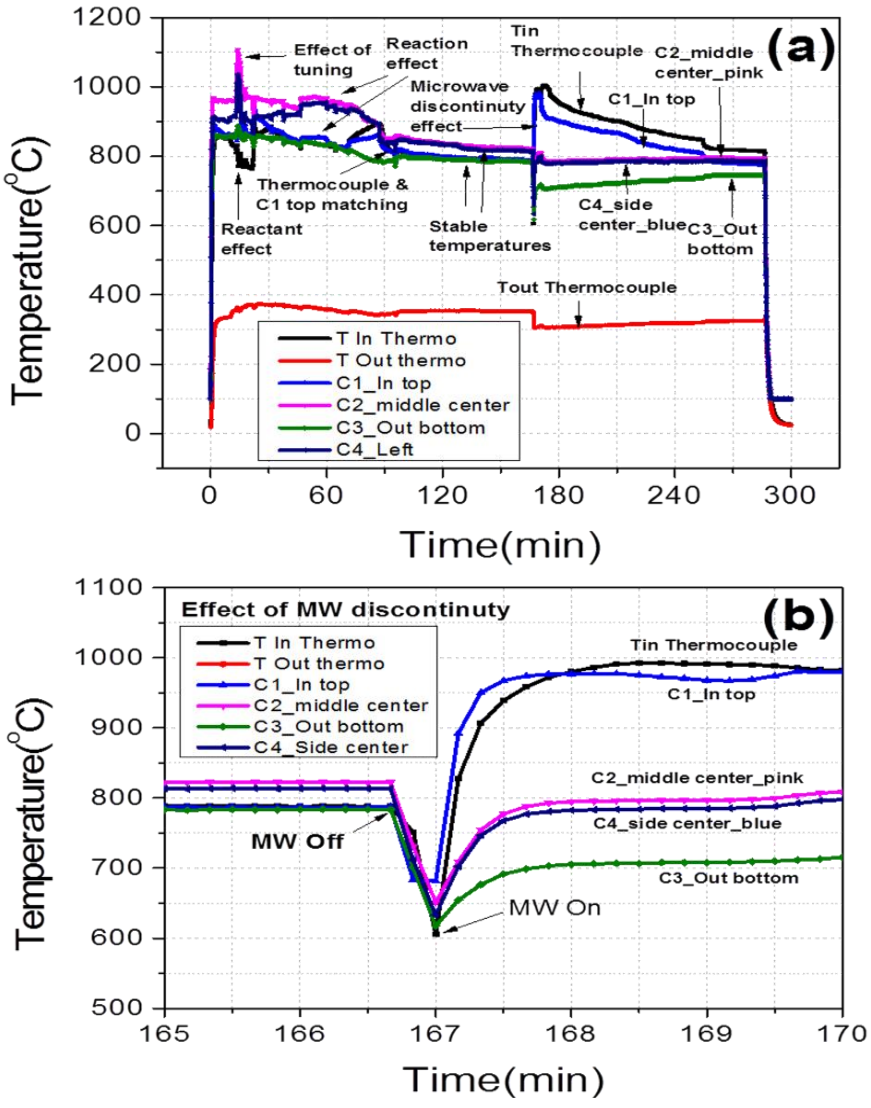

Figure 3.11. (a) Factors affecting temperature distribution in the catalytic bed during the reforming reaction, (b) effect of MW supply discontinuity on emissivity and temperature distribution.

A big drop in temperature from ~780 to 600 °C within 30 s was observed at ~166 min (**Fig. 3.11b**). Once the MW was ON again, a sudden increase in temperature was observed after this gap. This

incident changed the emissivity after 166 min. The temperature profiles at top, middle and bottom are separated after 166 min, but the temperature differences were observed to decrease until 270 min. In order to get a good match again with the temperature values shown by the thermocouple, a new emissivity was calculated with new thermocouple readings after 166 min. The reason for this change in temperature and emissivity values can be explained by the thermal images shown in **Fig. 3.10b** and **c**. The shift of hot spot or zone from the left side of the catalytic bed (**Fig. 3.10b**) to the top of the bed, where the thermocouple is placed (**Fig. 3.10c**), clearly explains the sudden increase in temperature as the hot spot is very close to the thermocouple and the location where it is calculated. The physical reason behind the change in emissivity is the sudden increase in temperature or shift of hot spot in the catalytic bed. This increase in temperature happened because of two things; first, when MW power was OFF, the temperature dropped from 780 to 600 °C, while reactant gases were still flowing through the bed. Now, due to the sudden interruption of microwave energy input, reactant conversions were decreased and the concentration levels of H_2, CO, CO_2, and CH_4 changed in the catalytic bed after 30 s. Therefore, in this complex gas mixture environment, the dielectric properties of the whole catalytic bed changed. The second reason was that when MW power was switched ON again, the catalyst was already at a temperature ~600 °C, and so its dielectric properties were higher than at room temperature, resulting in different response to absorb MW.

3.3.8. Axial and radial temperature distribution during the reaction

Fig. 3.12a shows temperature values at the center, left, right, top and bottom positions extracted after thermal data post-processing. If a corrected emissivity is provided to the thermal camera, then the temperature measurements in a 2D fashion will provide insight into the temperature distribution and heating patterns.

Fig. 3.10b shows the locations at which the temperature data have been extracted from the thermal video of the reaction run. It is particularly interesting to map the axial and radial temperature distributions that occurred during the reaction run. **Fig. 3.12a** shows the stable temperature differences at different points of the catalytic bed before the MW OFF issue and the clear shift, or separation, of temperature differences after MW ON after 30 s of time gap. **Fig. 3.12b** shows the differences in temperature in the mentioned location. In the case of stable temperature before 166 min, the center and left point difference is 5−10 °C. The center-top and center-bottom temperature differences are in the range of 50−60 °C. The center-right temperature difference is ~120 °C, as the hot spot is on left side only; hence there is a significant temperature difference between the center and right positions. After 166 min, the hot zone shifts to the top part of the catalytic bed and influences the temperature distribution inside the catalytic bed. In this case, a clear separation of temperature differences is observed in **Fig. 3.12b**. The −180 °C deference around 167 min shows that now the top part of the catalytic bed is hotter than the center part, which was indicated by the thermocouple reading and clearly shown in the thermal image (**Fig. 3.10c**).

After this change in location of the hot spot, the top-center difference became 180 °C. The center-left temperature difference became ~10−15 °C. The center-right temperature difference decreased from 120 to 100 °C, and the center-bottom one increased to 80−90 °C. A very big difference of ~280 °C from top to bottom after 167 min was observed. This top-bottom temperature difference decreased with an increase in time and eventually became ~50 °C at the end of 300 min.

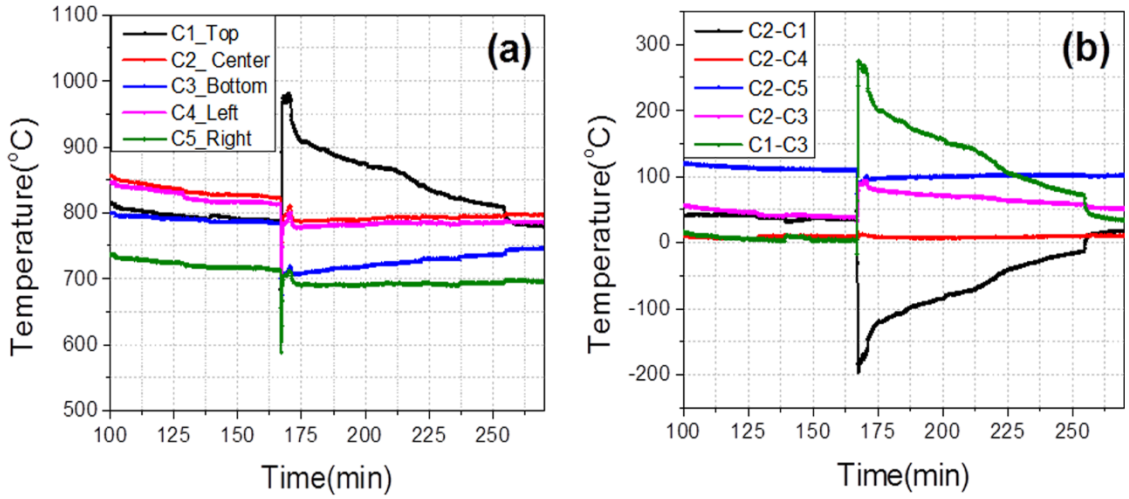

Figure 3.12. (a) Temperature distribution in the catalytic bed during the reaction with an emissivity value of 0.737. (b) Differences in temperature values at different locations of the catalytic bed with an emissivity value of 0.737.

3.4. Conclusions

The thermal camera-thermocouple dual temperature measurement method developed in this work allows for real-time high temperature (300− 1000 °C) measurements in MW-heated catalytic reactors. This method was applied for a temperature distribution study in a platinum-on-carbon catalytic bed used for methane dry reforming. For this purpose, a custom-designed microwave cavity was employed to focus the microwave field on the catalyst bed and monitor its temperature in a 2D fashion by means of a thermal camera. The effect of different factors affecting the temperature measurements and emissivity values under microwave heating were investigated. The effects of camera range, the presence of different media and reactant gases in the process domain, object-to-camera distance, heating system and microwave field distribution were discussed in detail. The multiparameter emissivity dependence in such a complex reaction system does not ensure correct temperature recording by the thermal camera alone; therefore, at least one contact sensor is highly recommended. The developed method successfully detected hot spot generation and provided an explanation for the non-homogeneous heating profiles during MW processing. Careful handling and continued temperature monitoring with a thermal camera is very helpful to avoid potential risk hazards in MW-heated catalytic reactors.

3.5. Supporting Information:

3.5.1. Challenges to reproduce experimental results and risk factors involved

The problem of system failure due to pyrolytic carbon formation has already been reported in the literature for high-temperature reactions in a quartz tube under microwave heating. In our work, over a period of ~15 hrs of MW heating, the quartz tube eventually broke. As shown in **Fig. 3.15 a**, the black-colored fresh catalyst is readily visible through a fresh transparent quartz tube. However, after several heating and reaction experiments for nearly 15 hours, a solid layer of white and black color was formed on the inside of the quartz tube wall (**Fig 3.15c**). Analysis of this layer has not been done, as it is not within the scope of this work; it could be a pyrolytic layer as reported already, degradation of the quartz tube due to heating above its thermal stability limit or combination of both, damaging the tube both from the interior and the exterior. The thermal camera helps in case of reactor damage and reveals tube breakage, as shown in **Fig. 3.15d**, which is impossible to know when using point sensors or pyrometers.

Reproducibility of heating profiles under microwaves is another major issue. During microwave heating, catalyst physical properties and composition may change resulting in different dielectric properties and eventually different heating patterns during future experiments. In addition, emissivity changes with temperature, different gases in the catalytic bed and surface properties of the quartz tube due to pyrolytic layer formation as mentioned earlier. Further, for given experimental settings, a sudden decrease in the reflected power may be observed, resulting in an unwanted steep temperature increase. Then, tuning of control elements can in principle adjust the reflected power, but doing so manually during the experiment involves the risk to overheat the catalytic bed and to damage the reactor and temperature sensor. Further, such tuning would be based on the heated load properties at the time; therefore, it is highly impossible to reproduce the same results if tuning is done every time.

Besides, microwave heating involves changes in hot spot location inside the reactor and affects the overall infrared radiation towards a thermal camera. A thermal camera is a very good option for non-contact measurements; however, in cases of uneven heating behavior of the system, emissivity values at different hot spots will change; this will compromise accurate temperature monitoring if the camera settings are not adjusted. Collectively, proper monitoring of high-temperature reactions under microwaves requires particular caution. To avoid any random behavior during the experiments, it is recommended to first check the thermal behavior of the system before planning and optimizing the actual experiments.

Table 3.1 Thermocouple and optical fiber temperature measurement comparison.

Time (sec)	MW power (W)	Thermocouple Temperature (˚C)	Optical fiber Temperature (˚C)
0	0	26.02	25.21
120	1	39.60	38.32
240	2	54.77	55.78
360	3	73.31	72.31
480	4	89.66	90.11
600	5	103.57	105.57
720	6	118.23	116.23
840	7	131.18	135.18
960	8	145.357	143.57

Table 3.2: Effect of gases on emissivity under microwave heating.

Pt.	N_2 Flow		CO_2 Flow		CH_4 Flow		CH_4:CO_2_1:1		CH_4:CO_2:N_2_1:1:1	
No	**Temp. (ºC)**	**Emi.**	**Temp. (ºC)**	**Emi.**	**Temp. (ºC)**	**Emi.**	**Temp. (ºC)**	**Emi.**	**Temp. (ºC)**	**Emi.**
1	230.71	0.132	300.28	0.551	302.91	0.428	307.89	0.557	303.60	0.408
2	390.7	0.168	397.29	0.513	402.22	0.482	395.55	0.463	404.82	0.398
3	496.9	0.205	517.26	0.473	499.56	0.461	500.37	0.442	519.90	0.388
4	631.23	0.208	600.26	0.459	613.16	0.439	611.82	0.433	617.80	0.380
5	730.01	0.195	690.35	0.457	703.17	0.429	706.35	0.436	714.28	0.361
6	815.6	0.193	817.90	0.419	820.03	0.433	826.48	0.419	809.65	0.369
7	917.96	0.227	923.16	0.375	886.25	0.430	915.37	0.412	907.83	0.448
8	1001.71	0.29	1000.28	0.400	946.72	0.422	1002.82	0.423	998.46	0.477

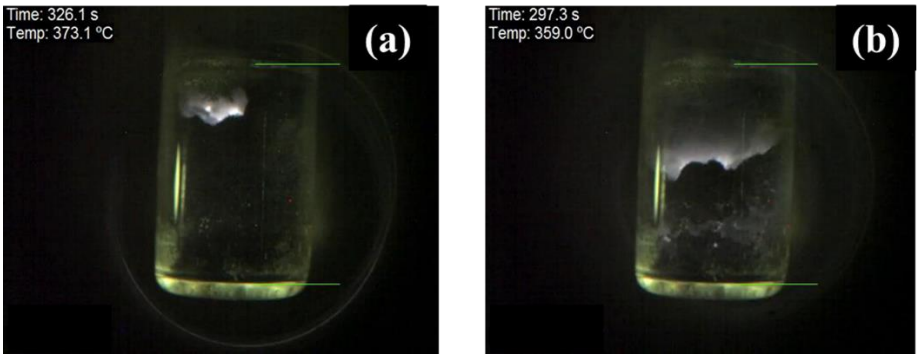

Figure 3.13 Reduction of the sample volume in the second (a) and third cycle (b)

Fig. 3.13 shows images of sample reduction occurred around 360−375 °C due to the shrinking of the catalytic materials responsible for the change in the dielectric properties. The original volume taken for the first measurement has been highlighted by top and bottom green lines in both images.

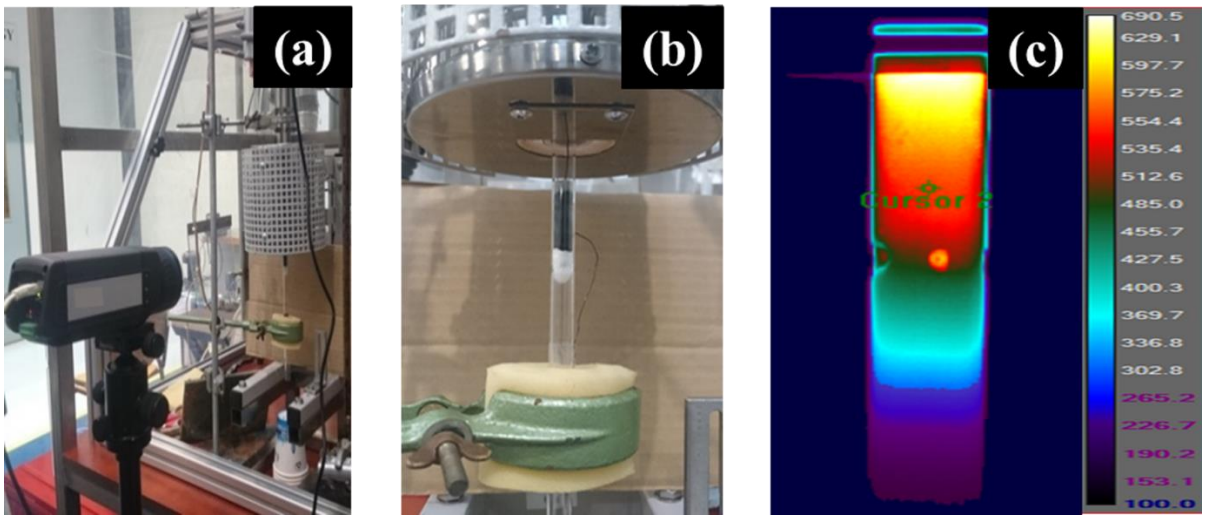

Figure 3.14 Emissivity measurement in conventional heating: (a) Set up arrangement, (b) thermocouple at the center of the catalytic bed and (c) Thermal image for emissivity calculation.

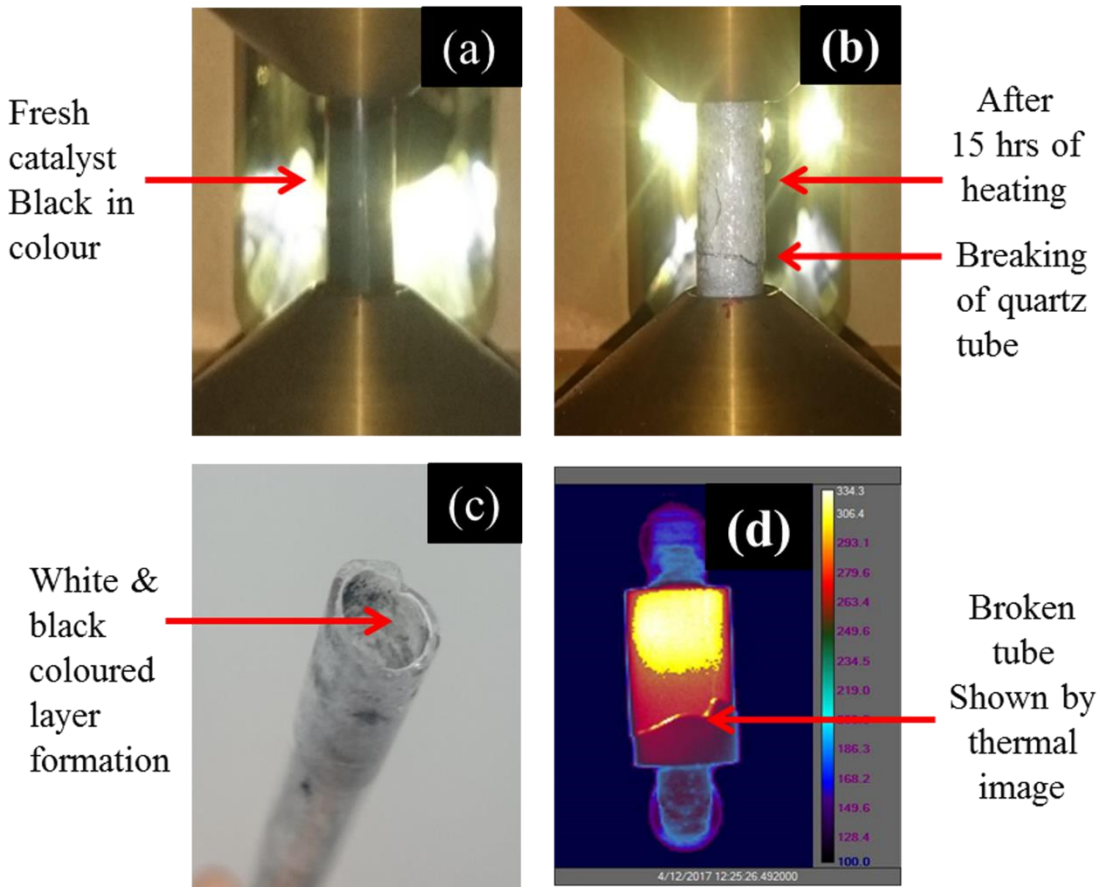

Figure 3.15. (a) Fresh catalyst loaded in the microwave cavity; the black colored catalyst is visible through the transparent quartz tube wall; (b) quartz tube after 15 hours of heating and reaction experiments under MW heating; (c) white and black colored solid layer formed on the inside of the quartz tube wall; (d) thermal image showing the quartz tube breakage.

4

4. Synthesis, characterization, and application of ruthenium-doped $SrTiO_3$ perovskite catalyst for microwave-assisted methane dry reforming

This Chapter is published as:

Lalit S. Gangurde, Guido S. J. Sturm, M. J. Valero-Romero, Reyes Mallada, Jesus Santamaria, Andrzej I. Stankiewicz, Georgios D. Stefanidis, Synthesis, characterization, and application of ruthenium-doped $SrTiO_3$ perovskite catalyst for microwave-assisted methane dry reforming, Chemical Engineering and Processing: Process Intensification, 127, 178-190, 2018.

Abstract

A series of ruthenium-doped strontium titanate ($SrTiO_3$) perovskite catalysts were synthesized by conventional and microwave-assisted hydrothermal methods. The structure was analyzed by X-Ray diffraction (XRD) confirming the formation of the perovskite phase with some TiO_2 anatase phase in all the catalysts. Microwave irradiation decreases the temperature and time of synthesis from 220 °C for 24 h (conventional heating) to 180 °C for 1 h, without affecting the formation of perovskite. A 7 wt. % ruthenium-doped $SrTiO_3$ catalyst showed the best dielectric properties, and thus its catalytic activity was evaluated for the methane dry reforming reaction under microwave heating in a custom fixed-bed quartz reactor. Microwave power, CH_4:CO_2 vol. % feed ratio and gas hourly space velocity (GHSV) were varied in order to determine the best conditions for performing dry reforming with high reactants conversions and H_2/CO ratio. Stable maximum CH_4 and CO_2 conversions of ~99.5% and ~94%, respectively, at H_2/CO ~0.9 were possible to reach with the 7 wt. % ruthenium-doped $SrTiO_3$ catalyst exposed to maximum temperatures in the vicinity of 940 °C. A comparative theoretical scale-up study shows significant improvement in H_2 production capability in the case of the perovskite catalyst compared to carbon-based catalysts.

Graphical Abstract:

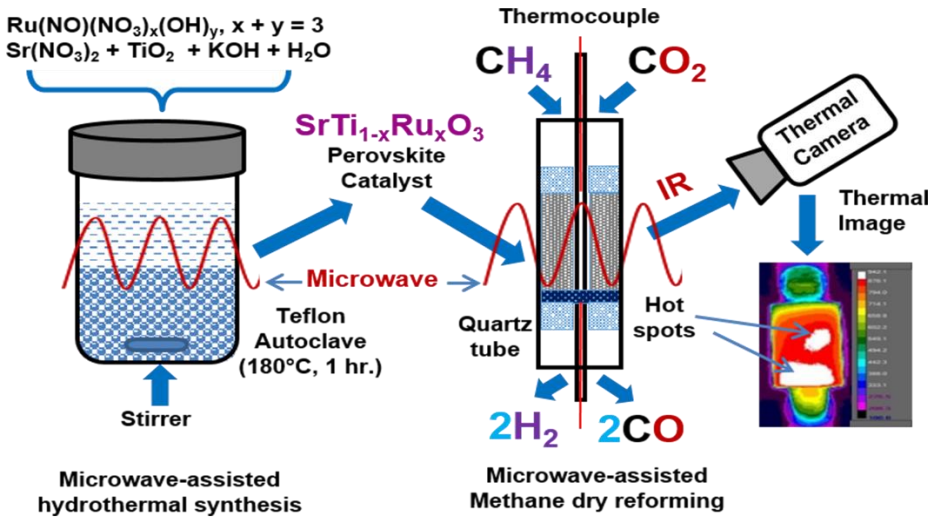

4.1. Introduction

Resource- and energy-efficient methane transformation to liquid fuels and chemicals is a research topic with societal, environmental and industrial relevance owing to the great variety of methane sources, including existing gas networks, small natural gas fields, shale gas, coal beds, agricultural biogas and deep-sea methane hydrates [18][19], the pressing issue of methane flaring in remote locations [17] and its significant contribution to the greenhouse effect [80][81][82].

A group of chemical routes to valorize methane includes its transformation into syngas (a mixture of CO and H_2) via steam reforming, dry reforming, partial oxidation and auto-thermal reforming. Among these processes, despite deactivation issues, dry reforming of methane (DRM) has 20% lower operating cost compared to the other mentioned processes [49]. DRM was first investigated as early as 1888 [83]. Fischer and Tropsch thoroughly explored DRM in 1928 [83]. This process reforms CH_4 and CO_2, both being greenhouse gases, into high purity syngas with negligible CO_2 content. The syngas from DRM can be used as a direct feed for Fischer-Tropsch synthesis for selective synthesis of higher hydrocarbons [49].

The primary challenge for industrial implementation of DRM is the unavailability of commercial catalysts that can operate at the high temperatures (800–1000 ^oC) required for CH_4 and CO_2 activation without catalyst deactivation issues due to carbon deposition [17]. The reported order of activity of noble and transition metals for DRM is Rh, Ru > Ir > Ni, Pt, Pd > Co > Fe, Cu [84]. Ruthenium has been reported to be the most active element combined with various supports such as Al_2O_3, La_2O_3, Y_2O_3, ZrO_2, TiO_2, MgO, SiO_2, carbon, and zeolites [84]. However, the high-temperature requirement of the highly endothermic DRM process leads to inevitable problems of metal sintering and rapid catalyst deactivation. Therefore, catalytic materials with high thermal stability, activity and coking resistance are required [19].

Rapid and selective microwave heating has been reported to improve the performance of heterogeneous catalytic processes compared to conventional heating in one or more of the following terms (faster reaction rate, better product distribution, higher energy efficiency) [57,58,85–87]. One of the key factors determining the extent of these effects is the ability of the catalytic material to dissipate microwave energy (i.e., to become efficiently heated by microwaves). Therefore, it is important to measure the dielectric properties of the catalytic materials in the range of actual process conditions to verify the extent of their susceptibility to microwave heating.

Carbon materials have been used in the literature for microwave-assisted methane dry reforming as they are good MW receptors and catalytically active [88][37]. Dominguez et al. studied biogas to syngas by microwave-assisted dry reforming in the presence of char [36]. They reported that CH_4 conversion falls after some minutes due to blockage of the active centers by carbon deposits. Nevertheless, CH_4 conversion can be improved by the presence of CO_2, due to gasification of the

carbon deposits. This effect was more noticeable in microwave heating than in conventional heating. It was also reported that constant removal of the carbon deposits was favored by the high K content in the char [36]. Most of the metal catalysts (e.g., Ni/Al_2O_3) that are active for DRM in conventional heating cannot be used directly for MW-assisted DRM because of their inability to reach the optimum reaction temperature due to their low dielectric properties. To address this issue, Fidalgo et al. mixed activated carbon with a metal-based catalyst to heat the latter up to the temperature required for MW-assisted DRM [89].

However, in our experiments, on microwave-assisted methane dry reforming over platinum on carbon catalyst, the amount of carbon catalyst decreased over a period of time (~ 270 min) and formed a carbon layer on the inner surface of the quartz wall of the reactor, thereby softening and eventually breaking the quartz tube wall [54]. Collectively, there is a room for the development of catalysts for MW-assisted methane dry reforming; such catalysts must have good microwave absorption ability, should be resistant to coke formation, should not get consumed during the reaction and produce high syngas yield.

Perovskite (ABO_3) materials have become attractive catalysts as they prevent the agglomeration of metal ions by retaining their structure during high temperature reforming reactions [90]. They have potential applications in oxygen separators, solid oxide fuel cells and membrane reactors [91]. A typical perovskite is a structure with general composition type ABO_3. Perovskite oxides contain lanthanide elements at 'A' sites (for example, Ce, La, Pr) and a transition element at 'B' sites, such as Ni, Rh, Pt, etc. The significant advantages of the perovskite structure from the catalysis point of view are (1) its well-defined bulk structure with good oxygen storage capacity, (2) compositions at A and B cationic sites can be widely varied, (3) better thermal stability with valency control and (4) excellent redox properties [13]. Liu et al. studied several low-cost perovskite catalysts for auto-thermal reforming of n-dodecane and concluded that ruthenium-doped perovskite catalysts have superior reforming efficiency with good resistance to sulfur as compared to perovskite catalysts without ruthenium [92].

In this work, we have synthesized a series of Ru-doped $SrTiO_3$ perovskite catalysts by conventional and microwave-assisted hydrothermal methods. The catalysts have been characterized by X-ray diffraction (XRD), N_2 physisorption (BET surface area), inductively coupled plasma optical emission spectrometry (ICP-OES) and high-angle annular dark-field scanning transmission electron microscopy (HAADF-STEM) coupled to energy dispersive X-ray (EDX) analysis. The dielectric properties have been measured in the temperature range 20–850 °C. The catalyst with the best dielectric properties was selected for application to DRM in a custom-built microwave reactor system. An experimental parametric study was carried out to investigate the role of microwave power, CO_2 concentration in the reaction mixture and gas hourly space velocity, as well as the catalyst stability. In this study, two-dimensional (2D) temperature monitoring was applied using an approach combining a thermal camera and thermocouples [54]. Finally, a comparison in terms of H_2 production between the synthesized perovskite catalyst and a carbon-based catalyst

from the literature has been carried out for a theoretical scale-up scenario of the MW-assisted methane dry reforming process.

4.2. Experimental

4.2.1. Reagents and materials

Strontium nitrate ($Sr(NO_3)_2$, 99% ACS reagent), ruthenium(III) nitrosyl nitrate solution ($Ru(NO)(NO_3)_x(OH)_y$, x + y = 3), titanium dioxide (TiO_2, 99 %) and potassium hydroxide (KOH, 99%) were purchased from Sigma-Aldrich. All chemicals were used without any further purification.

4.2.2. Conventional hydrothermal (CHT) synthesis

A series of Ru-doped strontium titanate ($SrTiO_3$) perovskite catalysts were synthesized by conventional (C) and microwave-assisted (MW) hydrothermal methods. In the case of conventional hydrothermal method, stoichiometric amounts of $Sr(NO_3)_2$ (5.77, 5.70, 5.64 and 5.57 gm) and TiO_2 (2.18, 2.07, 1.96 and 1.85 gm), respectively, were separately dissolved in deionized water under stirring until complete solution. Subsequently, 0, 7.26, 14.36 and 21.29 ml of ruthenium (III) nitrosyl nitrate solution was added. The colloidal solution was stirred at room temperature for 10–20 min, and then a solution of 9M of KOH was added dropwise and kept for 6 h under stirring. The reaction mixture was then transferred to a teflon-lined stainless steel autoclave for hydrothermal treatment at 220 °C for 24 h [93]. After cooling down, the precipitates obtained were filtered off, washed with deionized water several times and dried at 80 °C for 6 h. The resulting solids were calcined at 800 ºC for 3 h to obtain the perovskite phase [94]. A heating rate of 5 ºC min^{-1} and static air conditions were applied to all the drying and calcination steps mentioned above. The samples prepared by conventional hydrothermal synthesis are denoted as y$Ru/SrTiO_3$-C-zh, where y is the Ru content in *wt. %*, C stands for conventional heating, and z is the heating time in hours.

4.2.3. Microwave-assisted hydrothermal (MWHT) synthesis

In the case of microwave-assisted hydrothermal synthesis, the reaction mixture was prepared in a similar way to that mentioned in the conventional hydrothermal synthesis section. The only difference here is that the reaction mixture is placed in a teflon-lined autoclave inside a MILESTONE ETHOS Plus microwave cavity with automatic temperature control. The synthesis was performed at 220 °C for 6 h without stirring. Microwave synthesis while stirring the solution at a temperature of 180 °C for 1 h was also performed in order to reduce synthesis time and temperature. For 1 h MW synthesis with stirring, a MW setup (Mycrosynth plus model ACT38)

with automatic temperature control (ATC-TO) was used. After the hydrothermal treatment, the reaction products were filtered off, washed with deionized water, dried and calcined under the conditions explained earlier in conventional hydrothermal synthesis. The samples prepared by microwave heating are denoted as yRu/$SrTiO_3$-MW-zh, where y is the Ru content in *wt. %*, MW stands for microwave heating, and z is a heating time in hours.

4.2.4. Characterization methods

The crystalline phases of the powder catalysts were examined by X-ray powder diffraction (XRD) using a Bruker D8 Advance diffractometer. It is equipped with a Vantec position sensitive detector and a graphite monochromator. The measurements were performed at room temperature, using monochromatic Co Kα radiation (k = 0.179026 nm) in the 2θ region between 20 and 70°. The diffractometer was operating at 35 kV and 40 mA. The average crystallite size of perovskite in the catalysts was estimated from the Scherrer equation applied to the most intense diffraction (2θ = 37.77 °) using the shape factor K = 0.9. The phase compositions were semi-quantitatively estimated using Bruker Eva S-Q software. The reference intensity ratio (RIR) were taken from the PDF2 database (International Centre for Diffraction Data, 2004). A single reflection is used per phase; absorption correction is omitted, and the result is adjusted so that the sum of X_{phase} = 1. The reflections used were those with the highest intensities and without interference with other phases.

The dielectric properties of the prepared catalytic materials were measured by the DIMAS group at the Universitat Politecnica of Valencia, from 20 to 850 °C, in a dual mode cylindrical cavity by following the methodologies described elsewhere [77][78]. The catalytic samples were placed in a quartz tube, which was located inside the dual mode cylindrical cavity. The dielectric properties were measured while simultaneously heating the sample at 20 °C/min in N_2 atmosphere.

Textural properties of the materials were analyzed by N_2 adsorption-desorption at 77 K in a Tristar II 3020 Micromeritics sorptometer. Before each experiment, all the samples were outgassed at 200 °C for 16 h. From the N_2 adsorption/desorption isotherm, the specific surface area (S_{BET}) was determined from the BET equation [95]. The total pore volume (V_{total}) was determined from the adsorbed volume of N_2 at a relative pressure of 0.99.

Elemental analysis was performed using a PerkinElmer Optima instrument. Approximately 25 mg of each sample were digested in 4.5 ml 30% HCl + 1.5 ml 65% HNO_3 + 0.2 ml 40% HF using microwaves. The digestion time in the microwave oven was 30 min at maximum power. After digestion, the samples were diluted to 50 ml with MQ water and then analyzed by Inductively Coupled Plasma Optical Emission Spectrometry (ICP-OES) 5300DV.

High-resolution transmission electron micrographs were collected using (TEM/STEM) FEI Talos F200X, which operates at an accelerating voltage of 200 kV. To determine the specific distribution

of elements present in the synthesized materials, energy dispersive X-ray (EDX) elemental maps were analyzed. Particle size distribution histograms were also obtained by counting around 100 particles from each sample.

4.2.5. Microwave-assisted dry reforming of methane (DRM)

Eq. 1.1(chapter 1) represents the global DRM reaction that involves intermediate steps and side reactions. The intermediate steps (**Eqs. 1.2 and 1.3**) of methane cracking and carbon dioxide gasification both occur at high temperatures [36]. The most common side reactions (**Eqs. 1.4** and **1.5**) are the reverse water gas shift reaction (RWGS) (**Eq. 1.4**), which occurs at temperatures lower than 820 °C and the Boudouard reaction (**Eq. 1.5**), which occurs below 700 °C, contributing to the formation of carbon deposits [49].

The methane dry reforming experiments were performed in a specially developed microwave reactor system as discussed in Chapter 2. **Fig. 3.1**(Chapter 3) shows the schematic diagram of the microwave reactor setup. For all the experiments, 1 g of 7Ru/$SrTiO_3$-MW-1h (425-850 μm particle size), the catalyst with the highest loss tangent value among the tested series, was used to perform the DRM tests. The catalyst was loaded in a quartz tube (290 mm length × 8 mm i.d.) as shown in **Fig. 3.2a**. Two N-type thermocouples (−200 to +1250 °C) were placed at the top and bottom part of a catalyst bed to measure the emperature at these positions. The quartz tube loaded with the catalyst was then inserted into the custom-designed microwave reactor, as shown in **Fig.3.2b**.

The feed consisted of a mixture of CH_4 and CO_2. The total flow rate was varied from 50 to 225 ml min^{-1} to achieve variable CH_4 and CO_2 conversion levels according to the residence time of the reactants. The conversions of CH_4 and CO_2 were calculated by **Eqs. 3.2** and **3.3**, respectively (Chapter 3), considering the global DRM reaction (**Eq. 1.1**, Chapter 1) only. Approximately 100% of the MW power forwarded by the solid state generator to the sample is converted to heat; i.e., negligible reflected power is detected. MW power is mostly dissipated in the reactor itself, but, as reported by Cherbanski et al. [96], part of it may also be dissipated in the cavity walls, or in the hardware elements around the reactor.

The temperature of the catalytic material depends on its microwave heating ability under real process conditions. Therefore, methane dry reforming experiments were performed first with different MW powers to find out the optimum temperature response. After finding the optimum MW power, the influence of CO_2 concentration in the feed and of the total gas hourly space velocity (GHSV) on CH_4 conversion and overall reaction performance was studied. The total GHSV is defined by the ratio of total flow rate (cm^3h^{-1})/mass of catalyst (g), where the total flow rate is the sum of the flow rates of CH_4 and CO_2. Finally, a stability test was performed at the optimum conditions of MW power, CH_4 to CO_2 ratio and GHSV for 3 h.

4.3. Results and discussion

4.3.1. Catalyst characterization

Fig. 4.1a and **b** show the XRD patterns of Ru-doped $SrTiO_3$ perovskite catalysts synthesized by different methods, over different heating times, at different temperatures with or without stirring. **Fig. 4.1a** shows a comparison of XRD patterns of all the yRu/$SrTiO_3$-C-24h conventionally synthesized catalysts with the 7Ru/$SrTiO_3$-MW-1h catalyst. **Fig. 4.1b** shows a comparison of all the yRu/$SrTiO_3$-MW-6h microwave synthesized catalysts with the 7Ru/$SrTiO_3$-MW-1h catalyst. Bare $SrTiO_3$ (**Fig. 4.1a**) prepared by the conventional hydrothermal method exhibits diffractions at 37.8, 46.6, 54.4 and 68.2°, resulting from the presence of a perovskite cubic phase (PDF 73-0661). Ru-doped $SrTiO_3$ (3, 5 and 7 wt. % Ru) prepared by both conventional and microwave-assisted methods also exhibit perovskite reflections as the predominant phase (**Fig. 4.1a** and **b**). However, those samples prepared under conventional heating also exhibit diffractions attributed to the anatase phase of TiO_2 as an impurity. These diffractions included intense peaks at 29.5 and 56.8º resulting from the presence of the anatase (101) and (200) crystal planes, respectively (PDF 78-2486).

Table 4.1 summarizes the semi-quantitative phase composition and the crystallite sizes of $SrTiO_3$ in the catalysts based on the Scherrer equation. The values of the specific surface area obtained by the BET method and the total pore volume derived from the N_2 adsorption data are also reported in **Table 4.1**. In general, the composition of $SrTiO_3$ is above 70 wt. % in all the catalysts; however, the presence of anatase increases for those samples prepared by microwave heating at the lowest reaction time and temperature, 7Ru/$SrTiO_3$-MW-1h. Furthermore, the anatase composition decreases with increasing Ru loading and with increasing MW irradiation time and temperature; for example, it decreases from 26 wt.% for the bare $SrTiO_3$ (0Ru/$SrTiO_3$-C-24h) to 14 wt.% for the 7 wt.% Ru-doped $SrTiO_3$ (7Ru/$SrTiO_3$-C-24h) catalyst. The average crystallite sizes of bare $SrTiO_3$ and Ru-doped $SrTiO_3$ samples also showed differences, with smaller particles being formed in the samples with higher Ru loading. For instance, the average $SrTiO_3$ crystallite size decreases from 36.1 nm for 0Ru/$SrTiO_3$-MW-6h to 29.6 nm for 7Ru/$SrTiO_3$-MW-6h. These results suggest that the incorporation of Ru to $SrTiO_3$ could prevent particles sintering during the calcination step at 800 ºC. It is thus confirmed that the microwave-assisted preparation method can save energy and time due to the faster kinetics of crystallization [97].

Interestingly, the XRD of all the Ru-doped $SrTiO_3$ samples do not show any peak shifting or reflections corresponding to RuO_2 oxide formation, as reported before for Ru supported on $SrTiO_3$ [84]. This fact points out the high dispersion of ruthenium in $SrTiO_3$ prepared by hydrothermal methods, both under conventional and microwave heating, despite the low BET surface areas and pore volume obtained.

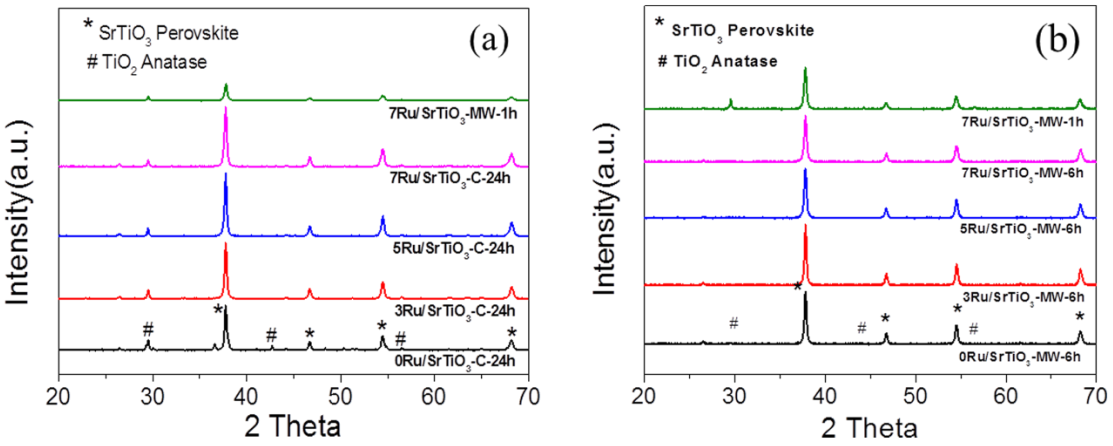

Figure 4.1. XRD patterns of (a) Ru-doped perovskite samples prepared by conventional HT synthesis for 24 h compared to MWHT for 1 h, and (b) Ru-doped perovskite samples prepared by MWHT synthesis for 6 h compared to MWHT 1 h.

Table 4.1: Physical and chemical properties of all synthesized Ru-doped $SrTiO_3$ catalysts.

Catalyst	XRD			N_2 isotherm		ICP-OES
	d_{SrTiO3} (nm)	S-Q^a_{TiO2} (wt %)	S-Q^a_{SrTiO3} (wt %)	S_{BET} (m^2/g)	V_{total} (cm^3/g)	Ru (wt%)
0Ru/$SrTiO_3$-C-24h	37.9	26.2	73.8	5	0.022	0
3Ru/$SrTiO_3$-C-24h	36.6	19.5	80.5	6	0.001	2.2
5Ru/$SrTiO_3$-C-24h	37.6	18.4	81.6	6	0.001	4.4
7Ru/$SrTiO_3$-C-24h	31.3	14.1	85.9	6	0.001	6.8
0Ru/$SrTiO_3$-MW-6h	36.1	1.9	98.1	8	0.032	0
3Ru/$SrTiO_3$-MW-6h	37.5	0.8	99.2	6	0.025	2.4
5Ru/$SrTiO_3$-MW-6h	30.0	1	99	6	0.020	4.8
7Ru/$SrTiO_3$-MW-6h	29.6	2.2	97.8	4	0.014	6.3
7Ru/$SrTiO_3$-MW-1h	29.8	22.2	77.8	8	0.026	7.2

[a] **Semi-quantitative (S-Q) weight percentage of the phases obtained from XRD.**

The dielectric properties of the yRu/$SrTiO_3$-C-24h series samples have been measured and presented in **Fig. 4.2**, while the specified weights and densities are presented in **Table 4.2**. The primary purpose of the dielectric properties measurements was to find a suitable catalyst for microwave heating and then use it for further characterization and the methane dry reforming reaction. Therefore, the dielectric properties of yRu-/$SrTiO_3$-MW-6h series and 7Ru/$SrTiO_3$-MW-1h catalyst were not measured. The dielectric properties measurement procedure was explained in our recent work [54]. Specifically, heating up to 850 °C with a heating rate of 20 °C/min was carried out. In **Fig. 4.2a** and **b**, the variation of the dielectric constant and loss factor with increasing temperature is presented for the yRu/$SrTiO_3$-C-24h series. For all the samples, the dielectric constant decreases with increasing temperature, whereas the loss factor increases with increasing

temperature. Further, the dielectric constant and dielectric loss factor values increase with an increase in Ru content. From this comparison, it is clear that the 7Ru/$SrTiO_3$-C-24h catalyst has the highest dielectric properties in the tested series.

On the basis of the dielectric characterization presented, the 7 wt. % Ru/$SrTiO_3$-C-24h catalyst was selected for further microwave-assisted synthesis study. To study the role of reduction of synthesis temperature, time and stirring, microwave synthesis of this catalyst has been done at 220 °C for 6 h without stirring and at 180 °C for 1 h with stirring. As explained earlier, 1 h microwave hydrothermal synthesis with stirring has shown similar XRD peaks and confirmed the perovskite phase formation. The obtained catalyst is denoted as 7Ru/$SrTiO_3$-MW-1h. Only the 7Ru/$SrTiO_3$-C-24h and 7Ru/$SrTiO_3$-MW-1h catalysts have been considered for further characterization and comparison purpose. **Table 4.1** shows the elemental analysis results by ICP-OES. It indicates that higher concentration of the Ru element is present in the MW-synthesized catalyst (7Ru/$SrTiO_3$-MW-1h) as compared to the conventionally synthesized catalyst (7Ru/$SrTiO_3$-C-24h).

Table 4.2: Weights and densities of yRu/$SrTiO_3$-C-24h series used for dielectric properties measurements.

Sample	Catalyst Code	Weight(g)	Density(g/cm^3)
1	0Ru/$SrTiO_3$-C-24h	1.498	1.2734
2	3Ru/$SrTiO_3$-C-24h	1.361	1.1673
3	5Ru/$SrTiO_3$-C-24h	1.271	1.0921
4	7Ru/$SrTiO_3$-C-24h	1.398	1.2120

To determine the dispersion of the different elements in the 7Ru/$SrTiO_3$-C-24h and 7Ru/$SrTiO_3$-MW-1h samples, high-angle annular dark-field scanning transmission electron microscopy (HAADF-STEM) images and energy dispersive X-ray (EDX) elemental maps have been produced. **Fig. 4.3** and **4.4** show the HAADF-STEM and EDX mapping of the 7Ru/$SrTiO_3$-C-24h and 7Ru/$SrTiO_3$-MW-1h catalysts, respectively. As shown in **Fig. 4.3**, for 7Ru/$SrTiO_3$-C-24h, the distribution of Ru, Sr, Ti and O elements is non-homogeneous indicating the random dispersion of the Ru element over the perovskite support. On the other hand, the 7Ru/$SrTiO_3$-MW-1h catalyst (**Fig. 4.4**) shows a homogeneous dispersion of all the elements, suggesting that stirring the mixture during the hydrothermal synthesis is crucial for proper dispersion of Ru. Therefore, not only MW irradiation improved the catalyst preparation in terms of time and energy, but also stirring enables good dispersion of the elements.

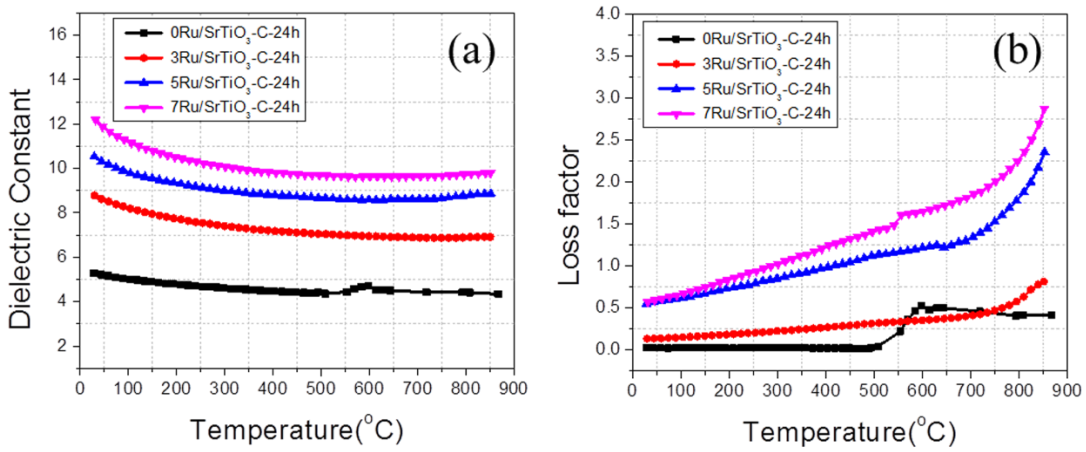

Figure 4.2. (a) Dielectric constant versus temperature and (b) loss factor versus temperature for the yRu/$SrTiO_3$-C-24h catalyst series.

Finally, the morphology of both catalysts prepared under conventional(C) and MW hydrothermal synthesis methods are compared. **Fig. 4.5** shows TEM images and particle size distributions of 7Ru/$SrTiO_3$-C-24h (**a, c**) and 7Ru/$SrTiO_3$-MW-1h (**b, d**). The 7Ru/$SrTiO_3$-C-24h catalyst, prepared under conventional heating, shows a wider range of particles sizes, from around 120 nm to around 300–500 nm particles (in lower proportion). 7Ru/$SrTiO_3$-MW-1h shows a more homogeneous particle size distribution of around 100 nm. The production of bigger particles shown in **Fig. 4.5(a, c)** might be due to the longer hydrothermal reaction time and higher temperatures than in the case of MW heating, where the shorter reaction time and lower temperature result in more homogeneous particle sizes due to the stirring effect. Nonhomogeneous particles sizes and bigger particles could favour nonhomogeneous MW field distribution during the reaction. In the case of 7Ru/$SrTiO_3$-MW-1h, the homogeneous distribution of Ru and the homogeneous particle size with better dielectric properties could contribute to better heat transfer in the catalyst bed under MW irradiation. Therefore, only the 7Ru/$SrTiO_3$-MW-1h catalyst has been selected for the microwave-assisted methane dry reforming reaction.

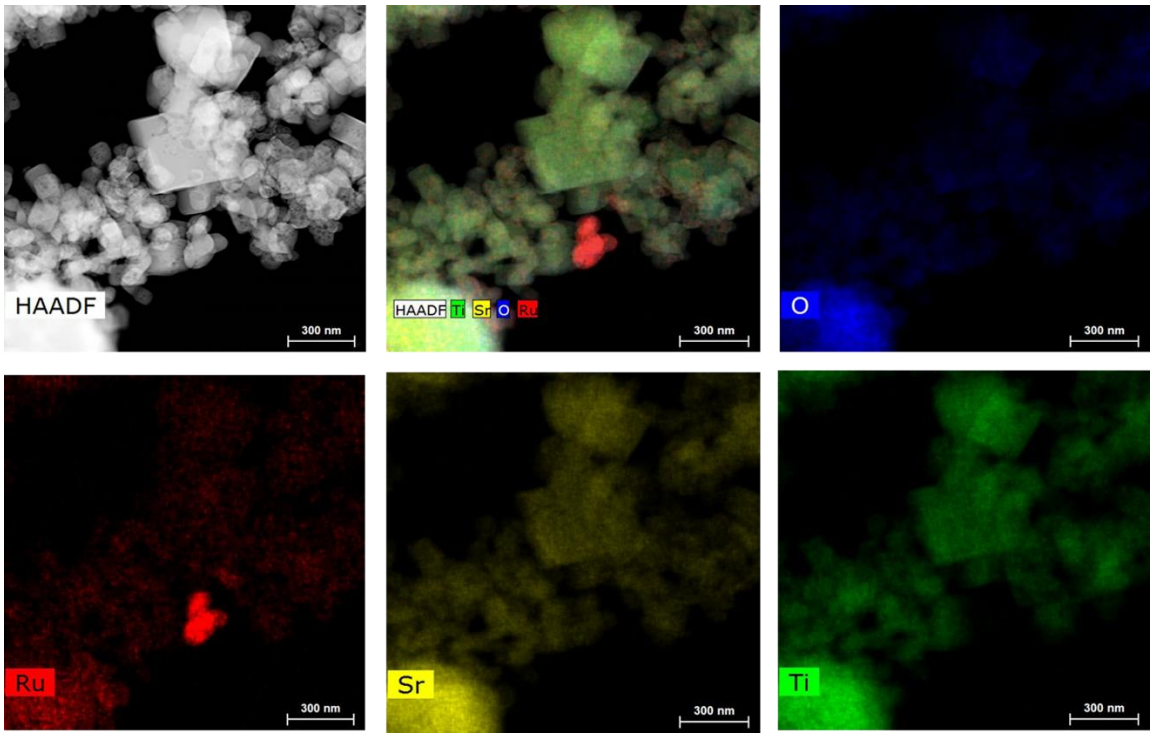

Figure 4.3. HAADF-STEM image and EDX elemental maps of O, Ru, Sr, and Ti for the 7Ru/$SrTiO_3$-C-24h catalyst.

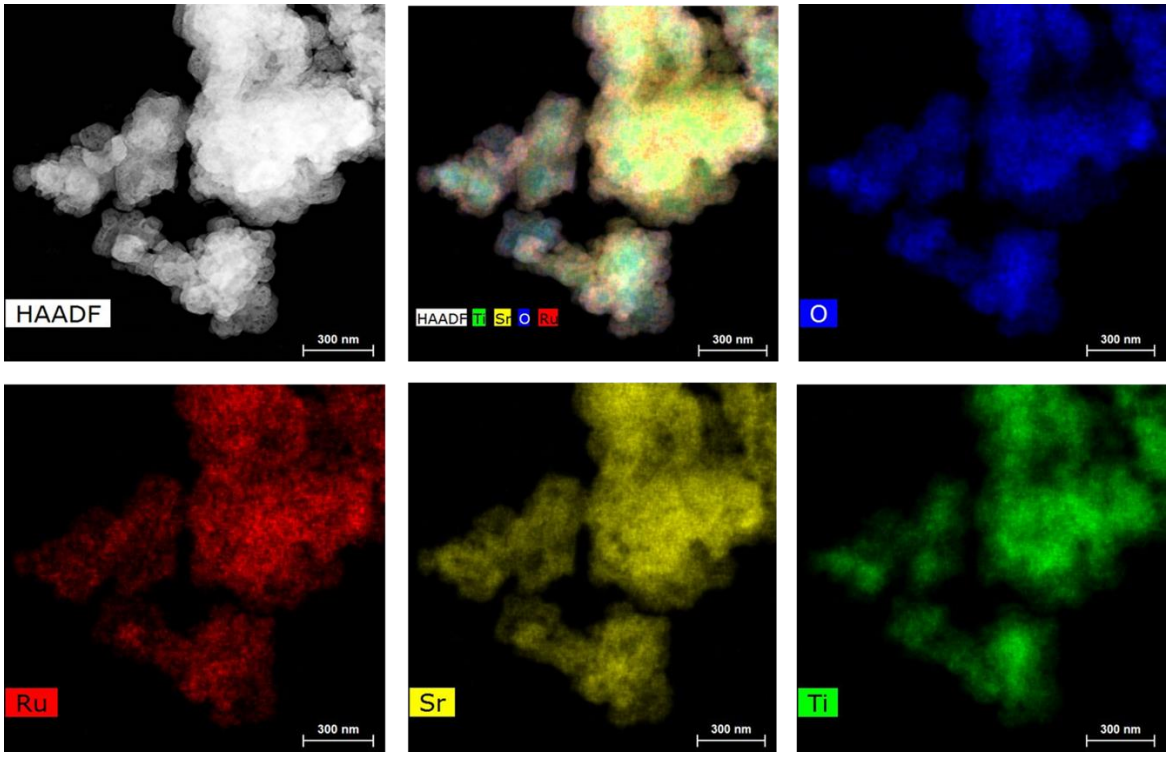

Figure 4.4. HAADF-STEM image and EDX elemental maps of O, Ru, Sr, and Ti for the 7Ru/$SrTiO_3$-MW-1h catalyst.

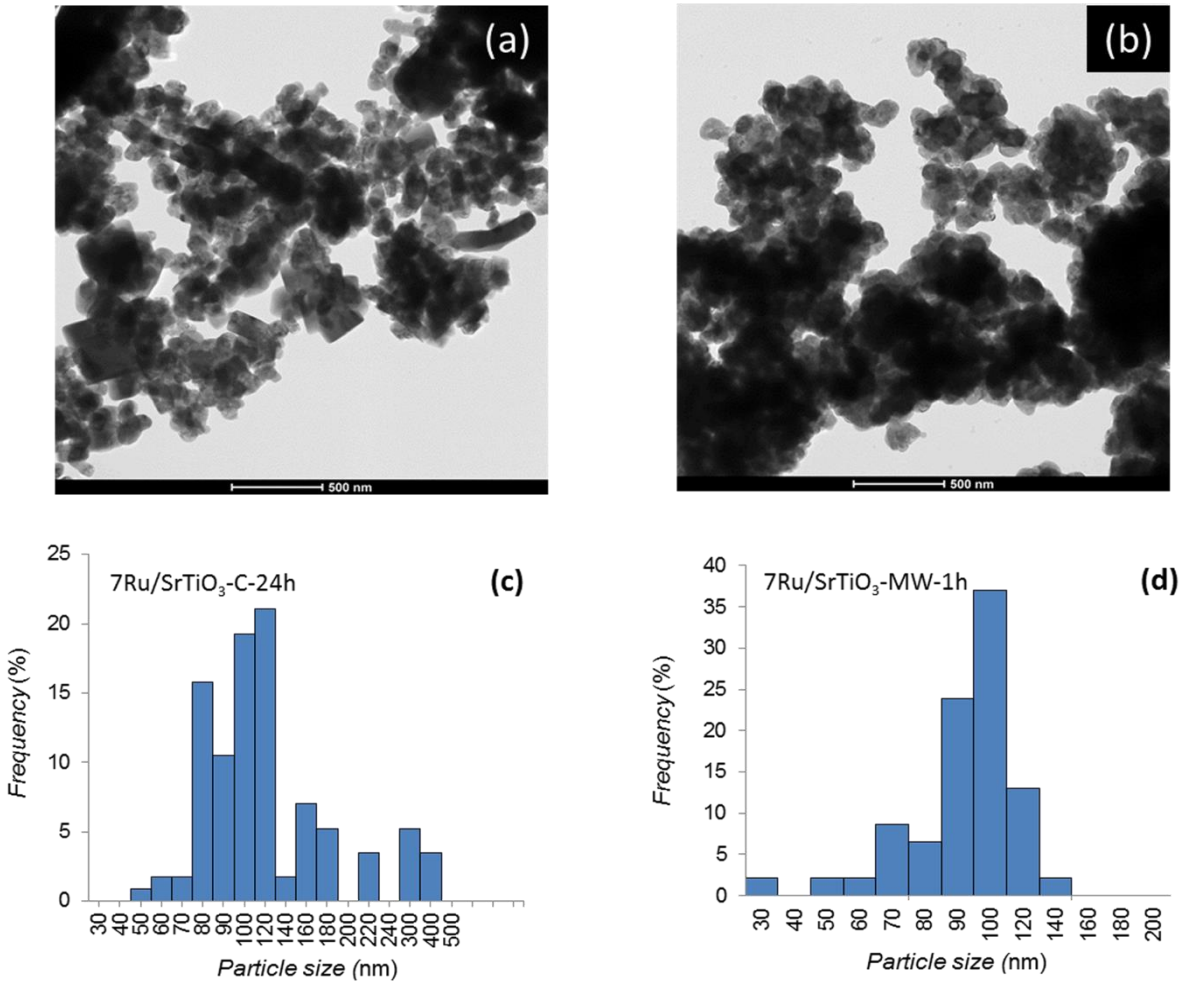

Figure 4.5. TEM images and particle size distributions of 7Ru/$SrTiO_3$-C-24h (a, c) and 7Ru/$SrTiO_3$-MW-1h (b, d)

4.3.2. Catalytic reactor performance

4.3.2.1 Reactor thermal response at varying MW input

A parametric study with variable MW power input was performed to a) obtain understanding of the thermal response of the catalytic bed as function of MW power at real reaction conditions and avoid any kind of quartz reactor damage due to overheating [63,98]; b) find the power settings at which reactor temperature is high enough to maximize reactants conversion. **Fig. 4.6** shows (a) CH_4 and CO_2 conversion and (b) H_2/CO ratio and temperature of the catalytic bed under real reaction conditions of the methane dry reforming process as function of MW power in the range 30 to 90 W. Each MW power was tested for 20 min and then increased by 10 W up to 90 W.

Fig. 4.6a shows that CH_4 and CO_2 conversions expectedly increase with increasing MW power and CO_2 conversion is always lower than that of CH_4. **Fig. 4.6b** shows that the H_2/CO ratio

increased from 0.60 to 0.89 and remained ~0.86 at ~90 W where the top bed temperature observed was 1067.6 °C (**Fig. 4.6b**). **Fig. 4.6b** shows that the temperature at the top of the catalytic bed increased with increasing MW power from 414.9 °C at 30 W to 1067.6 °C at 90 W. As temperature distribution is not homogeneous in the catalytic bed, the reaction will not be occurring homogeneously over the catalytic bed. Therefore, it was found from this study that in order to reach a temperature of ~1000 °C or get maximum reactants conversions, a minimum power of 90 W is required.

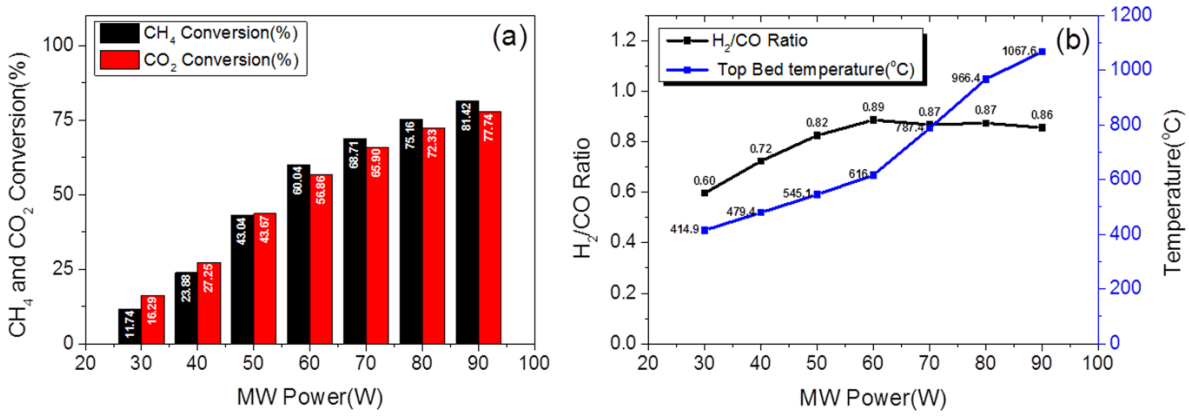

Figure 4.6. Effect of microwave power on (a) CH_4 and CO_2 conversion, (b) H_2/CO ratio and temperature at the top of the bed for the 7Ru/$SrTiO_3$-MW-1h catalyst. (Reaction conditions: CH_4:CO_2 vol. % feed ratio 50:50, GHSV = 3000 $cm^3g^{-1}h^{-1}$)

4.3.2.2 Effect of CO_2 concentration in the feed

Fig. 4.7 shows the effect of CO_2 concentration in the gas feed on the reactants conversion and the temperature at the top of the reactor filled with the 7Ru/$SrTiO_3$-MW-1h catalyst. The total flow of reactant gas mixture was 50 ml/min with a constant MW power of 90 W. The CO_2 concentrations (vol. %) applied were 45, 50, 55 and 60 % in total flow. Each flow has been applied for 30 min. It has been reported in the literature that CH_4 conversion decreases after a long reaction time due to carbon deposition [99][100]. Carbon deposition or coke formation during the DRM process is the major reason for deactivation of the catalytic sites in conventional heating.

Dry reforming of methane ($CH_4 + CO_2 \leftrightarrow 2H_2 + 2CO$) involves combination of two reactions namely, catalytic methane decomposition ($CH_4 \rightarrow C + 2H_2$) and CO_2 gasification ($C + CO_2 \leftrightarrow 2CO$) [36]. It has been reported that under microwave heating, increasing concentration of CO_2 in the reaction mixture results in increased gasification rate of the deposited carbon and thereby faster regeneration of the active sites and increase in CH_4 conversion [36][37][101]. This is in agreement with our experimental results too. **Fig. 4.7a** and **b** show that as CO_2 concentration (vol. %) increases from 45 to 60% at constant MW power input of 90 W, CH_4 conversion increases from 69.37 to 93.91%, while H_2/CO ratio decreases from 0.97 to 0.81 and the temperature at the top of the bed decreases from 702 to 657.5 °C.

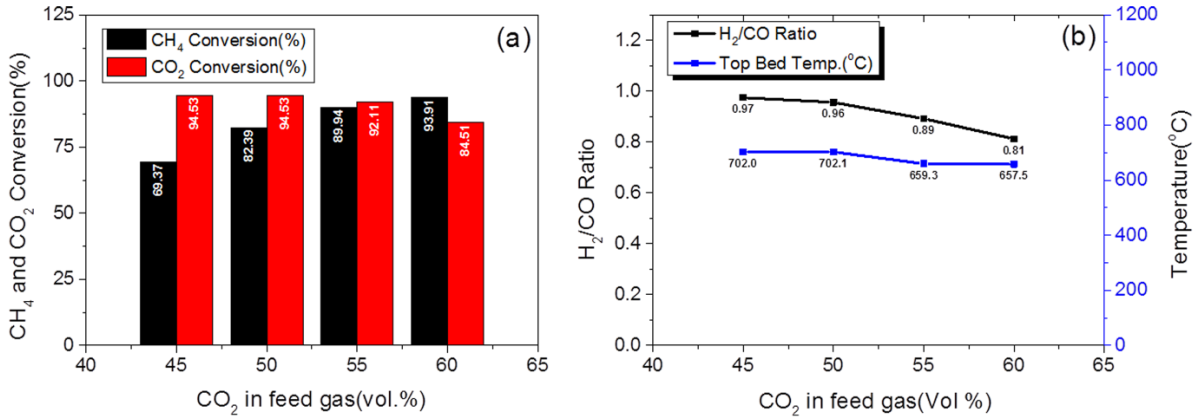

Figure 4.7. Effect of CO_2 concentration (vol. %) on (a) CH_4 and CO_2 conversion, (b) H_2/CO ratio and temperature at the top of the bed for the 7Ru/$SrTiO_3$-MW-1h catalyst. (Reaction Conditions: GHSV = 3000 $cm^3g^{-1}h^{-1}$, MW power: 90 W)

4.3.2.3 Gas hourly space velocity (GHSV) study

Fig. 4.8 shows the effect of total GHSV on (a) CH_4 and CO_2 conversion, (b) H_2/CO ratio and the temperature at the top of the catalytic bed for the 7Ru/$SrTiO_3$-MW-1h catalyst. Increase in the total flow requires higher MW power input to maintain a targeted top bed temperature and high conversions. The GHSV and corresponding powers applied are reported in **Table 4.3**. As we observed that a temperature of ~700 °C at the top of the catalytic bed was the optimum one to get maximum conversions, we tried to maintain that temperature, and therefore power has been increased or decreased as per the behavior of the catalytic material to maintain the targeted top catalytic bed temperature.

Each flow has been applied for 30 min. **Fig. 4.8a** shows that CH_4 and CO_2 conversions were high up to a total GHSV of 10500 $cm^3g^{-1}h^{-1}$, but at 12000 $cm^3g^{-1}h^{-1}$, the conversions dropped at ~61.78% and ~63.57% for CH_4 and CO_2, respectively. Lower conversions accompanied by a simultaneous increase in temperature, as the reaction is endothermic, were observed for the last two (highest) GHSV tests, which indicates that the reactants residence time is not sufficient to reach the high conversions (>90%) obtained at GHSVs <10500 $cm^3g^{-1}h^{-1}$. Finally, **Fig. 4.8b** shows that an increase in the total GHSV does not have much influence on the H_2/CO ratio, which remained in the range from 0.85 to 0.9.

Table 4.3: GHSV study with CH_4:CO_2 vol. % feed ratio 45:55 and corresponding MW powers applied.

Test. No.	Total flow (ml/min)	MW Power used (W)	Total GHSV ($cm^3g^{-1}h^{-1}$)
1	50	90	3000
2	75	105	4500
3	100	110	6000
4	125	120	7500
5	150	135	9000
6	175	150	10500
7	200	165	12000
8	225	160	13500

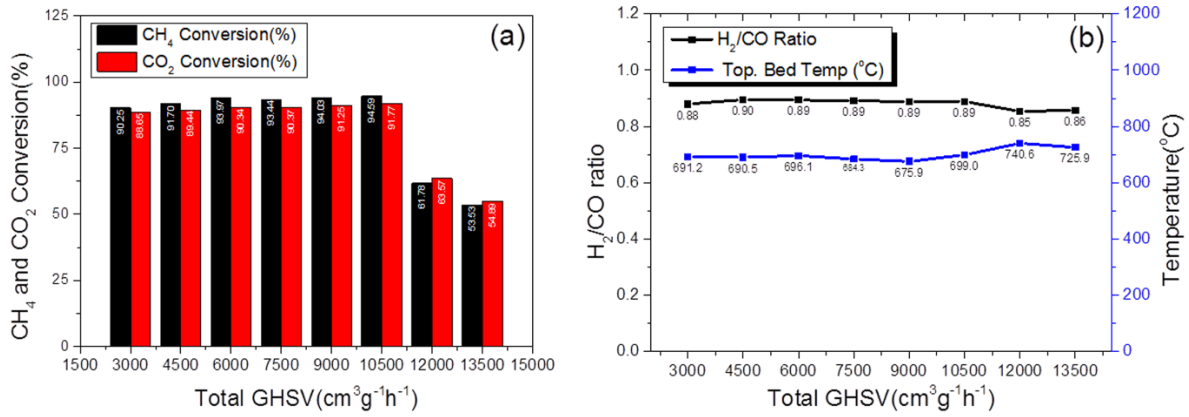

Figure 4.8. Effect of total GHSV on (a) CH_4 and CO_2 conversion, (b) H_2/CO ratio and temperature at the top of the catalytic bed for the 7Ru/$SrTiO_3$-MW-1h catalyst. (Reaction conditions: CH_4:CO_2 vol. % feed ratio 45:55; corresponding MW powers applied are specified in Table 4.3)

4.3.2.4 Catalyst stability study

Fig. 4.9 shows time-on-stream (TOS) evolution of (a) CH_4 and CO_2 conversions, (b) top and bottom thermocouple temperatures of the catalyst bed, (c) MW power and the H_2/CO ratio and (d) % MW energy utilization efficiency during methane dry reforming on the 7Ru/$SrTiO_3$-MW-1h catalyst. The TOS study has been performed at GHSV = 9000 $cm^3g^{-1}h^{-1}$, MW Power 150 W and CH_4:CO_2 vol. % feed ratio of 45:55. It was concluded from the GHSV study presented in **Table 4.3** that maximum conversion at 9000 $cm^3g^{-1}h^{-1}$ GHSV requires MW power of 135 W. Therefore, the reaction was initially started with 135 W, and after some time, the MW power was increased to 150 W, corresponding to a top thermocouple temperature of ~500 °C, as shown in **Fig. 4.9b**, to maintain maximum conversions of reactants.

Fig. 4.9a and **c** show that the CH_4 and CO_2 conversions depend on the MW power applied. **Fig. 4.9d** shows that 100% microwave energy utilization efficiency was achieved during 180 min of TOS due to the excellent MW absorption ability of the catalyst and the reactor configuration that allows for concentration of the MW field on the catalyst itself. Both reactants conversions increased with increase in the MW power and reached maximum values at 150 W. **Fig. 4.9a** shows that CO_2 conversion was lower than CH_4, due to the excess of CO_2 in the feed (CH_4:CO_2 vol. % feed ratio 45:55) during the stability test. As a result, the H_2/CO product ratio was lower than one (~ 0.9).

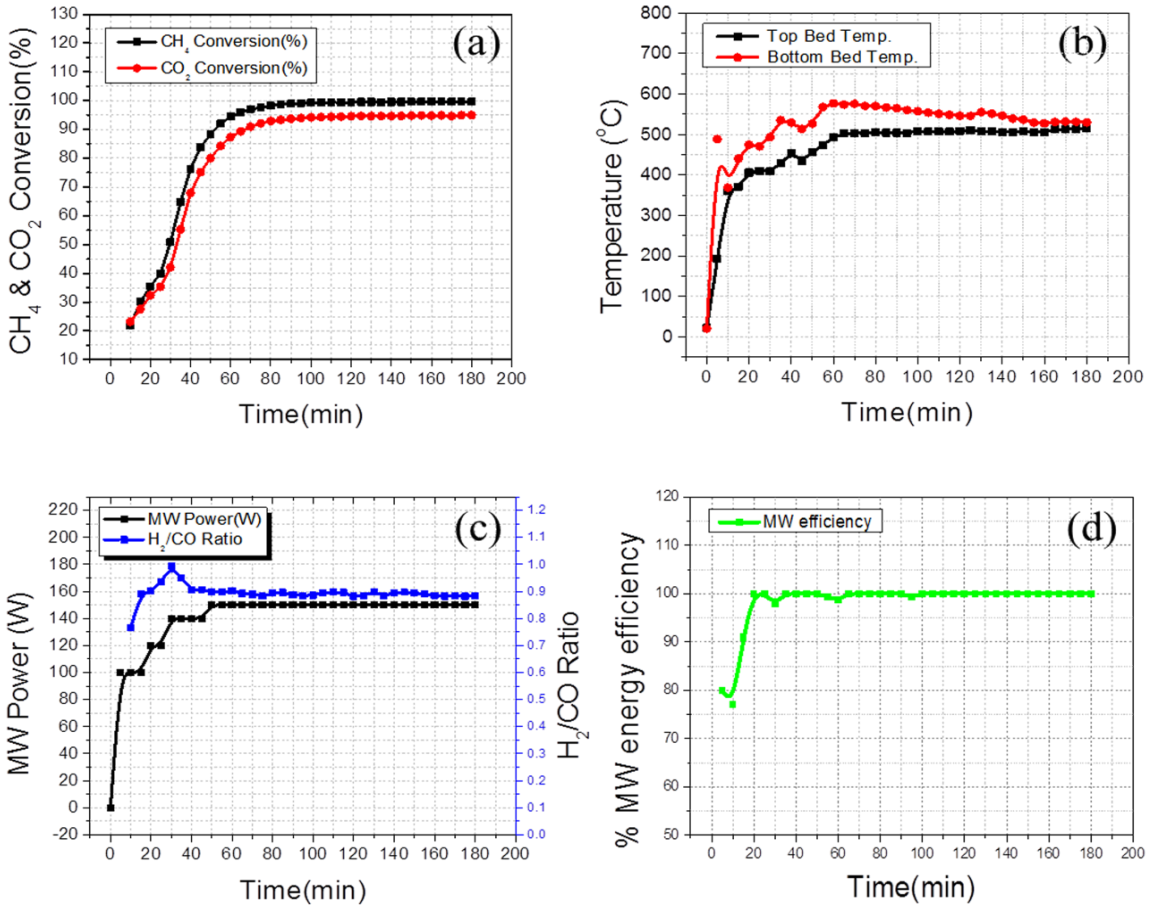

Figure 4.9. Time-on-stream (TOS) evolution of (a) CH_4 and CO_2 conversions, (b) top and bottom thermocouple temperature of the catalyst bed, (c) MW power and the H_2/CO ratio, and (d) % MW energy utilization efficiency during methane dry reforming over the 7Ru/$SrTiO_3$-MW-1h catalyst. (Reaction conditions: CH_4:CO_2 vol. % feed ratio 45:55, GHSV = 9000 $cm^3g^{-1}h^{-1}$, MW Power: 150 W)

Zhang et al. studied CO_2 reforming of methane on Pt-based catalysts using microwave heating [34]. They reported that the higher reactants conversions under microwave heating, compared to conventional heating, is attributed to the formation of hot spots, which are at a higher temperature than the average catalytic bed temperature [34]. Therefore, to verify such temperature gradients during the stability test, the temperature distribution in the catalytic bed was monitored by a thermal camera in a 2D fashion. The following section (**4.3.3**) provides a more detailed explanation of hotspots generation and the induced spatial temperature deferences.

In addition to MW hotspot effect, placement of Ru in the perovskite structure also plays an essential role as it prevents metal sintering at high temperatures (~800 °C)[84]. The improved catalytic behavior of the Ru-containing catalysts could be related to the participation of bulk oxygen during the reaction that enhances reactants adsorption [90]. Further, the constant removal of carbon deposits under MW heating promotes catalyst regeneration. Therefore, the stable high conversions observed at relatively low top bed temperature ~500 °C are due to the presence of hot spots in the catalyst bed, the stability of perovskite structure that prevents sintering, the good redox properties of the perovskite catalyst, and, possibly, the regeneration of the active catalytic sites due to continuous coke removal through CO_2 gasification under MW heating [37].

4.3.3. Hotspot detection and temperature gradient analysis

Fig. 4.10 shows the migration of hot spots at (a) 5, (b) 15, (c) 85 and (d) 180 min in the 7Ru/$SrTiO_3$-MW-1h catalyst bed during the stability test. As thermocouples are placed at the top and bottom part of the catalytic bed, they cannot measure hot spot temperatures inside the catalytic bed. Therefore, we have used the thermocouple and thermal camera dual approach to measure or track the thermal changes occurring in the catalytic bed [54]. **Table 4.4** presents the calculated differences in the hot spot temperatures and the top and average bed temperatures corresponding to the thermal images of **Fig. 4.10**. All the average bed temperatures and average hot spot temperatures are calculated with a constant emissivity value of 0.8. A more detailed presentation of the thermal camera measurements is given in our recently published article [54].

Fig. 4.10a shows that, during the stability test, hotspot generation starts from the bottom part of the catalytic bed (first 5 minutes). At 15 min, the hotspot position is detected at the center of the catalytic bed (**Fig. 4.10b**) and at 85 minutes, two hotspots are observed, one at the center and one at the bottom part of the catalytic bed (**Fig. 4.10c**). Finally, at 180 min, one extended hotspot is observed at the bottom part of the catalytic bed (**Fig. 4.10d**). The change in the position of the maximum temperature area inside the reactor results in a change in the temperature readings of the top and bottom thermocouples, but, as expected based on **Fig. 4.10**, the temperature measured by the top thermocouple is always lower than that of the bottom one (**Fig. 4.9b**).

As specified in **Table 4.4**, the top thermocouple temperatures reported at 5, 15, 85 and 180 min are 192.5, 370.6, 504.1 and 514.7 °C, respectively. The average catalytic bed temperatures calculated by thermal camera analysis are 474.8, 736.37, 849.07 and 828.04 °C. Therefore, it is clear that one-point measurement in case of microwave heating will always provide local temperature values. Hence the comparison of MW heated reactions with conventionally heated reactions using point sensors like thermocouples or optical fibers can be misleading. The temperature difference observed between the average hotspot temperature, and the average catalytic bed temperature is in the range of 77 to 117 °C. The average hotspot and (top) thermocouple temperature difference is

in the range of 386.5 to 442.78 °C, which is difficult to trace by point sensors. Therefore, the maximum attained conversions of ~ 99.5% and ~ 94% for CH_4 and CO_2 at ~500 °C, a temperature relatively lower than the required temperature range, are due to the presence of hotspots in the temperature range 813.38 to 942.3 °C detected by thermal camera 2D monitoring. The primary reason for hot spot formation might be the uneven microwave field distribution in the catalytic bed. Santos et al. performed 3D electromagnetic field simulation of a ceramic sample in a microwave oven using COMSOL software and reported that the electromagnetic field pattern changes during MW heating, and so, the hot spots have some type of dynamic behavior [102][103]. The second reason could be the areas where coke formation might have occurred during the MW power variation study. As carbon (coke) is a good MW absorber, it might either generate hot spots or get gasified during the stability test, giving rise to hotspot migration (**Fig. 4.10**).

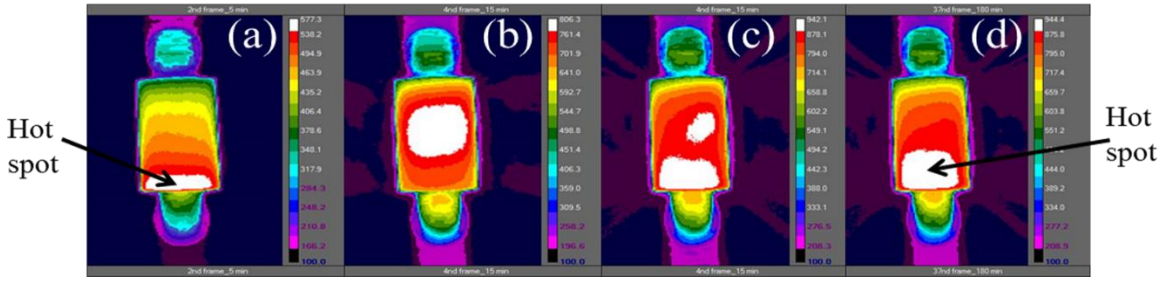

Figure 4.10. Migration of hot spots during stability test over 7Ru/$SrTiO_3$-MW-1h catalyst at (a) 5, (b) 15, (c) 85 and (d) 180 minutes. (Reaction conditions: CH_4:CO_2 vol. % feed ratio 45:55, GHSV = 9000 $cm^3g^{-1}h^{-1}$, MW Power: 150 W)

Table 4.4: Differences in average hotspot temperature, average catalytic bed temperature, and top and bottom thermocouple temperatures. (Thermal data processed at emissivity 0.8).

Image No	Time (min)	Thermocouple Temperatures(°C)		Average bed temp(°C)	Average hotspot temp (°C)	Average hotspot and average bed temp diff. (°C)	Average hotspot and top thermocouple temp diff. (°C)
		Top T	Bottom T				
(a)	5	192.5	488.5	474.8	579.0	104.25	386.5
(b)	15	370.6	440.4	736.37	813.38	77.01	442.78
(c)	85	504.1	566.6	849.07	936.4	87.38	432.3
(d)	180	514.7	529.7	828.04	942.3	117.3	427.6

4.3.4. Energy consumption comparison

Table 4.5 shows a comparison of the newly synthesized perovskite catalyst with carbon-based catalysts reported in the literature for microwave-assisted methane dry reforming [89]. It is shown that H_2 throughput is improved in the case of 7Ru/$SrTiO_3$-MW-1h. The amount of catalyst used in the present work has been reduced from 12–15 g to only 1 g in previous studies [89]. The catalytic stability test has been performed at 9000 GHSV as compared to 400 and 3000 GHSV in the case

of FY5 (activated carbon) and activated carbon mixed with Ni/Al_2O_3 catalyst, respectively (**Table 4.5**). The scale-up energy consumption and H_2 production values based on our experimental results are calculated in a similar way (included as supporting information) as in Fidalgo et al. [89] and compared with the results in [89]. **Table 4.6** presents a comparison on H_2 production and energy consumption in the case of perovskite catalyst and the carbon-based catalysts. Calculations are done on the basis of 1 m^3h^{-1} CH_4 flow rate. The H_2 throughput produced by FY5 is 0.3 $m^3h^{-1}kg^{-1}$ vs. 8.1 $m^3h^{-1}kg^{-1}$ (27 times higher) in the case of $7Ru/SrTiO_3$-MW-1h. The estimated energy consumption is 44.4 kW h m^{-3} of H_2 produced for FY5 vs. 18.58 kW h m^{-3} of H_2 produced (2.38 times less) for $7Ru/SrTiO_3$-MW-1h.

Table 4.5: Catalytic performance comparison of the perovskite catalyst with carbon-based catalysts reported in the literature for microwave-assisted methane dry reforming.

Catalyst used	Thermo-couple Temp. (°C)	Feed composition (vol. %)		Amount of catalyst (g)	Flow of CH_4 (ml/min)	Total GHSV cm^3h^{-1} g^{-1}	Total VHSV Lh^{-1} g^{-1}	MW Power (kW) used at 2.45 GHz	Reactant conversions in %		Reference
		CH_4	CO_2						CH_4	CO_2	
FY5 (Activated carbon)	700	40	60	15	40	400	0.4	13.5	96.2	97	[89]
50%FY5 + 50% Ni/Al_2O_3	800	50	50	12	300	3000	3	11.8	88.1	93.3	[89]
$7Ru/SrTiO_3$-MW-1h	500	45	55	1	67.5	9000	9	0.150	99.5	94	This work.

Table 4.6: Energy consumption and H_2 production comparison of the perovskite catalyst with carbon-based catalysts reported in the literature.

Catalyst	FY5 (Activated carbon)	50%FY5 + 50%Ni/Al_2O_3	$7Ru/SrTiO_3$-MW-1h	Units
Reference	[89]	[89]	This work	-
Calculation basis	1	1	1	m^3 h^{-1} of CH_4
Volume of reactor	912.73	912.73	58.27	cm^3
Amount of catalyst	6.25	0.7	0.2466	kg
Mass inflow rate of CH_4	0.72	0.72	0.72	kg h^{-1}
Mass outflow rate of H_2	0.17	0.16	0.18	kg h^{-1}
Volume outflow rate of H_2	1.92	1.762	1.99	m^3 h^{-1}
Volume outflow rate of H_2 per kg of catalyst	0.3	2.6	8.1	m^3 $h^{-1}kg^{-1}$
H_2/CO ratio	0.66	1	0.9	-
Supplied power to the reactor	84.4	8.3	36.99	kW
Energy consumption w.r.to CH_4 flow	84.4	8.3	36.99	kW h m^{-3} of CH_4
Energy consumption w.r.to H_2 flow	44.4	4.6	18.58	kW h m^{-3} of H_2

4.4. Conclusions

In this work, a series of ruthenium-doped strontium titanate perovskite catalysts were synthesized by conventional and microwave-assisted hydrothermal methods. Significant synthesis temperature and time reduction from 220 °C for 24 h in conventional heating to 180 °C for 1 h under microwave heating were achieved. XRD analysis of the catalyst powder confirmed the presence of Ru in the $SrTiO_3$ perovskite structure in all synthesized catalysts. Increase in the dielectric property values were observed with increase in ruthenium content and temperature. Higher dielectric property values were obtained for the 7 wt. *%* Ru-doped $SrTiO_3$ catalyst in a tested catalyst series with variable Ru content. Further, ICP-OES analysis and HRTEM+EDX elemental mapping showed improved Ru dispersion and more homogeneous distribution of particle sizes, respectively, in the case of MW-assisted hydrothermal synthesis as compared to the conventional hydrothermal synthesis.

Based on the aforementioned dielectric and chemical characterization study, microwave-assisted methane dry reforming was performed on the 7 wt. % Ru-doped $SrTiO_3$ perovskite catalyst (7Ru/$SrTiO_3$-MW-1h). The influence of different CH_4:CO_2 vol. % feed ratios were studied with respect to their impact on CH_4 conversion. The CH_4:CO_2 vol. % feed ratio 45:55 was found to maximize methane conversion. Different gas hourly space velocities (GHSVs) of total reactant flows were investigated too. Maximum conversions of ~99.5*%* and ~94*%* for CH_4 and CO_2, respectively, were achieved during a 3h stability test at 9000 $cm^3g^{-1}hr^{-1}$ GHSV, with the selected 7 wt. % Ru-doped $SrTiO_3$ catalyst, which was exposed at maximum temperatures in the vicinity of 940 °C. Scale-up calculations on the basis of 1 m^3h^{-1} CH_4 inlet flow rate, as previously set in the literature Ref. [89], on the 7Ru/$SrTiO_3$-MW-1h catalyst show significant improvement in H_2 production capability as compared to carbon-based catalysts.

4.5. Supporting Information

Energy Consumption calculations

Table 4.7: Experimental testing conditions with different units for comparison purpose.

Total Flow rate	150 ml/min	9 Lh^{-1}	9000 cm^3h^{-1}
CH_4 Flow rate	67.5 ml/min	4.05 Lh^{-1}	4050 cm^3h^{-1}
CO_2 Flowrate	82.5 ml/min	4.95 Lh^{-1}	4950 cm^3h^{-1}
Weight of Catalyst used	1 g	0.001 kg	0.001 kg
MW Power Supplied	150 W	0.150 kW	0.150 kW
GHSV	-	9 $Lg^{-1}h^{-1}$	9000 $cm^3g^{-1}h^{-1}$
CH_4:CO_2 Volume % ratio used	-	-	45:55
CH_4 conversion	-	-	99.5 %
CO_2 conversion	-	-	94%

The volume of quartz reactor used in reference [89]

$$\text{The volume of quartz tube} = \pi \times (Diameter)^2 \times Length$$
$$= \pi \times (2.6\ cm)^2 \times 43\ cm = \mathbf{912.73\ cm^3}$$

The volume of quartz reactor used in our work

$$\text{The volume of quartz tube} = \pi \times (Diameter)^2 \times Length$$
$$= \pi \times (0.8\ cm)^2 \times 29\ cm = \mathbf{58.27\ cm^3}$$

Scale up calculations

For 1 m^3h^{-1} of CH_4 reforming:

To perform the reforming of 1 m^3h^{-1} of CH_4 inlet flow rate at 9 $Lg^{-1}h^{-1}$ VHSV space velocity, the required amount of catalyst is calculated as follows

Note: we need to consider 45:55 volume % of CH_4: CO_2 ratio. Therefore, the total flow rate of the reactants becomes 2.22 m^3h^{-1}.

$$\text{VHSV} = \frac{Total\ flow(m^3h^{-1})}{Amount\ of\ catalyst(kg)} = 9\ Lh^{-1}g^{-1} = \frac{2.22\ m^3h^{-1}}{Amount\ of\ catalyst(kg)}$$

$$Amount\ of\ catalyst = \frac{2.22\ m^3h^{-1}}{9\ Lh^{-1}g^{-1}} = 0.2466\ kg$$

Therefore, 0.2466 kg of 7Ru/$SrTiO_3$-MW-1h catalyst will be needed to process a total flow rate of 2.22 m^3h^{-1} of 45%CH_4-55%CO_2.

We used 150 W of MW power for 1 g of the catalyst at 9 $Lh^{-1}g^{-1}$ GHSV. The power needed to keep the reaction system running at 2.22 m^3h^{-1} total flow is calculated as

$$\text{Specific Power} = \frac{Power\ required\ for\ 2.22\ m^3h^{-1}}{Amount\ of\ Catalyst\ used}$$

Therefore if we assume our specific power is 150 $kWkg^{-1}$.

$$150\ (\text{kWk}g^{-1}) = \frac{Power\ Required(kW)}{0.2466\ kg}$$

Then, the power required for 1m^3h^{-1} CH_4 conversion is 36.99 kW.

The hydrogen flowrate based on 1 m^3 hr^{-1} CH_4 flowrate and experimentally obtained CH_4 conversion is calculated as

$$\text{Flow rate of hydrogen} = \text{inlet } CH_4 \text{ flow rate} \times \%\ CH_4 \text{ Conversion} \times 2$$

Flow rate of hydrogen = 1 m^3hr^{-1}×0.995×2 = 1.99 m^3hr^{-1}

Energy Consumption w.r.t 1 m^3 hr^{-1} CH_4 flow keeping VHSV constant

$$\text{Energy Consumption w. r. t } CH_4 \text{ flow} = \frac{Power\ required(kW)}{Flowrate\ of\ methane(m^3h^{-1})} = \frac{36.99}{1} = 36.99\ \text{kW h m}^{-3}$$

Energy Consumption w. r. t H_2 flow keeping VHSV constant

$$\text{Energy Consumption w. r. t. } H_2 \text{ flow} = \frac{Power\ Required(kW)}{Flowrate\ of\ Hydrogen(m^3h^{-1})} = \frac{36.99}{1.99} = 18.58\ \text{kW h m}^{-3}$$

The density of CH_4 at NTP is 0.668 and at STP is 0.717 kg/m^3

The density of H_2 at NTP is 0.0899 and at STP is 0.0899 kg/m^3

Therefore, the inlet flow rate of CH_4 in terms of kg h^{-1} is calculated by its density

Density = $\frac{Mass(kg)}{Volume\ (m^3)}$ = 0.717 = $\frac{Mass(kg)}{1\ (m^3)}$

Therefore, the mass flow rate of CH_4 is 0.72 kg/h.

The mass flow rate of hydrogen produced is calculated from

0.0899 = $\frac{Mass(kg)}{1.99(m^3)}$

So, H_2 is produced at 0.18 kg/h.

The amount of H_2 produced per kg of the catalyst is calculated from

H_2 Produced per kg cat. = $\frac{\text{Outlet } H_2 \text{ flow in } m^3h^{-1}}{\text{Amount of catalyst in kg}} = \frac{1.99\ m^3h^{-1}}{0.2466\ \text{kg cat.}} = 8.1\ m^3h^{-1}kg^{-1}$

5

5. CO_2 reforming of CH_4 under microwave heating over hybrid catalytic systems of ruthenium-doped $SrTiO_3$ and nickel supported catalysts

Abstract

In this work, we test combinations of four commercial nickel-supported metal oxide catalysts (Ni/Al_2O_3, $Ni/CaAl_2O_4$, Ni/Al_2MgO_4 and Ni/SiO_2-Al_2O_3) with a 7 wt. % Ruthenium (Ru)-doped $SrTiO_3$ perovskite catalyst as hybrid catalytic systems for syngas production by CO_2 (dry) reforming of CH_4 under microwave (MW) heating. First, the dielectric properties of the nickel-based commercial catalysts were investigated to determine their microwave absorption ability and potential for microwave heating. The experimental results showed that the introduction of the Ru-doped perovskite catalyst plays an essential role in improving the microwave heating ability of the hybrid systems under typical dry reforming temperatures (up to 850 °C). The four catalytic systems were also evaluated under dry reforming reaction conditions in terms of CH_4 and CO_2 conversion and H_2/CO ratio as a function of MW power, gas hourly space velocity (GHSV) and time on stream. The combination of $Ru/SrTiO_3$ and Ni/Al_2O_3 was found to form the best hybrid catalyst system in terms of microwave absorption ability, syngas production capacity and catalytic stability. Finally, a comparative theoretical scale-up study shows improvement in H_2 production capacity in case of a combination of Ni/Al_2O_3 and $Ru/SrTiO_3$ as compared to the combination of Ni/Al_2O_3 and FY5.

Graphical Abstract:

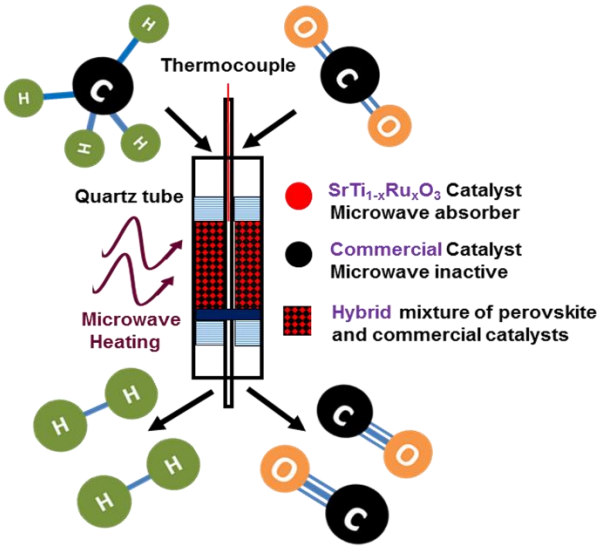

5.1. Introduction

Microwave (MW)-assisted dry reforming of methane (DRM) is a chemical process of interest in the context of power-to-chemical technologies [22] due to its high potential for methane and carbon dioxide valorization in an economic and sustainable manner [104][21][105]. The primary product of this reaction is syngas, which can be converted to a variety of chemicals through the Fischer-Tropsch process [106][107][108]. Due to the high temperatures required for the DRM reaction (700–1000 °C) [109][110][111], a catalyst with both good reactivity and dielectric properties (capacity to absorb microwaves and convert it into heat) are required. Carbon-based catalysts are commonly used for microwave-heated methane reforming reactions due to their excellent microwave absorption properties and good catalytic activity [107][111][48][112]. For these reasons, the combination of activated carbons with more active metal-based catalysts, such as nickel and platinum on various oxide supports has also been investigated. Hotspot generation and fast regeneration of active catalytic sites are the majorly reported effects in the literature responsible for higher CH_4 and CO_2 conversions under microwave heating as compared to conventional heating at similar reaction temperatures [37][71][34][56][36].

The main challenge with most of the common metal catalysts (e.g., Ni/Al_2O_3, $Ni/CaAl_2O_4$, Ni/Al_2MgO_4 and Ni/SiO_2-Al_2O_3) is that they cannot reach optimum reaction temperatures under MW exposure due to their poor dielectric properties [48]. In addition, they would not heat up comparably in a microwave reactor, which in turn hinders an accurate comparison among them and limits their eligibility for being used in a microwave reaction process. Further, an issue with carbon-based catalysts is that they form a pyrolytic carbon layer and, unavoidably, they are consumed during the reaction [37][112][54][113]. Noble metal-based catalysts like Pt and Ru are known to be good microwave absorbers, catalytically active and resistant to carbon formation, but also rather expensive and thus less attractive for industrial applications [54][114].

In an effort to intensify microwave-assisted dry reforming, we have investigated a hybrid catalytic approach in which different commercial and relatively inexpensive Ni-based catalysts, having poor microwave absorption capacity, are individually mixed with an in-house developed 7 wt. % Ru-doped perovskite catalyst ($Ru/SrTiO_3$) that has excellent microwave properties and catalytic activity. Mixing of the commercial and in-house catalyst particles can improve the heating of the catalyst bed as a whole, reduce susceptibility to coke formation, promote the activity of Ni-supported catalysts with a noble metal (Ru) and reduce the cost involved, as compared to using high content noble metal-based catalysts only [114]. The different combinations of the commercial Ni-based catalysts with the Ru-doped perovskite catalyst have been compared. The best catalyst pair has been selected, and the optimal heating and flow conditions have been identified. Finally, a catalyst performance test as a function of time on stream (TOS) has been carried out.

5.2. Experimental section

5.2.1. Catalytic systems and dielectric properties measurement method

Four different commercial Ni-supported metal oxide catalysts were used as received. **Table 5.1** summarizes the catalysts composition, the catalysts notation, and their supplier. In short, the selected commercial samples consist of nickel oxide supported on different inorganic supports such as alpha alumina (Katalco23) and calcium aluminate (Katalco57), provided by Johnson Matthey, magnesium aluminate (R-67-7H), supplied by Haldor Topsoe, and, finally, silica/alumina (Ni/SiO_2-Al_2O_3) purchased from Sigma Aldrich. The dielectric properties of these catalysts were measured in specially designed equipment at the Institute of Information and Communication Technologies (ITACA) of the University of Valencia, Spain [77]. The catalysts were heated from 20 °C to 850 °C with a heating rate of 20 °C/min under continuous N_2 flow. The dielectric properties were then determined based on the shift of the center of the resonant frequency and the quality factor of the microwave cavity due to the presence of material inside it with respect to an empty cavity [115–118]. In our previous work, an in-house developed 7 wt. % ruthenium-doped $SrTiO_3$ catalyst ($Ru/SrTiO_3$) was found to be an excellent heterogeneous catalyst for DRM under microwave heating [119]. Therefore, this catalyst was also used in the present work for comparison.

Table 5.1: Commercial catalysts used

Catalyst	Notation	Company/Supplier	Composition
Ni/Al_2O_3	Katalco23	Johnson Matthey	Nickel oxide(10-25%) on alpha alumina
$Ni/CaAl_2O_4$	Katalco57	Johnson Matthey	Nickel oxide(10-25%) on calcium aluminate
Ni/Al_2MgO_4	R-67-7H	Haldor Topsoe	Nickel oxide (>15 wt. %) on magnesium aluminate
Ni/SiO_2-Al_2O_3	$Ni\text{-}SiO_2/Al_2O_3$	Sigma Aldrich	Nickel (61-69 wt. %) on silica/alumina

5.2.2. Microwave reactor system

A schematic and photos of the parts comprising the custom microwave setup developed for the experiments are shown in the supporting information document (**Figure S5.1a and S5.1b**). For all experiments, 1 g of hybrid (mixed) catalyst (425–850 μm particle size) was fixed inside the reactor quartz tube (290 mm length × 8 mm i.d.) using quartz wool plugs. A solid-state microwave generator (Miniflow 200 SS, 2.45 GHz, 200 W max.) was used to deliver MW energy to the catalytic bed. Two N-type thermocouples (–200 to +1250 °C) were placed at the top and at the bottom part of the catalyst bed to measure the temperature at these positions. The surface temperature of the catalytic bed was monitored in 2D by a thermal camera, model FLIR A655sc (7.5–14 μm, –40 to 2000 °C). The temperature was recorded every 5 min during the experiments.

The reactants and products in the gas phase were analyzed online by a Varian CP4900 micro-GC, equipped with two columns, 20 m MS5A and 10 m PPU, and analyzed by a TCD detector. The conversion of CH_4 and CO_2 were calculated by **equations (5.2)** and **(5.3)**, respectively, considering only the global dry reforming of methane reaction (DRM) (**eq. 5.1**), after 5 min of time on stream.

Global DRM Reaction: $CH_4 + CO_2 \rightarrow 2CO + 2H_2$ $\Delta H_{298K} = +247$ kJ.mol^{-1} **(5.1)**

CH_4 Conversion, % = $100 \times [\frac{(H_2)Out}{2}]/[(CH_4)_{out} + \frac{(H_2)out}{2}]$ **(5.2)**

CO_2 Conversion, % = $100 \times [\frac{(CO)_{out}}{2}]/[(CO_2)_{out} + \frac{(CO)_{Out}}{2}]$ **(5.3)**

Where $(CH_4)_{Out}$, $(H_2)_{out}$, $(CO_2)_{out}$ and $(CO)_{out}$ are methane, hydrogen, carbon dioxide and carbon monoxide concentrations in the effluent gas (% by volume), respectively. H_2 and CO production in moles are calculated by equations (4) and (5), respectively.

H_2 in moles = CH_4 inlet flow in L $\times$ % CH_4 conversion $\times$ 2 $\times$ 22.414 L **(5.4)**

CO in moles = CO_2 inlet flow in L $\times$ % CO_2 conversion $\times$ 2 $\times$ 22.414 L **(5.5)**

The combination of both a thermal camera and two thermocouples placed at the top and at the bottom of the catalyst bed is used in all experiments performed. This dual approach is used for three reasons; 1) the thermocouples alone can only measure temperature at a single point outside of the catalytic bed due to the risk of thermocouple damage by formation of hot-spots in which temperature may exceed 1250 °C (the maximum thermocouple limit); 2) due to the formation and migrating nature of hot spots in the catalytic bed, recording of the spatial temperature distribution is necessary and this can only be enabled by the use of a thermal camera; 3) the emissivities of the quartz tube and the catalyst change during the reaction, resulting in inaccuracies in temperature measurements by the thermal camera alone [54]. Therefore, a feedback mechanism by thermocouples is needed. To this end, simultaneous temperature monitoring by a thermal camera and thermocouples was used to analyze temperature evolution and distribution during microwave-assisted DRM. The details of the approach are given in previous work (Ref. [54]).

5.2.3. Methane dry reforming reaction conditions

Table 5.2 summarizes the reaction conditions applied during microwave-assisted DRM over the four hybrid catalytic systems ($Ru/SrTiO_3$ + Ni-supported catalysts**)**. Four different test series have been carried out, denoted by series numbers 1 to 4 in **Table 5.2**; 1) thermal response of the catalytic materials under microwave heating, 2) evolution of microwave power and reactants conversion, 3)

gas hourly space velocity (GHSV) study and 4) reactor performance test as a function of time on stream. The standard reaction conditions are described in series number 0 (**Table 5.2**). All methane dry reforming reactions were performed at atmospheric pressure. It is important to note that the microwave power absorption response of each hybrid catalytic system is different, leading to different catalytic bed temperatures. The endothermic nature of the reaction and possible hot spot migration makes it very challenging to maintain the same stable temperature in different hybrid catalytic systems in order to compare them. Therefore, reactant conversions in each case were monitored until the highest conversions were attained, or temperatures ~1000 °C were reached. Hence different settings of MW power, temperature, and GHSV values are required for different hybrid catalytic systems in order for each of them to reach the best performance.

Table 5.2. Operating conditions for microwave-assisted methane dry reforming over the four hybrid catalytic systems of the four Ni-based commercial catalysts mixed in 1:1 ratio with 7 wt. % ruthenium-doped $SrTiO_3$ perovskite catalyst

Sr. No.	Test	Description	Ru/$SrTiO_3$ + Ni-supported catalyst
0	Standard reaction conditions	Catalyst amount / g	1
		particle size / μm	425–850
		Pressure / atm	~1
		CH_4:CO_2 vol. % ratio	45:55
		CH_4:CO_2 feed ratio	0.82
1	Thermal response of the catalytic materials under microwave heating	Nitrogen feed / cm^3_{STP}/min	50
		MW power / W	0–100
2	Evolution of microwave power and reactants conversion	CH_4:CO_2 vol. % ratio	45:55
		Total flow rate / cm^3_{STP}/min	50
		MW power / W	40-140
3	Gas hourly space velocity (GHSV) study	Total flow rate / cm^3_{STP}/min	50–150
		GHSV / cm^3_{STP}/h g $_{cat}$	3000–9000
		MW power / W	100–140
4	Reactor performance as a function of time on stream	Total flow rate / cm^3_{STP}/min	50–75
		GHSV / cm^3_{STP}/h g $_{cat}$	3000–4500
		MW power / W	100–140
		Total reaction time / min	180

The first test "thermal response of the catalytic materials under microwave heating" was a heating test conducted under nonreactive conditions (N_2 flow of 50 cm^3_{STP}/min) to approximately verify the power level at which the reaction temperature range was attained. In this test, power was increased by 5 W every 5 min. The second test ("evolution of microwave power and reactants conversion") was carried out to determine the power at which the catalysts were showing the highest CH_4 and CO_2 conversions for DRM. In this case, the microwave power was increased by 10 W every 20 min. The third test "gas hourly space velocity (GHSV) study" was carried out to determine the optimal total flow rate to reach maximum conversions. The GHSV test was carried out at the constant power determined in the "evolution of microwave power and reactants conversion" test. For each flow rate, the conversion was monitored for 30 min. The fourth test conducted was the "reactor performance test as a function of time on stream." This test was done under the optimal operating conditions for each catalyst, obtained from the previous experiments (tests 1, 2 and 3 described in **Table 5.2**), to determine catalyst stability over longer reaction times (~180 min) and verify possible catalyst deactivation.

5.3. Results and discussion

5.3.1. Dielectric properties and the need of a hybrid catalytic system

The dielectric properties of the catalytic materials were measured up to 850 °C. **Figure 5.1a** shows a comparison of the dielectric constants of the Ni-based commercial catalysts and $Ru/SrTiO_3$. It can be seen that the Ni/Al_2O_3 catalyst is outperforming the other commercially available catalysts at higher temperatures. When comparing all commercial catalysts with the $Ru/SrTiO_3$ catalyst, it can be seen that $Ru/SrTiO_3$ has a much higher dielectric constant across the whole temperature range. **Figure 5.1b** shows the dielectric loss factor of the four commercial catalysts and $Ru/SrTiO_3$. The loss factor of Ni/Al_2O_3 is almost zero at room temperature, but increases with temperature to around 1. The other three catalysts maintain a loss factor close to zero up to ~400 °C; at higher temperatures, the loss factor starts to slowly increase up to 0.2–0.3. Thus, only a negligible amount of microwave power is dissipated as heat in the commercially available catalysts, and very little heating can be achieved. In comparison to the four commercial catalysts, $Ru/SrTiO_3$ has the highest dielectric loss factor, ranging from 0.57 at room temperature to 2.25 at 800 °C. Overall, **Figure 5.1** confirms that the dielectric properties of the commercial catalysts are not suitable to heat them up to the required reaction temperature with 200 W of microwave power (max. power limit of the solid-state microwave generator used). Therefore, they are not good candidates for direct heating in microwave-assisted heterogeneous catalytic reactions.

In a previous work of our group, a series of ruthenium-doped strontium titanate ($SrTiO_3$) perovskite catalysts, with different ruthenium loadings, were synthesized by a microwave-assisted hydrothermal method [119]. It was observed that the increase in ruthenium content in $SrTiO_3$

perovskite improved its dielectric properties. A 7 wt. % Ru-doped $SrTiO_3$ catalyst, denoted in the present work as $Ru/SrTiO_3$, was found to be the best catalyst for microwave-assisted methane dry reforming among the tested samples. However, use of the ruthenium-based catalyst only would be expensive for large-scale operations. On the other hand, its combination with a Ni-based commercial catalyst would enable the latter to reach the required reaction temperature while reducing the total cost on scale up.

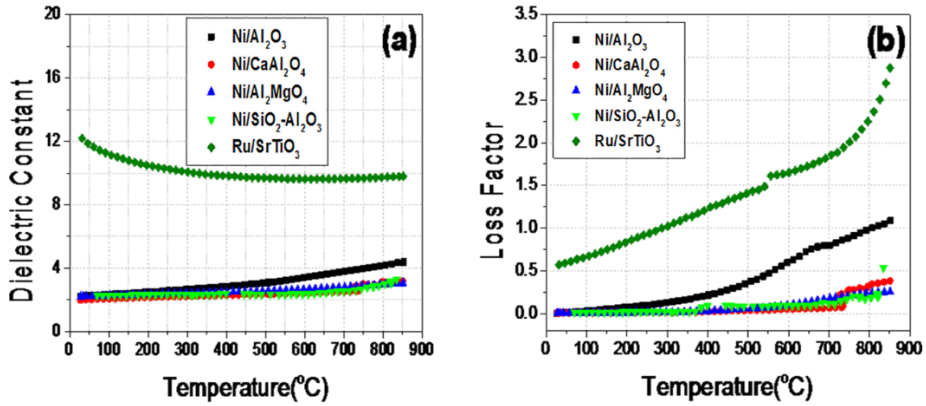

Figure 5.1. Comparison of dielectric properties of Ni-based commercial catalysts and 7 wt. % Ru-doped $SrTiO_3$ ($Ru/SrTiO_3$) perovskite catalysts: (a) dielectric constant versus temperature and (b) loss factor versus temperature.

Overall, in order to improve the microwave heating ability of the commercial Ni-based catalysts, different synthetic strategies were investigated. The first one consisted of impregnating Ni/Al_2O_3 catalyst with 6 wt. % of Ru via incipient wetness impregnation with aqueous ruthenium (III) nitrosyl nitrate solution. After impregnation, samples were calcined at 400 °C for 3h under static air conditions. 1 g of 6 wt% Ru-impregnated Ni/Al_2O_3, denoted as $6Ru@Ni/Al_2O_3$, was sieved to obtain 425–850 μm particles and loaded into the quartz reactor tube. The sample was then heated in the microwave reactor under N_2 flow. It was not possible to heat this impregnated catalyst above 300 °C using the maximum microwave power of 200 W.

Kumar et al. [120] have reported that metals like aluminum and nickel when dispersed on titanium (IV) oxide (TiO_2) nanoparticles increase their overall dielectric properties. Therefore, the second approach was the mixing of TiO_2 powder (425–850 μm) with $6Ru@Ni/Al_2O_3$ of the same particle size at a ratio of 1:1 (0.5 g of TiO_2 and 0.5 g of $6Ru@Ni/Al_2O_3$). No significant improvement in the heating profile was found after TiO_2 addition and testing in the microwave reactor. The third approach consisted of adding strontium oxide to the samples prepared in the first two approaches ($6Ru@Ni/Al_2O_3$ and $6Ru@Ni/Al_2O_3 + TiO_2$) at a ratio of 1:1. Upon heating in the microwave reactor, no increment in the heating profile was observed after addition of the strontium oxide.

Finally, the fourth and last synthesis procedure was based on mixing $Ru/SrTiO_3$ (in the perovskite form) with the Ni-based catalysts. The $Ru/SrTiO_3$ catalyst was directly mixed with each

commercial Ni-based catalyst at a ratio 1:1 (0.5 g of $Ru/SrTiO_3$ and 0.5 g of Ni-supported catalyst) all having particle sizes 425-850 μm. This approach was successful in attaining the required temperature range within the available MW power limit (200 W). Therefore, these samples were used for methane dry reforming as described in the following sections.

5.3.2. Thermal response of the catalytic materials under microwave heating

As the catalysts have different chemical compositions, they will not obtain the same temperatures when heated inside a microwave reactor at a given applied power. For this reason, a study on the relation between microwave power and catalyst bed temperature using both the top bed thermocouple and the thermal camera was performed for each catalytic system under a N_2 flow rate of 50 cm^3_{STP}/min. The information from this study was later used to determine the microwave power needed for each hybrid catalyst to reach the desired reaction temperature during DRM. **Figure 5.2a** presents the top catalyst bed temperature as a function of MW power for each hybrid catalytic system; **Figures 5.2b, c, d,** and **e** show the temperature contours produced by the thermal camera for the $Ru/SrTiO_3+Ni/SiO_2-Al_2O_3$ sample at applied MW powers of 70, 75, 80 and 85 W, respectively.

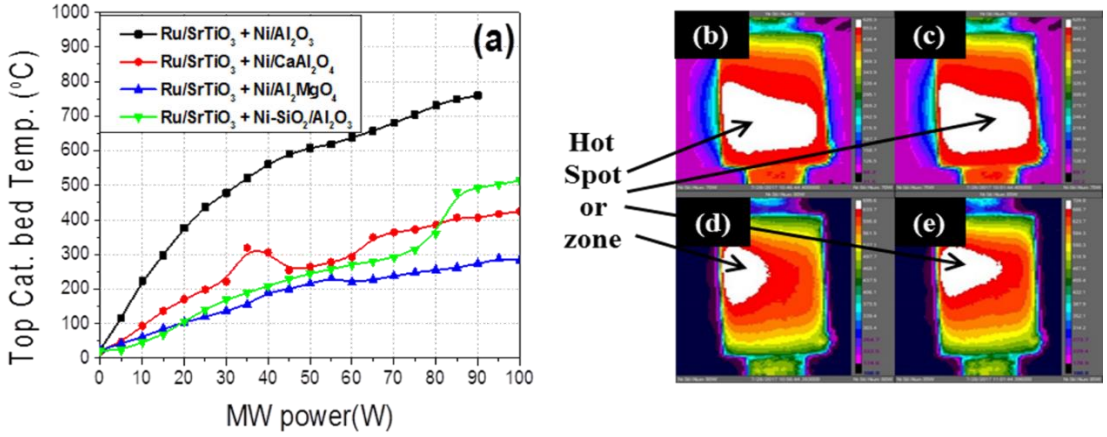

Figure 5.2. (a) Top bed temperature measurement in each hybrid catalytic system comprising each of the four commercial catalysts and the in-house developed $Ru/SrTiO_3$ catalyst in the power range from 0 to 100 W. (b-e) Migration of hotspot inside the $Ru/SrTiO_3+Ni/SiO_2-Al_2O_3$ catalyst sample with increase in MW power; (b) 70 W, (c) 75 W, (d) 80 W and (e) 85 W.

In **Figure 5.2a**, ascending temperature trends with increasing power input are presented. Although these general trends are expected, some abrupt temperature changes are also recorded, e.g., for $Ru/SrTiO_3+Ni/SiO_2-Al_2O_3$ at ~80 W and for $Ru/SrTiO_3+Ni/CaAl_2O_4$ at ~35 W, manifesting hotspot migration inside the catalyst bed. Indeed, this is confirmed by the thermal images in **Figures 5.2b-e**, which show that the hottest (white) zone inside the reactor moves towards the top of the bed (closer to the inlet), at higher powers (80–85 W, **Figures 5.2d** and **e**) compared to lower

ones (70–75 W, **Figures 5.2b** and **c**). As the thermocouple is located at the top of the bed, its temperature reading is affected by hotspot migration. Overall, these results confirm that 2D temperature monitoring in the catalyst bed is necessary to track the location of hot spots and avoid materials damage during a microwave heating process.

5.3.3. Evolution of microwave power and reactants conversion

The effect of different microwave powers on the overall reactor performance was experimentally determined. **Figures 5.3a-f** show methane conversion, carbon dioxide conversion, H_2/CO ratio, top catalyst bed temperature, bottom catalyst bed temperature and average catalyst bed temperature, respectively, after 20 min of TOS, as a function of MW power (40–140 W) at a CH_4/CO_2 inlet ratio of 0.82 and 3000 $cm^3g^{-1}h^{-1}$ GHSV (50 cm^3_{STP}/min). The reaction was performed either until conversions were stabilized to maximum values or until the top catalytic bed temperature reached ~1000 °C; in the latter case, the reaction was stopped to avoid thermocouple damage.

Based on the heating experiments discussed in **Section 5.3.2**, it was decided to perform all reactant conversion tests starting from 40 W. As shown in Figures **5.3a** and **b**, up to 60 W, the conversions of CH_4 and CO_2 with Ru/$SrTiO_3$+Ni/Al_2O_3 are higher compared to the other three catalysts, despite the lowest top bed temperature reached (172.52 ºC at 60 W with Ru/$SrTiO_3$+Ni/Al_2O_3; **Figure 5.3d** and **Table S5.2**). In the 60-120 W range, Ru/$SrTiO_3$+Ni/$CaAl_2O_4$ gives higher conversions than Ru/$SrTiO_3$+Ni/Al_2O_3. At powers higher than 120 W, Ru/$SrTiO_3$+Ni/Al_2O_3 and Ru/$SrTiO_3$+Ni/$CaAl_2O_4$ give nearly equal conversions for CH_4 and CO_2. The maximum conversions achieved by the two catalysts were ~99% for CH_4 and ~92% for CO_2 at 140 W. According to these results, it was decided that 140 W be the maximum applied MW power for all the experiments since the CH_4 conversion achieved with Ru/$SrTiO_3$+Ni/Al_2O_3 and Ru/$SrTiO_3$+Ni/$CaAl_2O_4$ was ~99%. Interestingly, the Ru/$SrTiO_3$+Ni/Al_2MgO_4 catalyst had a top catalyst bed temperature value in excess of 550 °C at 40 W and reached 1000 °C at 110 W (see **Figure 5.3d** and **S5.5**); therefore, no higher power levels were tested in order to avoid damage of the thermocouple. In the case of Ru/$SrTiO_3$+Ni/SiO_2-Al_2O_3 catalyst, rapid temperature rise was also observed from 400 °C at 110 W to 1027 °C at 130 W (**Table S5.2**). Hence the experiment was stopped at 130 W to avoid thermocouple damage.

The conversions achieved by Ru/$SrTiO_3$+Ni/Al_2MgO_4 are lower than those of Ru/$SrTiO_3$+Ni/Al_2O_3 and Ru/$SrTiO_3$+Ni/$CaAl_2O_4$, but higher than the conversions with the Ru/$SrTiO_3$+Ni/SiO_2-Al_2O_3 catalyst in the range (40–100 W). At higher powers (100–130 W range), Ru/$SrTiO_3$+Ni/SiO_2-Al_2O_3 has shown an increase in conversion up to 88% for CH_4 and 82% for CO_2 at 130 W. This increase in conversion could be associated with the drastic increase in the top bed temperature at 130 W (**Figure 5.3d**) due to hotspot migration close to the top thermocouple (inlet side where reactants concentration is high) (see **Figure S5.6**). **Figure 5.3c** shows that for

$Ru/SrTiO_3+Ni/Al_2O_3$, $Ru/SrTiO_3+Ni/CaAl_2O_4$, and $Ru/SrTiO_3+Ni/Al_2MgO_4$, the obtained syngas ratio gradually increases with the MW power up to ~80 W and then it remains constant to 0.84. In the case of $Ru/SrTiO_3+Ni/SiO_2$-Al_2O_3, the H_2/CO ratio has an increasing trend up to 100 W, where it becomes 1; at higher powers, H_2/CO decreases down to the value of 0.84 (at 130 W) that was obtained with the other catalysts as well.

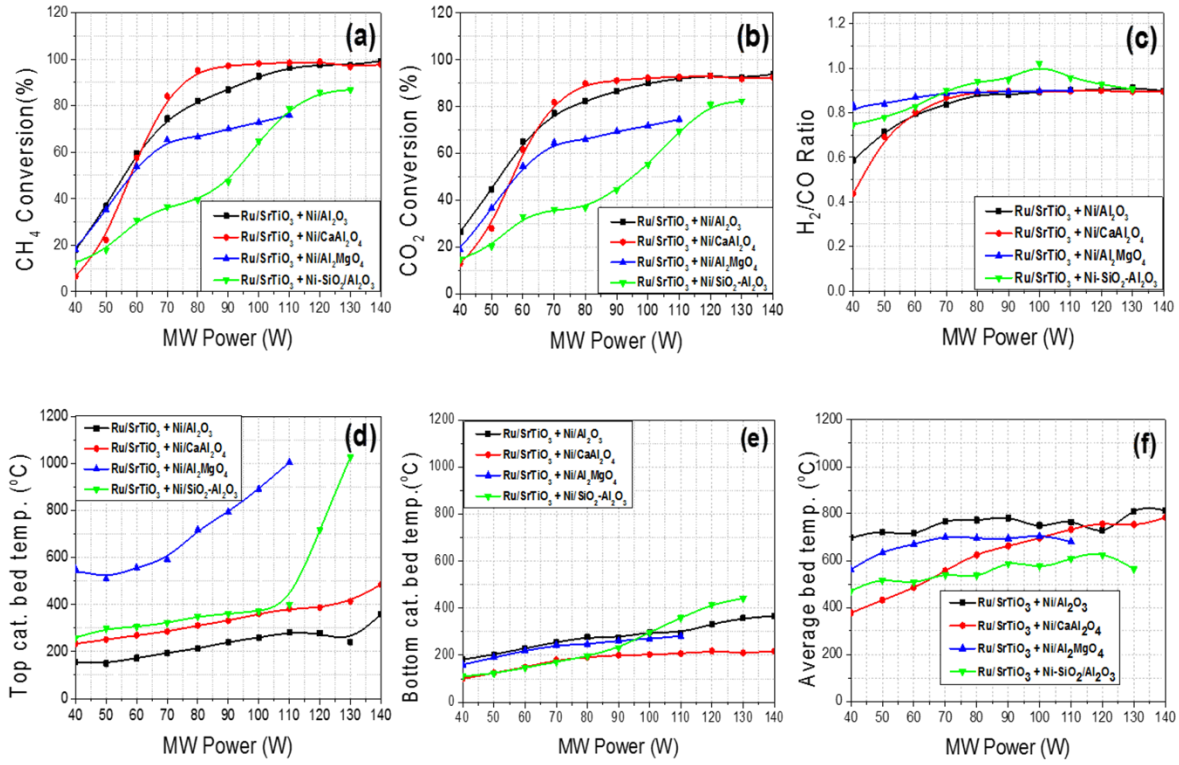

Figure 5.3. (a) CH_4 conversion, (b) CO_2 conversion, (c) H_2/CO ratio, (d) top catalyst bed temperature, (e) bottom catalyst bed temperature and (f) average catalyst bed temperature by thermal camera, after 20 min of TOS, as a function of MW power (40–140 W). CH_4/CO_2 inlet ratio=0.82 and GHSV=3000 $cm^3g^{-1}h^{-1}$.

Comparing **Figure 5.2a** and **Figure 5.3d**, it is observed that different temperature profiles are developed while increasing MW power input in the case of N_2 flow and CH_4:CO_2 flow. In the case of reacting gases, the heating profiles will be different due to the continuous change in the gas composition flowing through the catalytic bed. For example, the top catalyst bed temperature for $Ru/SrTiO_3+Ni/Al_2MgO_4$ increased by 90 ºC only (from 200 ºC at 40 W to 290 ºC at 100 W) under N_2 flow (**Figure 5.2a**) and by 340 ºC (from 550 ºC at 40 W to 890 ºC at 100 W) under the CH_4/CO_2 flow in the applied microwave power range 40-100 W (**Figure 5.3d**). The reason for this temperature change is the generation and migration of hot spots, or zones, at different locations inside the catalytic bed in the events of the nonreactive and reactive environment, most likely due to coke formation in the latter case. This becomes clear upon a comparison of the relevant thermal images. Specifically, the hotspot generated in the case of N_2 flow was at the center of catalytic bed (**Figure S5.4**), while in the reactive case, the hotspot was at higher temperature level and migrated

from the centre to the top side of the catalytic bed (**Figure S5.5**) where the thermocouple is placed (compare **Figure S5.4** and **S5.5** in power range 40 to 100 W). In addition to the thermocouple readings and the 2D temperature contours provided by the thermal camera, average temperature values based on the 2D contours have also been calculated to further characterize the thermal environment in each experiment, as in our previous works [54,119]. **Figure S5.2** shows a thermal image of the $Ru/SrTiO_3+Ni/Al_2O_3$ catalytic bed at 180 min of operation during the time-on-stream (TOS) study along with the statistics viewer window. The 2D box with the red borderline in **Figure S5.2** is used to calculate the average (mean) catalytic bed temperature. The statistics viewer shows the average (mean), maximum and minimum temperature values present in the box.

Figure 5.3f shows the average bed temperature values for all the hybrid catalytic systems as a function of power (the maximum and minimum temperature values are presented in **Figure S5.3**). The average catalytic bed temperature values of $Ru/SrTiO_3+Ni/Al_2O_3$ are higher than the other three catalytic systems in agreement with the dielectric properties measurements shown in **Figure 5.1.** From the thermal point of view, this is also consistent with the higher CH_4 and CO_2 conversions obtained with $Ru/SrTiO_3+Ni/Al_2O_3$ compared to $Ru/SrTiO_3+Ni/Al_2MgO_4$ and $Ru/SrTiO_3+Ni/SiO_2$-Al_2O_3 (**Figures 5.3a** and **b**). On the other hand, the average temperature value of $Ru/SrTiO_3+Ni/CaAl_2O_4$ increases with increasing MW power input, but it is quantitatively lower compared to $Ru/SrTiO_3+Ni/Al_2O_3$ in the range 60-120 W (**Figure 5.3f**), while reactant conversions are somewhat higher for $Ru/SrTiO_3+Ni/CaAl_2O_4$ in this power range (**Figures 5.3a** and **b**). At microwave powers higher than 120 W, similar conversions and average temperatures have been obtained for both catalysts. It should be remarked therefore that the average, minimum and maximum temperatures, as well as the 2D temperature contours, reported herein and in the supporting information document, are meant to give as much insight as possible into the thermal response of the system in the different experiments. Nevertheless, in order for full justification of the relative differences in the conversion values obtained with the four catalysts, information on the varying 3D temperature distribution (given the strong non-linear reaction rate dependence on temperature) and the activity of the catalysts themselves at different temperature levels is also required.

5.3.4. Gas hourly space velocity study

The effect of different gas hourly space velocities on the overall catalyst performance was experimentally determined. **Figures 5.4a** and **b** present CH_4 and CO_2 conversions, respectively, after 30 min of TOS as a function of the GHSV, from 3000–9000 $cm^3g^{-1}h^{-1}$ (total flow rate: 50–150 cm^3/min) at an inlet CH_4/CO_2 ratio of 0.82 and varying MW power (140 W for $Ru/SrTiO_3+Ni/Al_2O_3$ and $Ru/SrTiO_3+Ni/CaAl_2O_4$, 100 W for $Ru/SrTiO_3+Ni/Al_2MgO_4$ and 120 W for $Ru/SrTiO_3+Ni/SiO_2$-Al_2O_3). **Figures 5.4c-f** show the H_2/CO ratio, the top bed temperature, the

bottom bed temperature and the average bed temperature, respectively, as a function of GHSV, for the four catalytic systems.

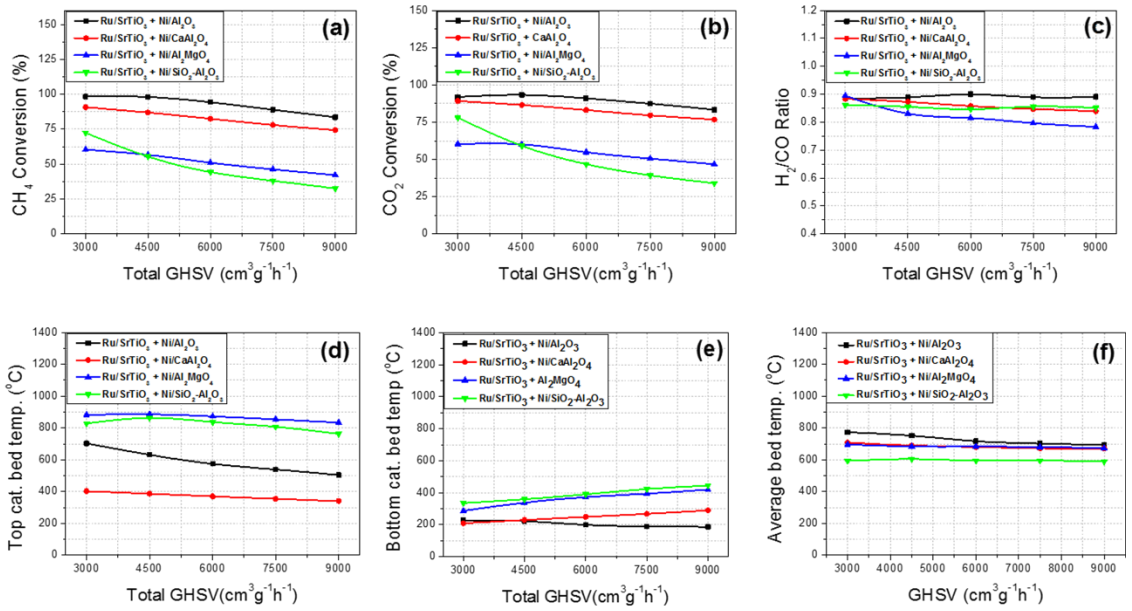

Figure 5.4. (a) CH_4 conversion, (b) CO_2 conversion, (c) H_2/CO ratio, (d) top catalyst bed temperature, (e) bottom catalyst bed temperature and (f) average catalyst bed temperature, after 30 min of TOS, as a function of the GHSV (3000–9000 $cm^3g^{-1}h^{-1}$). CH_4/CO_2 inlet ratio=0.82. The power input was 140 W for $Ru/SrTiO_3+Ni/Al_2O_3$ and $Ru/SrTiO_3+Ni/CaAl_2O_4$, 100 W for $Ru/SrTiO_3+Ni/Al_2MgO_4$ and 120 W for $Ru/SrTiO_3+Ni/SiO_2-Al_2O_3$.

A decreasing trend in CH_4 and CO_2 conversions vs. GHSV is obtained for all catalytic systems. For example, $Ru/SrTiO_3+Ni/Al_2O_3$ gives conversions of 98.36% and 91.90% for CH_4 and CO_2, respectively, at 3000 $cm^3g^{-1}h^{-1}$, which decrease to 83.58% and 83.41%, respectively, at 9000 $cm^3g^{-1}h^{-1}$. As shown in **Fig. 5.4c**, the H_2/CO ratio was in all cases between 0.8 and 0.9 in the range 3000 to 9000 $cm^3g^{-1}h^{-1}$. $Ru/SrTiO_3+Ni/Al_2O_3$ produces the highest H_2/CO ratio (0.9) across the whole GHSV range study. In general, $Ru/SrTiO_3+Ni/Al_2O_3$ gives relatively higher conversions across the whole GHSV range, despite $Ru/SrTiO_3+Ni/Al_2MgO_4$ and $Ru/SrTiO_3+Ni/SiO_2-Al_2O_3$ reaching higher catalyst top bed temperatures. These higher temperatures are again due to hotspots present near the top thermocouple positions (see **Figures S5.7c and S5.7d**). However, **Figure 5.4f** shows that the average temperature values of $Ru/SrTiO_3+Ni/CaAl_2O_4$, $Ru/SrTiO_3+Ni/Al_2MgO_4$, and $Ru/SrTiO_3+Ni/SiO_2-Al_2O_3$ were lower than in the case of $Ru/SrTiO_3+Ni/Al_2O_3$. Moreover, a decrease in reactants conversions is observed with increase in GHSV due to the decrease in the catalyst contact time.

5.3.5. Reactor performance as a function of time-on-stream (TOS)

Figures 5.5a-f present CH_4 conversion, CO_2 conversion, H_2/CO ratio, top bed temperature, bottom bed temperature and average bed temperature as a function of TOS. The conditions applied to these 180 min tests were chosen based on the tests 1, 2 and 3 mentioned in **Table 5.2** namely, $Ru/SrTiO_3+Ni/Al_2O_3$ at 4500 $cm^3g^{-1}h^{-1}$ GHSV and 140 W microwave power and $Ru/SrTiO_3+Ni/CaAl_2O_4$, $Ru/SrTiO_3+Ni/Al_2MgO_4$ and $Ru/SrTiO_3+Ni/SiO_2$-Al_2O_3 at 3000 $cm^3g^{-1}h^{-1}$ GHSV and 140 W, 100 W and 120 W of microwave power, respectively. The CH_4/CO_2 inlet ratio was 0.82.

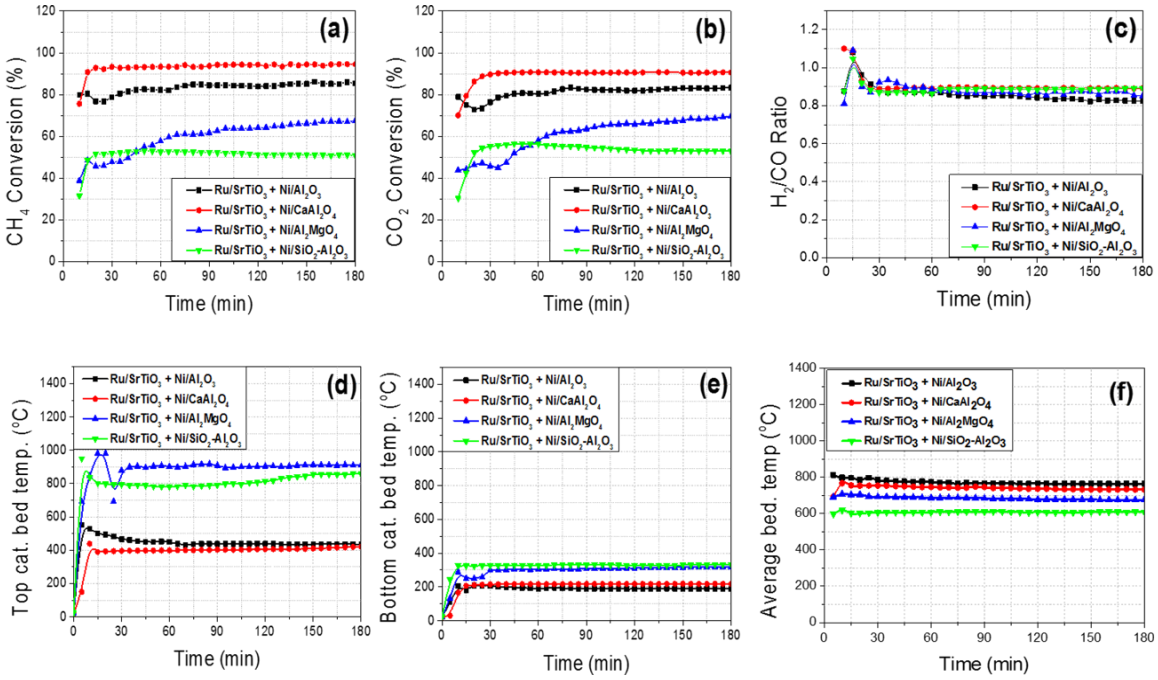

Figure 5.5. (a) CH_4 conversion, (b) CO_2 conversion, (c) H_2/CO ratio, (d) top catalyst bed temperature, (e) bottom catalyst bed temperature and (f) average catalyst bed temperature as a function of TOS for the four hybrid catalytic systems. GHSV=4500 $cm^3g^{-1}h^{-1}$ for $Ru/SrTiO_3+Ni/Al_2O_3$ and 3000 $cm^3g^{-1}h^{-1}$ for the other three catalysts. The applied MW power was 140 W for $Ru/SrTiO_3+Ni/Al_2O_3$ and $Ru/SrTiO_3+Ni/CaAl_2O_4$, 100 W for $Ru/SrTiO_3+Ni/Al_2MgO_4$ and 120 W for $Ru/SrTiO_3+Ni/SiO_2$-Al_2O_3. The CH_4/CO_2 inlet ratio was 0.82.

As shown in **Figures 5.5a** and **b**, $Ru/SrTiO_3+Ni/Al_2O_3$, $Ru/SrTiO_3+Ni/CaAl_2O_4$, and $Ru/SrTiO_3+Ni/SiO_2$-Al_2O_3 reached steady state conversions after 30 minutes of TOS. For $Ru/SrTiO_3+Ni/Al_2O_3$, CH_4 and CO_2 conversions (4500 $cm^3g^{-1}h^{-1}$ GHSV) increased from 78.69% and 76.35%, respectively, at 30 min, to 85.33% and 83.35%, respectively, at 180 min. For $Ru/SrTiO_3+Ni/CaAl_2O_4$, CH_4 and CO_2 conversions (3000 $cm^3g^{-1}h^{-1}$ GHSV) were 93.23% and 89.70%, respectively, at 30 min, and remained quite stable with time, 94.52% and 90.55%, respectively, at 180 min. On the other hand, CH_4 and CO_2 conversions gradually increase from 47.76% and 45.73%, respectively, to 67.47% and 69.58%, respectively, in the case of the

$Ru/SrTiO_3+Ni/Al_2MgO_4$ sample over the time range 30–180 min. Guczi et al. [121] have reported deactivation of catalysts having structure $Ni/MgAl_2O_4$ due to the formation of graphite-like carbon deposits, or carbon nanotubes, during methane dry reforming under conventional heating. On the contrary, no deactivation was observed in our case for $Ni/MgAl_2O_4$. The reason for this could be the application of MW heating and the surplus of CO_2 in the reaction mixture (CH_4/CO_2 feed ratio=0.82), which may promote regeneration of the coke deposited on the catalyst.

Table 5.3: Catalytic performance comparison of the perovskite catalyst with a carbon-based catalyst reported in the literature

Catalyst used	Temperature (°C)	Feed composition (vol. %)		Amount of catalyst (g)	Flow of CH_4 (ml/min)	Total GHSV ($cm^3h^{-1}g_{cat}^{-1}$)	Conversion (%)		H_2 produced ($m^3h^{-1}kg_{cat}^{-1}$)	Reference
		CH_4	CO_2				CH_4	CO_2		
50%FY5 + 50% Ni/Al_2O_3	Thermocouple temperature (800)	50	50	12	300	3000	88.1	93.3	2.6	[89]
50% $Ru/SrTiO_3$ + 50% Ni/Al_2O_3	average catalytic bed temperature range (765-815)	45	55	1	33.75	4500	85.33	83.35	3.45	This work.

The conversions with $Ru/SrTiO_3+Ni/SiO_2$-Al_2O_3 are in general lower than those obtained with the other three tested catalysts and slightly decrease as a function of TOS (**Figures 5.5a** and **b**). Particularly, CH_4 and CO_2 conversions slightly decreased from 51.84% and 55.18%, respectively, at 30 min, to 50.96% and 52.85%, respectively, at 180 min. **Figure 5.5f** shows the average bed temperature for each of the four hybrid catalysts as a function of TOS. The average temperature values for $Ru/SrTiO_3+Ni/Al_2O_3$, $Ru/SrTiO_3+Ni/CaAl_2O_4$, $Ru/SrTiO_3+Ni/Al_2MgO_4$ and $Ru/SrTiO_3+Ni/SiO_2$-Al_2O_3 are in the temperature ranges 765–798 °C, 732–767 °C, 676–708 °C and 609–619 °C, respectively (**Table S5.1**; time span: 10-180 min). In general, higher conversions are obtained with $Ru/SrTiO_3+Ni/Al_2O_3$ and $Ru/SrTiO_3+Ni/CaAl_2O_4$ for which higher temperatures are reached. Nevertheless, similar to the remark made in **section 5.3.3**, information both on the exact 3D temperature distribution in the reactor and the activity of the catalysts at different temperatures would be required to provide full reasoning on the relative conversion differences obtained with the four catalysts. The main purpose in this work is to identify an effective and stable hybrid catalytic system, among possible candidates, for microwave-assisted methane dry reforming at high temperatures.

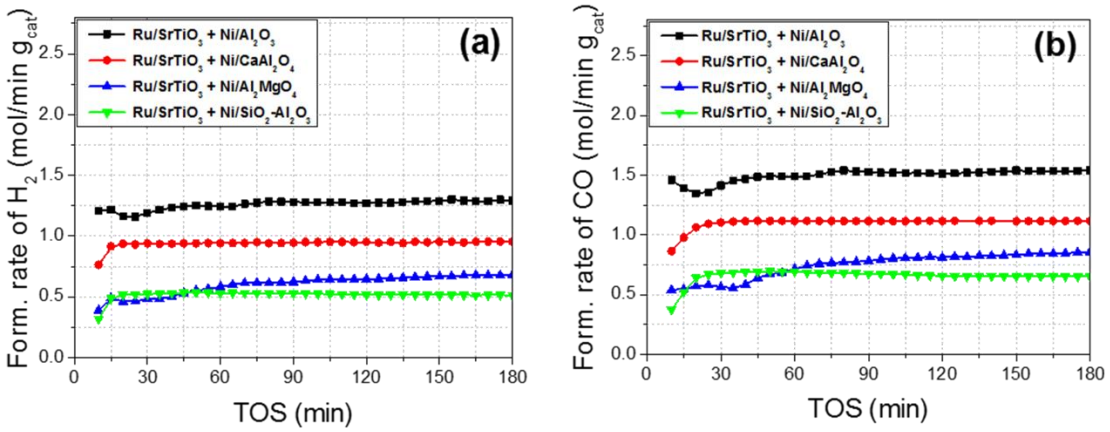

Figure 5.6. Formation rate of (a) H_2 and (b) CO as a function of TOS at a CH_4/CO_2 inlet ratio of 0.82 and GHSV = 4500 cm^3 $_{STP}$/h g $_{cat}$ for $Ru/SrTiO_3+Ni/Al_2O_3$ and 3000 cm^3 $_{STP}$/h g $_{cat}$ for other 3 catalysts with MW powers 140W for $Ru/SrTiO_3+Ni/Al_2O_3$ and $Ru/SrTiO_3+Ni/CaAl_2O_4$, 100 W for $Ru/SrTiO_3+Ni/Al_2MgO_4$ and 120W for $Ru/SrTiO_3+Ni/SiO_2-Al_2O_3$.

Figure 5.6 shows the formation rate of H_2 and CO for each catalytic system as a function of TOS. $Ru/SrTiO_3+Ni/Al_2O_3$ has shown higher CH_4, and CO_2 conversions with ~1.3 and ~1.5 moles of H_2 and CO produced $min^{-1}g_{cat}^{-1}$, as compared to the other three hybrid catalysts. The syngas production rate order of the hybrid catalytic systems is as follows: $Ru/SrTiO_3+Ni/Al_2O_3$ > $Ru/SrTiO_3+Ni/CaAl_2O_4$ > $Ru/SrTiO_3+Ni/Al_2MgO_4$ > $Ru/SrTiO_3+Ni/SiO_2-Al_2O_3$. Therefore, among the tested materials, $Ru/SrTiO_3+Ni/Al_2O_3$ has been found to be the best catalyst due to its good microwave absorption ability and its ability to operate at higher GHSVs producing higher syngas flow rates. **Table 5.3** compares the combination of 50% Ni/Al_2O_3 with 50% activated carbon (FY5) to that of 50% Ni/Al_2O_3 with 50% $Ru/SrTiO_3$. CH_4 and CO_2 conversions of ~85% and ~83%, respectively, at a GHSV of 4500 $cm^3g^{-1}h^{-1}$ were attained with 1 g of 50% $Ru/SrTiO_3$ + 50% Ni/Al_2O_3. In the case of 50% FY5 + 50% Ni/Al_2O_3, CH_4 and CO_2 conversions of ~88% and ~93%, respectively, have been reported, at a GHSV of 3000 $cm^3g^{-1}h^{-1}$ and 12 g of catalyst mixture. The scale-up potential of the two catalysts has been evaluated according to the approach described by Fidalgo et al. [89] concluding that the hybrid catalytic system of 50% $Ru/SrTiO_3$ + 50% Ni/Al_2O_3 is able to produce 3.45 m^3 H_2 $h^{-1}kg_{cat}^{-1}$, as compared to 2.6 m^3 H_2 $h^{-1}kg_{cat}^{-1}$ in the case of the carbon-based catalyst comprising 50% FY5 + 50% Ni/Al_2O_3 [89].

5.4. Conclusions

We evaluated four different hybrid catalytic systems, containing commercial nickel supported on metal oxide catalysts and 7 wt. % Ru-doped $SrTiO_3$ perovskite catalyst, in terms of syngas production via CO_2 (dry) reforming of CH_4 under microwave heating. The four hybrid catalytic systems are: $Ru/SrTiO_3+Ni/Al_2O_3$, $Ru/SrTiO_3+Ni/CaAl_2O_4$, $Ru/SrTiO_3+Ni/Al_2MgO_4$ and $Ru/SrTiO_3+Ni/SiO_2$-Al_2O_3. First, the dielectric properties of the commercial nickel-based catalysts were measured up to 850 °C to get insight into their microwave heating ability at realistic dry reforming temperatures. It was found that incorporation of the $Ru/SrTiO_3$ perovskite catalyst improves the microwave heating properties of the microwave-inactive Ni-supported metal oxide commercial catalysts. The thermal response of the hybrid catalytic systems and their performance, in terms of reactants conversions and syngas production rate, have been monitored as a function of microwave power and gas hourly space velocity. It can be concluded that ~100% CH_4 conversion can be attained if the reaction conditions are appropriately selected. The order of the four hybrid catalytic systems tested in terms of their total syngas production rate capacity is: $Ru/SrTiO_3+Ni/Al_2O_3$ > $Ru/SrTiO_3+Ni/CaAl_2O_4$ > $Ru/SrTiO_3+Ni/Al_2MgO_4$ > $Ru/SrTiO_3+Ni/SiO_2$-Al_2O_3. Based on scale-up calculations, 50% $Ru/SrTiO_3$ + 50% Ni/Al_2O_3 is able to produce 3.45 m^3 H_2 $h^{-1}kg_{cat}^{-1}$ as compared to 2.6 m^3 H_2 $h^{-1}kg_{cat}^{-1}$ that has been reported in the literature [89] for a carbon-based catalyst of 50% FY5 + 50% Ni/Al_2O_3.

5.5. Supporting Information:

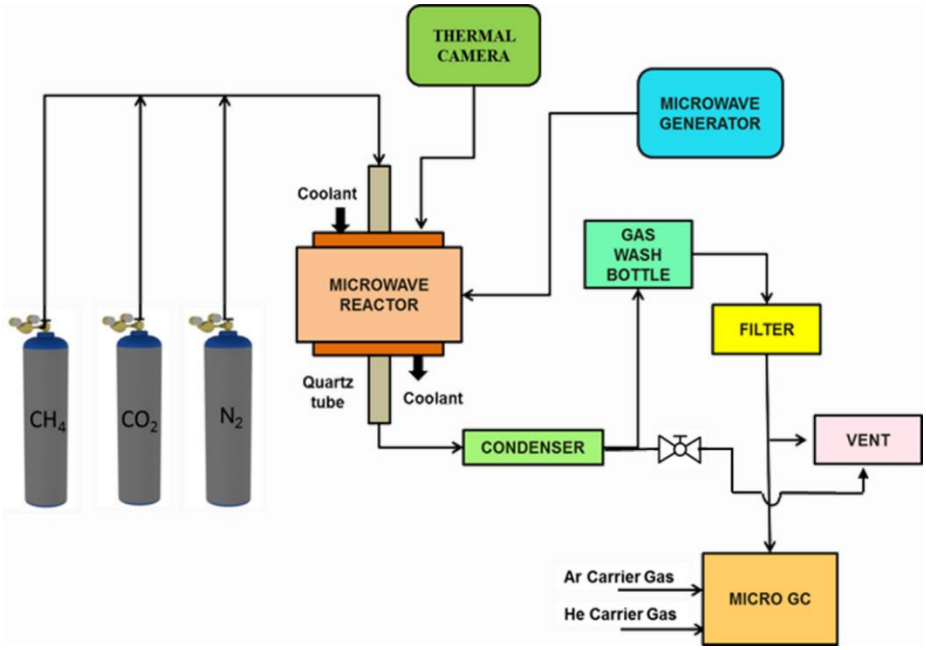

Figure S5.1a: Schematic of the microwave reactor system used.

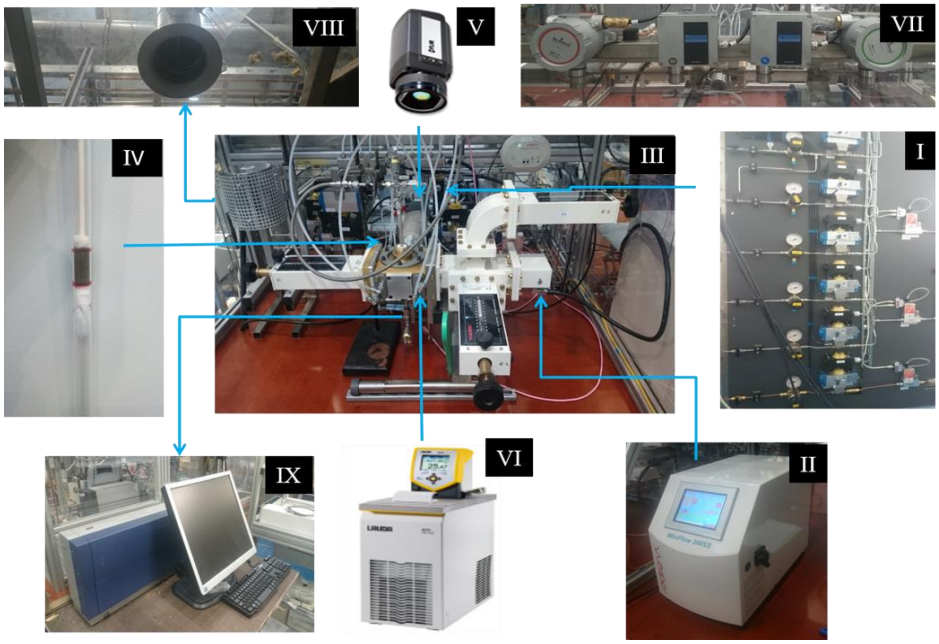

Figure S5.1b: Digital image of the microwave reactor system. It includes (I) a gas supply unit, (II) a solid state MW generator, (III) a microwave reactor assembly, (IV) a quartz tube loaded with a catalyst and a ceramic well, (V) a thermal camera, (VI) a thermostat for cooling, (VII) gas detectors, (VIII) ventilation, and (IX) a micro GC for product analysis.

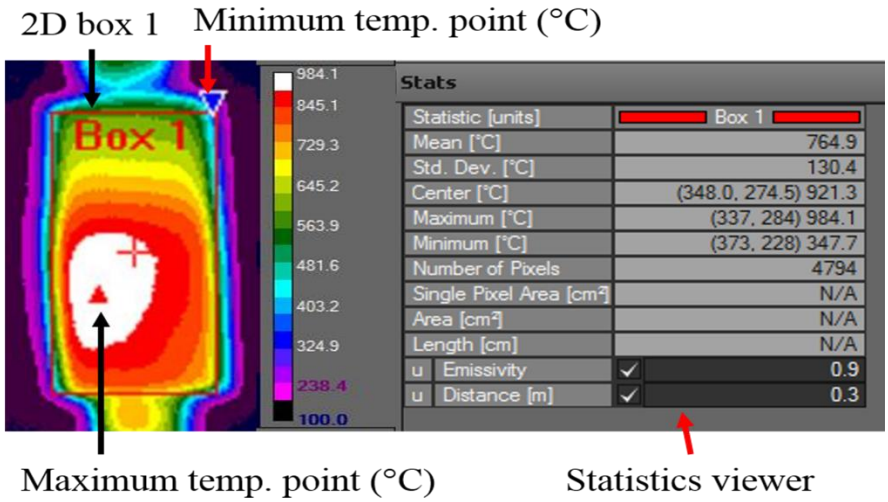

Figure S5.2: Thermal image of the Ru/$SrTiO_3$+Ni/Al_2O_3 catalytic bed at 180 min of operation during the time-on-stream (TOS) study along with the statistics viewer window. The 2D box with the red borderline is used to calculate the average (mean) catalytic bed temperature. The statistics viewer shows the average (mean), maximum and minimum temperature values present in the box. The temperature distribution in the four tested hybrid catalytic beds has been calculated in 2D using thermal camera videos at an emissivity value of 0.9.

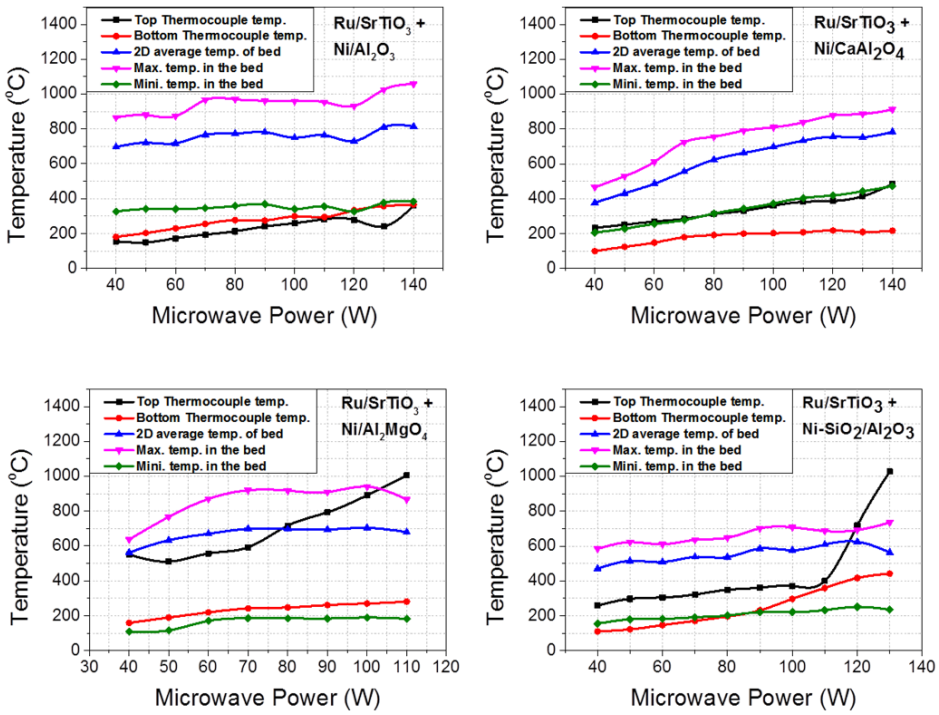

Figure S5.3: Top and bottom bed temperatures as well as maximum, minimum and average bed temperatures as a function of microwave power during dry reforming experiments with the four hybrid catalysts tested.

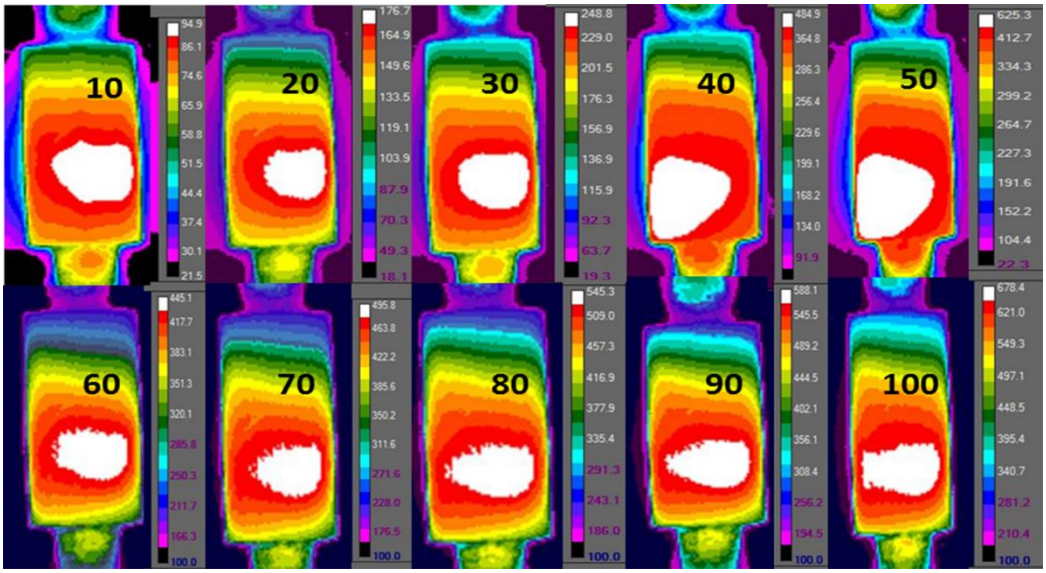

Figure S5.4: Thermal images of $Ru/SrTiO_3$ + Ni/Al_2MgO_4 catalyst during microwave heating under N_2 flow. Migration of hot spot (white area) occurs when varying the power input from 10 to 100 W.

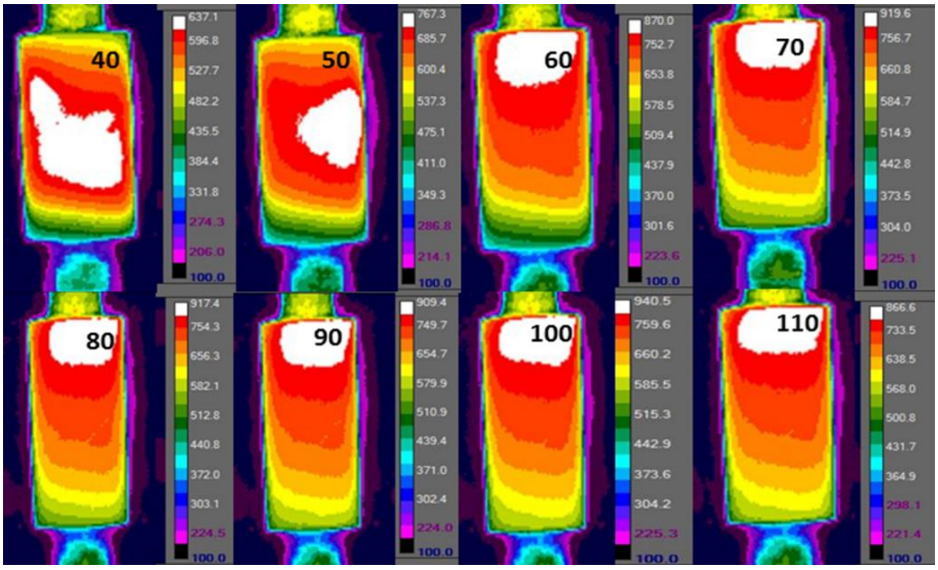

Figure S5.5: Thermal images of $Ru/SrTiO_3$ + Ni/Al_2MgO_4 catalyst during microwave heating under CH_4/CO_2 reactant mixture flow (dry reforming experiment). Migration of hot spot (white area) occurs when varying the power input from 40 to 100 W.

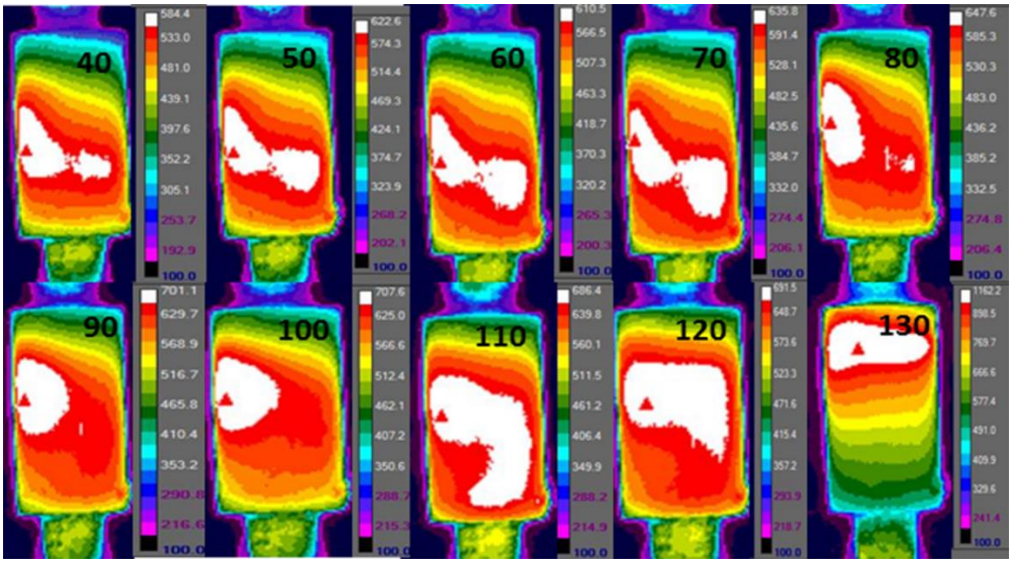

Figure S5.6: Thermal images of Ru/$SrTiO_3$ + Ni-SiO_2/Al_2O_3 catalyst during microwave heating under CH_4/CO_2 reactant mixture flow (dry reforming experiment). Migration of hot spot (white area) occurs when varying the power input from 40 to 130 W.

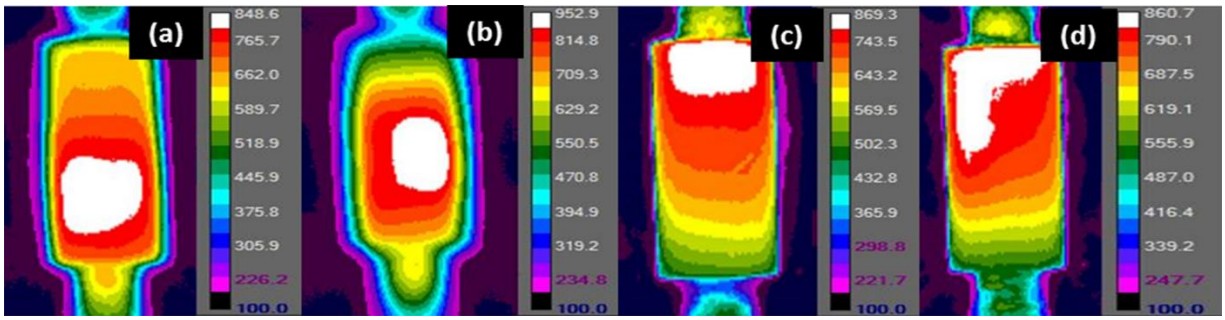

Figure S5.7: Thermal images of (a) Ru/$SrTiO_3$+Ni/Al_2O_3, (b) Ru/$SrTiO_3$+Ni/$CaAl_2O_4$, (c) Ru/$SrTiO_3$+Ni/Al_2MgO_4 and (d) Ru/$SrTiO_3$+Ni/SiO_2-Al_2O_3 during the GHSV parametric study. The images were taken at 9000 $cm^3g^{-1}h^{-1}$ GHSV.

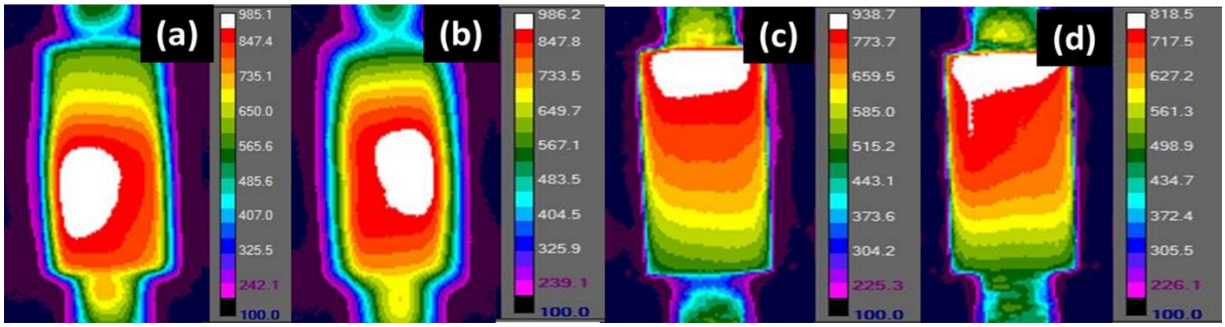

Figure S5.8: Thermal images of (a) Ru/$SrTiO_3$+Ni/Al_2O_3 at 4500 $cm^3g^{-1}h^{-1}$ GHSV and (b) Ru/$SrTiO_3$+Ni/$CaAl_2O_4$, (c) Ru/$SrTiO_3$+Ni/Al_2MgO_4 and (d) Ru/$SrTiO_3$+Ni/SiO_2-Al_2O_3 at 3000 $cm^3g^{-1}h^{-1}$ GHSV during the time-on-stream (TOS) study.

Table S5.1: Average bed temperature values for the four tested hybrid catalytic beds as a function of time-on-stream (TOS).

Time (min)	Ru/$SrTiO_3$ + Ni/Al_2O_3	Ru/$SrTiO_3$ + Ni/$CaAl_2O_4$	Ru/$SrTiO_3$ + Ni/Al_2MgO_4	Ru/SrTiO3 + Ni-SiO_2/Al_2O_3
5	812.4	693.1	691.7	598.4
10	797.7	767.3	707.7	618.9
15	797.2	755.8	704.4	601.2
20	787.5	753.4	704.6	602.3
25	797.2	754	695	604.1
30	784.7	753.9	693.3	606.4
35	780.9	753.5	692.9	607.3
40	778.2	751.4	691.1	607.5
45	776.5	750.1	691.6	607
50	774.9	748.1	690.9	607.6
55	776.9	745.8	688	607.7
60	775.9	746.1	685.5	607.8
65	771	744	686.3	610.2
70	769.8	743.7	687.7	609.5
75	763.5	743.4	687.7	609.8
80	768.6	743.3	687	611.3
85	767.9	747.7	685.5	611.8
90	767.5	746.1	684.3	609.9
95	766.2	741.1	681.4	612.1
100	765.9	740.8	682.1	611.6
105	766	739.5	682.4	609.3
110	764.9	738.5	681.2	608.7
115	764.8	736.8	680.4	607.6
120	767.5	736.6	679.1	608.3
125	764.9	736.7	679.4	607.4
130	765.4	735.4	679.1	607.1
135	765.3	734.5	678.8	607.2
140	764.9	734.2	677.9	606.4
145	764.9	733.2	678.1	607.4
150	765.5	733	678	609.6
155	764.3	732	676.1	610.1
160	764.3	732.4	676.2	610.7
165	764.2	732.8	676.1	609.9
170	764.3	734.4	675.5	609.7
175	764.9	732.3	675.6	610.1
180	764.9	732.4	675.6	609.2

Table: S5.2: Temperature values measured or calculated by the thermocouples and the thermal camera for the four tested hybrid catalytic beds during the "Evolution of microwave power and reactants conversion" study (Section 5.3.3 in main text).

1. $Ru/SrTiO_3 + Ni/Al_2O_3$					
MW Power (W)	**Top Thermocouple temp.**	**Bottom Thermocouple temp.**	**Average bed temp.**	**Max. temp. in the bed**	**Mini. temp. in the bed**
40	155.13	181.15	696.5	865.5	326.5
50	149.49	202.82	720.5	879.7	341.5
60	172.52	229.05	717.3	873.3	340.8
70	194.29	255.22	766.6	965.8	346
80	212.95	276.74	772.7	969.9	357.9
90	240.35	274.71	781.2	961.5	368.2
100	259.83	298.78	749.4	958.8	340
110	281.86	294.48	764.1	954	356.3
120	278.68	332.94	730	931.6	327.1
130	240.97	357.33	810.1	1024.9	377
140	359.35	366.38	813.7	1057.5	383.7
2. $Ru/SrTiO_3 + Ni/CaAl_2O_4$					
MW Power (W)	**Top Thermocouple temp.**	**Bottom Thermocouple temp.**	**Average bed temp.**	**Max. temp. in the bed**	**Mini. temp. in the bed**
40	233.25	99.74	376.9	466.2	205.8
50	250.66	124.52	430.8	529.1	228.3
60	269.35	148.25	485.6	611.5	255
70	284.8	179.21	556.3	723.7	277.2
80	311.17	191.61	623.8	755.4	315.5
90	330.8	199.87	662.4	790	343.4
100	360.38	202.39	696.5	809.6	372.8
110	381.66	207.14	732.5	838.1	403.9
120	387.15	217.66	755.4	877.3	418.6
130	413.75	209.27	752.6	885.7	442.2
140	484.32	216.43	783.5	911.7	472.6
3. $Ru/SrTiO_3 + Ni/Al_2MgO_4$					
MW Power (W)	**Top Thermocouple temp.**	**Bottom Thermocouple temp.**	**Average bed temp.**	**Max. temp. in the bed**	**Mini. temp. in the bed**
40	550.54	159.27	562	637.1	109.7
50	510.69	189.68	633.3	767.3	116.2
60	556.9	219.27	670	870	170.5

70	592.56	241.57	698.8	919.6	185.6
80	716.71	247.17	696.2	917.4	185.5
90	792.86	261.26	694.2	909.4	183.9
100	890.92	270.02	703.9	940.5	189.5
110	1004.6	280.84	679.9	866.6	182.8
4. Ru/$SrTiO_3$ + Ni-SiO_2/Al_2O_3					
MW Power (W)	**Top Thermocouple temp.**	**Bottom Thermocouple temp.**	**Average bed temp.**	**Max. temp. in the bed**	**Mini. temp. in the bed**
40	258.96	110.47	470.4	584.3	155.1
50	297.48	122.02	514.6	622.4	179.5
60	305.37	146.77	508.3	610.3	182.1
70	321.88	170.74	537.8	635.7	191.7
80	349.26	195.82	536.7	647.5	201.8
90	361.06	231.41	585.7	701	222
100	371.08	297.06	576.5	707.5	221.3
110	399.86	359.46	608.3	686.3	232.9
120	717.31	416.5	624.5	691.4	251.2
130	1027.13	441.73	563.5	734.9	234.9

6

6. Conclusions and Recommendations

6.1. Conclusions

The most important conclusions obtained from this work are collectively summarized in this section.

First, a custom-designed microwave reactor assembly (MRA) was designed and developed to enable effective microwave heating of catalytic materials to high temperatures (up to 1000 °C) for methane dry reforming. It was found that in order to capture the dynamic temperature changes inside the catalytic bed during the reaction, a combination of a thermal camera with at least one contact sensor for in situ emissivity calculations is necessary. On the reaction side, microwave-assisted methane dry reforming experiments over platinum on carbon catalyst were performed first. It was found that although nearly complete CH_4 and CO_2 conversions were obtained in the first 30 min, the amount of carbon catalyst decreased with time and formed a carbon layer on the inner surface of the quartz wall of the reactor, which resulted in softening and eventually melting of the quartz tube wall.

Further, a series of ruthenium-doped strontium titanate perovskite catalysts were synthesized by conventional and microwave-assisted hydrothermal methods. Significant synthesis temperature and time reduction were achieved when microwaves were applied; specifically, from 220 °C for 24 h in conventional heating to 180 °C for 1h under microwave heating. In addition, ICP-OES analysis and HRTEM+EDX elemental mapping showed that higher Ru dispersion and more homogeneous distribution of particle sizes are obtained in the case of MW-assisted hydrothermal synthesis as compared to conventional hydrothermal synthesis. Based on the results of the dielectric and chemical characterization of the different catalysts prepared, a 7 wt. % Ru-doped $SrTiO_3$ perovskite catalyst prepared over 1h of microwave-assisted hydrothermal synthesis was selected for application to methane dry reforming under microwave heating over a range of CH_4/CO_2 inlet ratio, power input and gas hourly space velocity (GHSV). Stable maximum conversions of ~99.5% and ~94% for CH_4 and CO_2, respectively, were achieved during a 3h stability test at CH_4:CO_2 vol.%=45:55, GHSV=9000 $cm^3g^{-1}hr^{-1}$ and forward power input of 150 W. Besides, scale-up calculations on the basis of 1 m^3h^{-1} CH_4 inlet flow rate through the 7Ru/$SrTiO_3$-MW-1h catalyst bed show significant improvement in H_2 production capability as compared to carbon-based catalysts previously reported in the literature.

In an effort to decrease the cost of the catalytic system, four different hybrid catalytic systems, containing relatively inexpensive commercial metal-oxide supported nickel catalysts and 7 wt. % Ru-doped $SrTiO_3$ perovskite, were evaluated for methane dry reforming. The four hybrid catalytic systems are: Ru/$SrTiO_3$+Ni/Al_2O_3, Ru/$SrTiO_3$+Ni/$CaAl_2O_4$, Ru/$SrTiO_3$+Ni/Al_2MgO_4 and Ru/$SrTiO_3$+Ni/SiO_2-Al_2O_3. Dielectric and thermal characterization of the catalysts in heating experiments showed that incorporation of the Ru/$SrTiO_3$ perovskite improves the microwave heating properties of the microwave-inactive Ni-supported metal oxides. As regards the dry

reforming process, it was found that ~100% CH_4 conversion (stable over 3 hours of time on stream) can be attained with proper selection of gas hourly space velocity and power. The order of the four hybrid catalytic systems tested in terms of their total syngas production rate capacity is: $Ru/SrTiO_3+Ni/Al_2O_3 > Ru/SrTiO_3+Ni/CaAl_2O_4 > Ru/SrTiO_3+Ni/Al_2MgO_4 > Ru/SrTiO_3+Ni/SiO_2$-$Al_2O_3$. Based on scale-up calculations, 50% $Ru/SrTiO_3$ + 50% Ni/Al_2O_3 is able to produce 3.45 m^3 H_2 $h^{-1}kg_{cat}^{-1}$ as compared to 2.6 m^3 H_2 $h^{-1}kg_{cat}^{-1}$ that has been reported in the literature for a carbon-based catalyst of 50% FY5 + 50% Ni/Al_2O_3.

6.2. Recommendations

The custom-made MRA has proven able to concentrate the microwave field to catalytic materials, but the generation of hotspots cannot be avoided. This makes it challenging to control uneven heating and temperature distribution due to the change in the dielectric properties of the catalytic materials with a change in temperature. A rapid temperature increase in a catalytic bed is sometimes very challenging to control manually. Therefore, an automated temperature-to-power control system for the existing reactor is recommended for future works. It is also important to develop a parallel technique to record thermocouple temperatures and automatically update them in the thermal camera calculator to instantly get the most accurate temperature distribution.

The Ru-doped $SrTiO_3$ catalyst has some advantages, compared to the Pt-C catalyst tested, such as stable volume, weight, and structure during the reaction at very high temperatures and reduced coke formation. Therefore, the Ru-doped $SrTiO_3$ perovskite catalyst was selected to form hybrid catalytic systems with Ni-based catalysts. Some of the hybrid materials though were not able to perform well in terms of CH_4 and CO_2 conversions at similar reaction conditions. One reason is the poor dielectric properties, but, further characterization of the physical and chemical properties of the fresh and spent catalysts as well as well as activity tests for all selected catalysts should be carried out to reach complete conclusions on this matter.

Finally, although some good catalysts for microwave-assisted methane dry reforming have been found, such as the Ru-doped $SrTiO_3$ catalyst and its hybrid formulation with Ni/Al_2O_3 and $Ni/CaAl_2O_4$, it is also recommended that the respective conventionally-heated dry reforming experiments with these catalysts be also performed. These experiments in combination with heat transfer simulations at reactor and particle scale will enable conclusive comparison of the two heating modes on the process performance itself and identify the reasoning behind the differences that will be obtained.

References

[1] X. Li, Diversification and localization of energy systems for sustainable development and energy security, Energy Policy. 33 (2005) 2237–2243. doi:10.1016/j.enpol.2004.05.002.

[2] EIA, International Energy Outlook 2017 Overview, U.S. Energy Inf. Adm. IEO2017 (2017) 143. doi:www.eia.gov/forecasts/ieo/pdf/0484(2016).pdf.

[3] REN21, Renewables 2013 Global Status Report, 2013. doi:ISBN 978-3-9815934-0-2.

[4] I. Carolina, D.L. Rios, F.J.S. Charnley, Skills and capabilities for a sustainable and circular economy : The changing role of design, J. Clean. Prod. 160 (2017) 109–122. doi:10.1016/j.jclepro.2016.10.130.

[5] G.Q. Chen, X.F. Wu, Energy overview for globalized world economy: Source, supply chain and sink, Renew. Sustain. Energy Rev. 69 (2017) 735–749. doi:10.1016/j.rser.2016.11.151.

[6] N. Abas, A. Kalair, N. Khan, Review of fossil fuels and future energy technologies, Futures. 69 (2015) 31–49. doi:10.1016/j.futures.2015.03.003.

[7] U.S.E.I. Administration, Annual Energy Outlook 2018 with projections to 2050 Table of contents, (n.d.).

[8] E. Summary, World Energy Outlook, (2017).

[9] C.A. Miller, E.P.A. Of, 3 . 02 Energy Resources and Policy : Vulnerability of Energy Resources and Resource Availability – Fossil Fuels (Oil , Coal , Natural Gas , Oil Shale), Elsevier, 2013. doi:10.1016/B978-0-12-384703-4.00304-X.

[10] A.E. MacDonald, C.T.M. Clack, A. Alexander, A. Dunbar, J. Wilczak, Y. Xie, Future cost-competitive electricity systems and their impact on US CO2 emissions, Nat. Clim. Chang. 6 (2016) 4–7. doi:10.1038/nclimate2921.

[11] C. Xiaoli, D.J. Tonjes, D. Mahajan, Methane emissions as energy reservoir : Context , scope , causes and mitigation strategies, Prog. Energy Combust. Sci. 56 (2016) 33–70. doi:10.1016/j.pecs.2016.05.001.

[12] C.A. Miller, E.P.A. Of, 3 . 02 Energy Resources and Policy : Vulnerability of Energy Resources and Resource Availability – Fossil Fuels (Oil , Coal , Natural Gas , Oil Shale), Elsevier, 2013. doi:10.1016/B978-0-12-384703-4.00304-X.

[13] F.A. Rahman, M.M.A. Aziz, R. Saidur, W.A.W.A. Bakar, M.R. Hainin, R. Putrajaya, N.A. Hassan, Pollution to solution: Capture and sequestration of carbon dioxide (CO2) and its utilization as a renewable energy source for a sustainable future, Renew. Sustain. Energy Rev. 71 (2017) 112–126. doi:10.1016/j.rser.2017.01.011.

[14] G.C. Project, Global carbon budget, (2014). http://www.globalcarbonproject.org/carbonbudget/index.htm.

[15] B. Studies, Trends in global co 2 emissions 2013 report, 2013.

[16] M. Saunois, P. Bousquet, B. Poulter, A. Peregon, P. Ciais, J.G. Canadell, E.J. Dlugokencky, G. Etiope, D. Bastviken, S. Houweling, G. Janssens-Maenhout, F.N. Tubiello, S. Castaldi, R.B. Jackson, M. Alexe, V.K. Arora, D.J. Beerling, P. Bergamaschi, D.R. Blake, G. Brailsford, V. Brovkin, L. Bruhwiler, C. Crevoisier, P. Crill, K. Covey, C. Curry, C. Frankenberg, N. Gedney, L. Höglund-Isaksson, M. Ishizawa, A. Ito, F. Joos, H.S. Kim, T. Kleinen, P. Krummel, J.F. Lamarque, R. Langenfelds, R. Locatelli, T. Machida, S. Maksyutov, K.C. McDonald, J. Marshall, J.R. Melton, I. Morino, V. Naik, S. O'Doherty, F.J.W. Parmentier, P.K. Patra, C. Peng, S. Peng, G.P. Peters, I. Pison, C. Prigent, R. Prinn, M. Ramonet, W.J. Riley, M. Saito, M. Santini, R. Schroeder, I.J. Simpson, R. Spahni, P.

Steele, A. Takizawa, B.F. Thornton, H. Tian, Y. Tohjima, N. Viovy, A. Voulgarakis, M. Van Weele, G.R. Van Der Werf, R. Weiss, C. Wiedinmyer, D.J. Wilton, A. Wiltshire, D. Worthy, D. Wunch, X. Xu, Y. Yoshida, B. Zhang, Z. Zhang, Q. Zhu, The global methane budget 2000-2012, Earth Syst. Sci. Data. 8 (2016) 697–751. doi:10.5194/essd-8-697-2016.

[17] S. Arora, R. Prasad, An overview on dry reforming of methane: strategies to reduce carbonaceous deactivation of catalysts, RSC Adv. 6 (2016) 108668–108688. doi:10.1039/C6RA20450C.

[18] J.M.F. Iii, The Different Catalytic Routes for Methane Liquid Fuels The Different Catalytic Routes for Methane Valorization : An Assessment of Processes for liquid Fuels, 4940 (2016). doi:10.1080/01614949308014605.

[19] A.I. Olivos-suarez, A. Sze, E.A. Pidko, J. Gascon, Strategies for the Direct Catalytic Valorization of Methane Using Heterogeneous Catalysis : Challenges and Opportunities, (2016). doi:10.1021/acscatal.6b00428.

[20] T. da Silva Veras, T.S. Mozer, D. da Costa Rubim Messeder dos Santos, A. da Silva César, Hydrogen: Trends, production and characterization of the main process worldwide, Int. J. Hydrogen Energy. 42 (2017) 2018–2033. doi:10.1016/j.ijhydene.2016.08.219.

[21] C. Xiaoli, D.J. Tonjes, D. Mahajan, Methane emissions as energy reservoir : Context , scope , causes and mitigation strategies, Prog. Energy Combust. Sci. 56 (2016) 33–70. doi:10.1016/j.pecs.2016.05.001.

[22] L. Mennicken, A. Janz, S. Roth, The German R&D Program for CO2 Utilization—Innovations for a Green Economy, Environ. Sci. Pollut. Res. 23 (2016) 11386–11392. doi:10.1007/s11356-016-6641-1.

[23] G.D. Stefanidis, A.N. Muñoz, G.S.J. Sturm, A. Stankiewicz, A helicopter view of microwave application to chemical processes: reactions, separations, and equipment concepts, Rev. Chem. Eng. 30 (2014) 1–26. doi:10.1515/revce-2013-0033.

[24] R.J. (Roger J.. Meredith, Institution of Electrical Engineers., Engineers' handbook of industrial microwave heating, Institution of Electrical Engineers, 1998.

[25] G.D. Stefanidis, A.N. Muñoz, G.S.J. Sturm, A. Stankiewicz, A helicopter view of microwave application to chemical processes: reactions, separations, and equipment concepts, Rev. Chem. Eng. 30 (2014) 1–26. doi:10.1515/revce-2013-0033.

[26] V. Gnaneswar Gude, P. Patil, E. Martinez-Guerra, S. Deng, N. Nirmalakhandan, Microwave energy potential for biodiesel production, (n.d.).

[27] D.M. Pozar, Microwave Engineering, Wiley, 1997. https://books.google.be/books?id=IDxTAAAAMAAJ (accessed November 22, 2016).

[28] J. Hunt, A. Ferrari, A. Lita, M. Crosswhite, B. Ashley, A.E. Stiegman, Microwave-Specific Enhancement of the Carbon − Carbon Dioxide (Boudouard) Reaction, (2013).

[29] W. Yunpu, D.A.I. Leilei, F.A.N. Liangliang, S. Shaoqi, L.I.U. Yuhuan, Journal of Analytical and Applied Pyrolysis Review of microwave-assisted lignin conversion for renewable fuels and chemicals, J. Anal. Appl. Pyrolysis. 119 (2016) 104–113. doi:10.1016/j.jaap.2016.03.011.

[30] Y. Pang, H. Lei, Degradation of p-nitrophenol through microwave-assisted heterogeneous activation of peroxymonosulfate by manganese ferrite, Chem. Eng. J. 287 (2016) 585–592. doi:10.1016/j.cej.2015.11.076.

[31] Y.S. Malghe, Nanosized SrTiO3 powder from oxalate precursor microwave aided synthesis and thermal characterization, J. Therm. Anal. Calorim. 102 (2010) 831–836. doi:10.1007/s10973-010-0786-9.

[32] K. Asadian, T. Ebadzadeh, Synthesis of Nanosized Ba(Zn1/3Nb2/3)O3 Using Microwave

Heating Process, J. Mater. Eng. Perform. 22 (2012) 898–902. doi:10.1007/s11665-012-0328-7.

[33] S.H. Jhung, J.-H. Lee, J.W. Yoon, Y.K. Hwang, J.-S. Hwang, S.-E. Park, J.-S. Chang, Effects of reaction conditions in microwave synthesis of nanocrystalline barium titanate, Mater. Lett. 58 (2004) 3161–3165. doi:10.1016/j.matlet.2004.06.006.

[34] X. Zhang, C.S. Lee, D.M.P. Mingos, D.O. Hayward, Carbon dioxide reforming of methane with Pt catalysts using microwave dielectric heating, 88 (2003) 129–139.

[35] X.-R. Zhang, L.-C. Wang, Y. Cao, W.-L. Dai, H.-Y. He, K.-N. Fan, A unique microwave effect on the microstructural modification of Cu/ZnO/Al2O3 catalysts for steam reforming of methanol., Chem. Commun. (Camb). (2005) 4104–6. doi:10.1039/b502997j.

[36] A. Domínguez, Y. Fernandez, B. Fidalgo, J.J. Pis, J.A. Menendez, Biogas to Syngas by Microwave-Assisted Dry Reforming in the Presence of Char, Energy & Fuels. 21 (2007) 2066–2071. doi:10.1021/ef070101j.

[37] B. Fidalgo, a Dominguez, J. Pis, J. Menendez, Microwave-assisted dry reforming of methane, Int. J. Hydrogen Energy. 33 (2008) 4337–4344. doi:10.1016/j.ijhydene.2008.05.056.

[38] W.-H. Chen, J.-G. Jheng, a. B. Yu, Hydrogen generation from a catalytic water gas shift reaction under microwave irradiation, Int. J. Hydrogen Energy. 33 (2008) 4789–4797. doi:10.1016/j.ijhydene.2008.06.059.

[39] W.-H. Chen, B.-J. Lin, Effect of microwave double absorption on hydrogen generation from methanol steam reforming, Int. J. Hydrogen Energy. 35 (2010) 1987–1997. doi:10.1016/j.ijhydene.2009.12.147.

[40] W. Deng, Y. Su, S. Liu, H. Shen, Microwave-assisted methane decomposition over pyrolysis residue of sewage sludge for hydrogen production, Int. J. Hydrogen Energy. 39 (2014) 9169–9179. doi:10.1016/j.ijhydene.2014.04.033.

[41] a Dominguez, B. Fidalgo, Y. Fernandez, J. Pis, J. Menendez, Microwave-assisted catalytic decomposition of methane over activated carbon for CO2CO2-free hydrogen production, Int. J. Hydrogen Energy. 32 (2007) 4792–4799. doi:10.1016/j.ijhydene.2007.07.041.

[42] Y. Xu, Z. Tian, Z. Xu, L. Lin, Reactions in a Mixture of CH 4 and CO 2 under the Action of Microwave Discharge at Atmospheric Pressure, 11 (2002) 28–32.

[43] T. Durka, G. D Stefanidis, T. Van Gerven, A. Stankiewicz, On the accuracy and reproducibility of fiber optic (FO) and infrared (IR) temperature measurements of solid materials in microwave applications, Meas. Sci. Technol. 21 (2010) 045108. doi:10.1088/0957-0233/21/4/045108.

[44] T. Durka, G.D. Stefanidis, T. Van Gerven, A.I. Stankiewicz, Microwave-activated methanol steam reforming for hydrogen production, Int. J. Hydrogen Energy. 36 (2011) 12843–12852. doi:10.1016/j.ijhydene.2011.07.009.

[45] T.L. Roussière, Catalytic Reforming of Methane in the Presence of CO 2 and H 2 O at High Pressure, (2013).

[46] D. Pakhare, J. Spivey, A review of dry (CO2) reforming of methane over noble metal catalysts, Chem. Soc. Rev. 43 (2014). doi:10.1039/c3cs60395d.

[47] P. Gangadharan, K.C. Kanchi, H.H. Lou, Evaluation of the economic and environmental impact of combining dry reforming with steam reforming of methane, Chem. Eng. Res. Des. 90 (2012) 1956–1968. doi:10.1016/j.cherd.2012.04.008.

[48] B. Fidalgo, J.A. Menéndez, SYNGAS PRODUCTION BY CO 2 REFORMING OF CH 4 UNDER MICROWAVE HEATING – CHALLENGES AND OPPORTUNITIES, (2013) 121–149.

[49] D. Pakhare, J. Spivey, A review of dry (CO2) reforming of methane over noble metal catalysts., Chem. Soc. Rev. (2014). doi:10.1039/c3cs60395d.
[50] M. Oghbaei, O. Mirzaee, Microwave versus conventional sintering : A review of fundamentals , advantages and applications, J. Alloys Compd. 494 (2010) 175–189. doi:10.1016/j.jallcom.2010.01.068.
[51] M. Omran, T. Fabritius, R. Mattila, Thermally assisted liberation of high phosphorus oolitic iron ore : A comparison between microwave and conventional furnaces, Powder Technol. 269 (2015) 7–14. doi:10.1016/j.powtec.2014.08.073.
[52] D. Li, Y. Nakagawa, K. Tomishige, Methane reforming to synthesis gas over Ni catalysts modified with noble metals, Appl. Catal. A Gen. 408 (2011) 1–24. doi:10.1016/j.apcata.2011.09.018.
[53] T. Durka, T. Van Gerven, A. Stankiewicz, Microwaves in Heterogeneous Gas-Phase Catalysis: Experimental and Numerical Approaches, Chem. Eng. Technol. 32 (2009) 1301–1312. doi:10.1002/ceat.200900207.
[54] L.S. Gangurde, G.S.J. Sturm, T.J. Devadiga, A.I. Stankiewicz, G.D. Stefanidis, Complexity and Challenges in Noncontact High Temperature Measurements in Microwave-Assisted Catalytic Reactors, Ind. Eng. Chem. Res. 56 (2017) 13379–13391. doi:10.1021/acs.iecr.7b02091.
[55] J.M. Osepchuk, A History of Microwave Heating Applications, IEEE Trans. Microw. Theory Tech. 32 (1984) 1200–1224. doi:10.1109/TMTT.1984.1132831.
[56] J. Sun, W. Wang, Q. Yue, C. Ma, J. Zhang, X. Zhao, Z. Song, Review on microwave-metal discharges and their applications in energy and industrial processes, Appl. Energy. 175 (2016). doi:10.1016/j.apenergy.2016.04.091.
[57] M. Omran, T. Fabritius, R. Mattila, Thermally assisted liberation of high phosphorus oolitic iron ore : A comparison between microwave and conventional furnaces, Powder Technol. 269 (2015) 7–14. doi:10.1016/j.powtec.2014.08.073.
[58] M. Oghbaei, O. Mirzaee, Microwave versus conventional sintering : A review of fundamentals , advantages and applications, J. Alloys Compd. 494 (2010) 175–189. doi:10.1016/j.jallcom.2010.01.068.
[59] L. Acevedo, S. Usón, J. Uche, Exergy transfer analysis of microwave heating systems, Energy. 68 (2014) 349–363. doi:10.1016/j.energy.2014.02.041.
[60] L. Acevedo, S. Usón, J. Uche, Numerical study of cullet glass subjected to microwave heating and SiC susceptor effects . Part II : Exergy transfer analysis, Energy Convers. Manag. 97 (2015) 458–469. doi:10.1016/j.enconman.2015.03.065.
[61] S. Chandrasekaran, S. Ramanathan, T. Basak, Microwave Material Processing — A Review, 58 (2012). doi:10.1002/aic.
[62] J. Goyette, R. Chahine, T.K. Bose, C. Akyel, R. Bosisio, Importance of the Dielectric Properties of Materials for Microwave Heating, Dry. Technol. 8 (1990) 1111–1121. doi:10.1080/07373939008959938.
[63] G.S.J. Sturm, M.D. Verweij, A.I. Stankiewicz, G.D. Stefanidis, Microwaves and microreactors: Design challenges and remedies, Chem. Eng. J. 243 (2014) 147–158. doi:10.1016/j.cej.2013.12.088.
[64] S. Horikoshi, A. Osawa, M. Abe, N. Serpone, On the generation of hot-spots by microwave electric and magnetic fields and their impact on a microwave-assisted heterogeneous reaction in the presence of metallic Pd nanoparticles on an activated carbon support, J. Phys. Chem. C. 115 (2011) 23030–23035. doi:10.1021/jp2076269.
[65] X. Zhang, D.O. Hayward, C. Lee, D.M.P. Mingos, Microwave assisted catalytic reduction

of sulfur dioxide with methane over MoS2 catalysts, Appl. Catal. B Environ. 33 (2001) 137–148. doi:10.1016/S0926-3373(01)00171-0.

[66] C.O. Kappe, How to measure reaction temperature in microwave-heated transformations, Chem. Soc. Rev. 42 (2013) 4977–4990. doi:10.1039/c3cs00010a.

[67] A. Ramirez, J.L. Hueso, R. Mallada, J. Santamaria, In situ temperature measurements in microwave-heated gas-solid catalytic systems. Detection of hot spots and solid-fluid temperature gradients in the ethylene epoxidation reaction, (2017). doi:10.1016/j.cej.2017.01.077.

[68] A. Ramírez, J.L. Hueso, R. Mallada, J. Santamaría, Ethylene epoxidation in microwave heated structured reactors, Catal. Today. (2016). doi:10.1016/j.cattod.2016.01.007.

[69] E. Pert, Y. Carmel, A. Birnboim, T. Olorunyolemi, D. Gershon, J. Calame, I.K. Lloyd, O.C. Wilson, Temperature measurements during microwave processing: the significance of thermocouple effects, J. Am. Ceram. Soc. 84 (2001) 1981–1986. doi:10.1111/j.1151-2916.2001.tb00946.x.

[70] H. Will, P. Scholz, B. Ondruschka, Heterogeneous gas-phase catalysis under microwave irradiation - A new multi-mode microwave applicator, Top. Catal. 29 (2004) 175–182. http://www.scopus.com/inward/record.url?eid=2-s2.0-3042801191&partnerID=40&md5=1b040fcfcddd920fdf20148d4c579fc1.

[71] L. Li, X. Jiang, H. Wang, J. Wang, Z. Song, X. Zhao, C. Ma, Title: Methane dry and mixed reforming on the mixture of bio-char and nickel-based catalyst with microwave assistance Methane dry and mixed reforming on the mixture of bio-char and nickel-based catalyst with microwave assistance, J. Anal. Appl. Pyrolysis. (2017). doi:10.1016/j.jaap.2017.03.009.

[72] G.S.J. Sturm, A.Q. Van Braam Houckgeest, M.D. Verweij, T. Van Gerven, A.I. Stankiewicz, G.D. Stefanidis, Exploration of rectangular waveguides as a basis for microwave enhanced continuous flow chemistries, Chem. Eng. Sci. 89 (2013) 196–205. doi:10.1016/j.ces.2012.11.039.

[73] S.D. Luo, Y.F. Yang, G.B. Schaffer, M. Qian, Calibration of Temperature Measurement by Infrared Pyrometry in Microwave Heating of Powder Materials : an Exothermic Reaction Based Approach, 47 (2013) 5–11.

[74] X. Shen, G. Xu, C. Shao, C. Cheng, Temperature dependence of infrared emissivity of doped manganese oxides in different wavebands (3–5 and 8–14μm), J. Alloys Compd. 479 (2009) 420–422. doi:10.1016/j.jallcom.2008.12.090.

[75] R.P. Madding, Emissivity measurement and temperature correction accuracy considerations, Spie Conf. Thermosense XXI. 3700 (1999) 393–401. doi:10.1117/12.342307.

[76] H.T. Pressures, V.A. Petrov, Measurement of the emissivity of quartz glass, (2016).

[77] J.M. Catalá-Civera, A.J. Canós, P. Plaza-González, J.D. Gutiérrez, B. García-Baños, F.L. Peñaranda-Foix, Dynamic Measurement of Dielectric Properties of Materials at High Temperature during Microwave Heating in a Dual Mode Cylindrical Cavity, IEEE Trans. Microw. Theory Tech. 63 (2015) 2905–2914. doi:10.1109/TMTT.2015.2453263.

[78] F.L. Penaranda-Foix, M.D. Janezic, J.M. Catala-Civera, A.J. Canos, Full-wave analysis of dielectric-loaded cylindrical waveguides and cavities using a new four-port ring network, IEEE Trans. Microw. Theory Tech. 60 (2012) 2730–2740. doi:10.1109/TMTT.2012.2206048.

[79] W.-H. Chen, H.-J. Liou, C.-I. Hung, A numerical approach of interaction of methane thermocatalytic decomposition and microwave irradiation, Int. J. Hydrogen Energy. 38 (2013) 13260–13271. doi:10.1016/j.ijhydene.2013.07.107.

[80] A. Gvakharia, E.A. Kort, A. Brandt, J. Peischl, T.B. Ryerson, J.P. Schwarz, M.L. Smith, C. Sweeney, Methane, Black Carbon, and Ethane Emissions from Natural Gas Flares in the Bakken Shale, North Dakota, Environ. Sci. Technol. 51 (2017) 5317–5325. doi:10.1021/acs.est.6b05183.

[81] L. Höglund-Isaksson, Bottom-up simulations of methane and ethane emissions from global oil and gas systems 1980 to 2012, Environ. Res. Lett. 12 (2017) 024007. doi:10.1088/1748-9326/aa583e.

[82] R. Heede, Tracing anthropogenic carbon dioxide and methane emissions to fossil fuel and cement producers, 1854-2010, Clim. Change. 122 (2014) 229–241. doi:10.1007/s10584-013-0986-y.

[83] M.C.J. Bradford, M. a. Vannice, CO 2 Reforming of CH 4, Catal. Rev. 41 (1999) 1–42. doi:10.1081/CR-100101948.

[84] H.R. Gurav, R. Bobade, V.L. Das, S. Chilukuri, Carbon dioxide reforming of methane over ruthenium substituted strontium titanate perovskite catalysts, Indian J. Chem. - Sect. A Inorganic, Phys. Theor. Anal. Chem. 51 (2012) 1339–1347.

[85] D. Stuerga, P. Gaillard, Microwave heating as a new way to induce localized enhancements of reaction rate. Non-isothermal and heterogeneous kinetics, Tetrahedron. 52 (1996) 5505–5510. doi:10.1016/0040-4020(96)00241-4.

[86] H.J. Yang, B.P. Mathew, D.G. Oh, K. Myung, J.H. Kwak, S.Y. Hong, Efficient copper catalysts for C[sbnd]H bond arylation under microwave heating: Direct access to multi-substituted pivanilides, Catal. Commun. 90 (2017) 83–86. doi:10.1016/j.catcom.2016.11.022.

[87] F. Karimi, B.A. Peppley, Comparison of conventional versus microwave heating for polyol synthesis of supported iridium based electrocatalyst for polymer electrolyte membrane water electrolysis, Int. J. Hydrogen Energy. 42 (2017) 5083–5094. doi:10.1016/j.ijhydene.2017.01.090.

[88] B. Fidalgo, a. Arenillas, J. a. Menéndez, Influence of porosity and surface groups on the catalytic activity of carbon materials for the microwave-assisted CO2 reforming of CH4, Fuel. 89 (2010) 4002–4007. doi:10.1016/j.fuel.2010.06.015.

[89] B. Fidalgo, J. a. Menéndez, Study of energy consumption in a laboratory pilot plant for the microwave-assisted CO2 reforming of CH4, Fuel Process. Technol. 95 (2012) 55–61. doi:10.1016/j.fuproc.2011.11.012.

[90] R.M. Navarro, M.C. Alvarez-Galvan, J.A. Villoria, I.D. González-Jiménez, F. Rosa, J.L.G. Fierro, Effect of Ru on LaCoO3 perovskite-derived catalyst properties tested in oxidative reforming of diesel, Appl. Catal. B Environ. 73 (2007) 247–258. doi:10.1016/j.apcatb.2006.12.013.

[91] J. Sunarso, S.S. Hashim, N. Zhu, W. Zhou, Perovskite oxides applications in high temperature oxygen separation, solid oxide fuel cell and membrane reactor: A review, Prog. Energy Combust. Sci. 61 (2017) 57–77. doi:10.1016/j.pecs.2017.03.003.

[92] D.J. Liu, M. Krumpelt, Activity and structure of perovskites as diesel-reforming catalysts for solid oxide fuel cell, Int. J. Appl. Ceram. Technol. 2 (2005) 301–307. doi:10.1111/j.1744-7402.2005.02032.x.

[93] A. Karaphun, S. Hunpratub, T. Putjuso, E. Swatsitang, Characterization and dielectric properties of SrTi 1− x Mn x O 3 ceramics, Jpn. J. Appl. Phys. 54 (2015) 06FH09. doi:10.7567/JJAP.54.06FH09.

[94] A. Karaphun, S. Hunpratub, E. Swatsitang, Effect of annealing on magnetic properties of Fe-doped SrTiO3 nanopowders prepared by hydrothermal method, Microelectron. Eng. 126

(2014) 42–48. doi:10.1016/j.mee.2014.05.001.
[95] S. Sartipi, S. Xiaohui, T. Cordero, Supporting Information-Carbon / H-ZSM-5 composites as supports for bi-functional Fischer-Tropsch, Catal. Sci. Technol. 5 (2016) 20–23.
[96] R. Cherbański, Calculation of critical efficiency factors of microwave energy conversion into heat, Chem. Eng. Technol. 34 (2011) 2083–2090. doi:10.1002/ceat.201100405.
[97] F. Matei-Rutkovska, G. Postole, C.G. Rotaru, M. Florea, V.I. Pârvulescu, P. Gelin, Synthesis of ceria nanopowders by microwave-assisted hydrothermal method for dry reforming of methane, Int. J. Hydrogen Energy. 41 (2016) 2512–2525. doi:10.1016/j.ijhydene.2015.12.097.
[98] G.S.J. Sturm, M.D. Verweij, T. Van Gerven, A.I. Stankiewicz, G.D. Stefanidis, On the parametric sensitivity of heat generation by resonant microwave fields in process fluids, Int. J. Heat Mass Transf. 57 (2013) 375–388. doi:10.1016/j.ijheatmasstransfer.2012.09.037.
[99] M.A. Goula, N.D. Charisiou, G. Siakavelas, L. Tzounis, I. Tsiaoussis, P. Panagiotopoulou, G. Goula, I. V. Yentekakis, Syngas production via the biogas dry reforming reaction over Ni supported on zirconia modified with CeO2 or La2O3 catalysts, Int. J. Hydrogen Energy. 42 (2017) 13724–13740. doi:10.1016/j.ijhydene.2016.11.196.
[100] V. Pawar, D. Ray, C. Subrahmanyam, V.M. Janardhanan, Study of Short-Term Catalyst Deactivation Due to Carbon Deposition during Biogas Dry Reforming on Supported Ni Catalyst, Energy and Fuels. 29 (2015) 8047–8052. doi:10.1021/acs.energyfuels.5b01862.
[101] J. a. Menéndez, a. Arenillas, B. Fidalgo, Y. Fernández, L. Zubizarreta, E.G. Calvo, J.M. Bermúdez, Microwave heating processes involving carbon materials, Fuel Process. Technol. 91 (2010) 1–8. doi:10.1016/j.fuproc.2009.08.021.
[102] T. Santos, L.C. Costa, M. Valente, J. Monteiro, J. Sousa, 3D Electromagnetic Field Simulation in Microwave Ovens : a Tool to Control Thermal Runaway, Proc. COMSOL Conf. (2010) 1–7.
[103] T. Santos, M.A. Valente, J. Monteiro, J. Sousa, L.C. Costa, Electromagnetic and thermal history during microwave heating, Appl. Therm. Eng. 31 (2011) 3255–3261. doi:10.1016/j.applthermaleng.2011.06.006.
[104] J.-M. Lavoie, Review on dry reforming of methane, a potentially more environmentally-friendly approach to the increasing natural gas exploitation., Front. Chem. 2 (2014) 81. doi:10.3389/fchem.2014.00081.
[105] F. Wang, L. Xu, J. Yang, J. Zhang, L. Zhang, H. Li, Y. Zhao, H.X. Li, K. Wu, G.Q. Xu, W. Chen, Enhanced catalytic performance of Ir catalysts supported on ceria-based solid solutions for methane dry reforming reaction, Catal. Today. 281 (2017) 295–303. doi:10.1016/j.cattod.2016.03.055.
[106] L. Xu, L. Duan, M. Tang, P. Liu, X. Ma, Y. Zhang, H.G. Harris, M. Fan, Catalytic CO2 reforming of CH4 over Cr-promoted Ni/char for H2 production, Int. J. Hydrogen Energy. 39 (2014) 10141–10153. doi:10.1016/j.ijhydene.2014.04.172.
[107] G. Zhang, A. Su, Y. Du, J. Qu, Y. Xu, Catalytic performance of activated carbon supported cobalt catalyst for CO2 reforming of CH4, J. Colloid Interface Sci. 433 (2014) 149–155. doi:10.1016/j.jcis.2014.06.038.
[108] S.S. Itkulova, G.D. Zakumbaeva, Y.Y. Nurmakanov, A.A. Mukazhanova, A.K. Yermaganbetova, Syngas production by bireforming of methane over Co-based alumina-supported catalysts, Catal. Today. 228 (2014) 194–198. doi:10.1016/j.cattod.2014.01.013.
[109] M.-S. Fan, A.Z. Abdullah, S. Bhatia, Hydrogen production from carbon dioxide reforming of methane over Ni–Co/MgO–ZrO2 catalyst: Process optimization, Int. J. Hydrogen Energy. 36 (2011) 4875–4886. doi:10.1016/j.ijhydene.2011.01.064.

[110] J.M. Bermúdez, a. Arenillas, J. a. Menéndez, Syngas from CO2 reforming of coke oven gas: Synergetic effect of activated carbon/Ni–γAl2O3 catalyst, Int. J. Hydrogen Energy. 36 (2011) 13361–13368. doi:10.1016/j.ijhydene.2011.07.124.
[111] G. Zhang, L. Hao, Y. Jia, Y. du, Y. Zhang, CO2 reforming of CH4 over efficient bimetallic Co–Zr/AC catalyst for H2 production, Int. J. Hydrogen Energy. 40 (2015) 12868–12879. doi:10.1016/j.ijhydene.2015.07.011.
[112] B. Fidalgo, J.A. Menéndez, Syngas Production By Co2 Reforming of Ch4 Under Microwave Heating – Challenges and Opportunities, Syngas Prod. Appl. Environ. Impact. (2011) 1–28.
[113] L. Li, X. Jiang, H. Wang, J. Wang, Z. Song, X. Zhao, C. Ma, Methane dry and mixed reforming on the mixture of bio-char and nickel-based catalyst with microwave assistance, J. Anal. Appl. Pyrolysis. 125 (2017) 318–327. doi:10.1016/j.jaap.2017.03.009.
[114] D. Pakhare, J. Spivey, A review of dry (CO2) reforming of methane over noble metal catalysts, Chem. Soc. Rev. 43 (2014). doi:10.1039/c3cs60395d.
[115] F.L. Penaranda-Foix, M.D. Janezic, J.M. Catala-Civera, A.J. Canos, Full-Wave Analysis of Dielectric-Loaded Cylindrical Waveguides and Cavities Using a New Four-Port Ring Network, IEEE Trans. Microw. Theory Tech. 60 (2012) 2730–2740. doi:10.1109/TMTT.2012.2206048.
[116] A.J. Canos-Marin, F.L. Penaranda-Foix, J.M. Catala-Civera, B. Garcia-Banos, Measurement of dielectric properties at high-temperatures in real-time with cylindrical cavity, in: 2010 IEEE MTT-S Int. Microw. Symp., IEEE, 2010: pp. 1–1. doi:10.1109/MWSYM.2010.5518314.
[117] J.M. Catala-Civera, A.J. Canos, P. Plaza-Gonzalez, J.D. Gutierrez, B. Garcia-Banos, F.L. Penaranda-Foix, Dynamic Measurement of Dielectric Properties of Materials at High Temperature During Microwave Heating in a Dual Mode Cylindrical Cavity, IEEE Trans. Microw. Theory Tech. 63 (2015) 2905–2914. doi:10.1109/TMTT.2015.2453263.
[118] ASTM D2520 - 13 Standard Test Methods for Complex Permittivity (Dielectric Constant) of Solid Electrical Insulating Materials at Microwave Frequencies and Temperatures to 1650°C, (n.d.).
[119] L.S. Gangurde, G.S.J. Sturm, M.J. Valero-Romero, R. Mallada, J. Santamaria, A.I. Stankiewicz, G.D. Stefanidis, Synthesis, characterization, and application of ruthenium-doped SrTiO3perovskite catalysts for microwave-assisted methane dry reforming, Chem. Eng. Process. - Process Intensif. 127 (2018) 178–190. doi:10.1016/j.cep.2018.03.024.
[120] A. Kumar, V. Agarwala, D. Singh, Microwave absorbing behavior of metal dispersed TiO2 nanocomposites, Adv. Powder Technol. 25 (2014) 483–489. doi:10.1016/j.apt.2013.07.006.
[121] L. Guczi, G. Stefler, O. Geszti, I. Sajó, Z. Pászti, A. Tompos, Z. Schay, Methane dry reforming with CO2: A study on surface carbon species, Appl. Catal. A Gen. 375 (2010) 236–246. doi:10.1016/j.apcata.2009.12.040.

Appendix

Table 0.1: Parts list description of P&ID.

No.	Tag	Description	T_{design} (°C)	$T_{operating}$ (°C)	P_{design} (bar*)	$P_{operating}$ (bara*)	Flow rate+
1.	V101	Pressure reducer for pneumatics		Ambient		< 8	
2.	V102	Ball valve on compressed air ring line		Ambient		< 8	
3.	V103	Pressure reducer for air		Ambient		< 8	
4.	V104	Pneumatic valve for air		Ambient		< 15	
5.	V105	Ball valve on argon ring		Ambient		< 15	
6.	V106	Pressure reducer of argon ring		Ambient		< 15	
7.	V107	Pneumatic ball valve for argon		Ambient		< 15	
8.	V108	One-way valve		Ambient	VACUUM-ATM	VACUUM-ATM	
9.	V109	Ball valve on N_2 ring line		Ambient		< 8	
10.	V110	Pressure reducer for N_2		Ambient		< 8	
11.	V111	Pneumatic ball valve for N2		Ambient		< 8	
12.	V112	Pressure reducer for H2		Ambient		< 8	
13	V113	Pneumatic ball valve for H2		Ambient		< 8	
14	V114	Pressure reducer for CH_4		Ambient		< 8	
15	V115	Pneumatic valve for CH4		Ambient		< 8	
16	V116	Pressure reducer for O2		Ambient		< 8	
17	V117	Pneumatic valve for O2		Ambient		< 8	
18	V118	Pressure reducer for CO2		Ambient		< 8	
19	V119	Pneumatic valve for CO2		Ambient		< 8	
20	V120	Pressure reducer for CO		Ambient		< 8	
21	V121	Pneumatic valve for CO		Ambient		< 8	
22	V122	Reactant bypass valve		Ambient	VACUUM-ATM	VACUUM-ATM	
23	V123	Pneumatic valve to plasma reactor		Ambient	VACUUM-ATM	VACUUM-ATM	
24	V124	Pneumatic valve to catalytic reactor		Ambient	VACUUM-ATM	VACUUM-ATM	
25	V125	Fluid back pressure valve		Ambient		ATM	
26	FI151	Omega FL-2044, Rotameter with integrated needle valve	-	Ambient	-	ATM+	-
27	MFC152	Bronkhorst F-201CV-5K0-AAD-22-V	-	Ambient	64	0.01 to 1.2	0.04 to 5ln/min(Air)

28	MFC153	Bronkhorst F-201CV-1K0-RAD-33-V	-	Ambient	64	0.01 to 1.2	8 to 1000 mln/min(air)
29	MFC154	Bronkhorst F-201-CV-500-RAD-33-V	-	Ambient	64	0.01 to 1.2	8 to 1000 mln/min(air)
30	MFC155	Bronkhorst F-201CV-500-RAD-33-V	-	Ambient	1.3	0.01 to 1.2	500 mln/min
31	MFC156	Bronkhorst L13-AAD-11-K30S	-	Ambient	1.5	0.01 to 1.2	72g/h mix
32	PMP1	Micro gear pump, Bronkhorst LP122-22-K	-	Ambient	64	ATM+	-
33	LFV	Liquid feeding vessel	-	Ambient	-	ATM	-
34	EVAP	Evaporator, Bronkhorst Type W-202A-122-K	-	Ambient	-	-	72g/h mix 6.5 ln/min
35	FLT	Filter	-	-	-	-	-
36	V130	Ball valve on H2 ring line					
37	V131	Ball valve on CH4 ring line					
38	V132	Ball valve on O2 ring line					
39	V133	Ball valve on CO2 ring line					
40	V134	Ball valve on CO ring line					
41	V135	Pressure reducer N2, MS Carrier gas					
42	V136	Pressure reducer Ar, MS carrier & shielding gas					
43	V137	Pressure reducer Ar, GC Carrier Gas					
44	V140	Pressure reducer He, GC Carrier Gas					
45	FI160	Catalytic reactor moisture barrier gas Omega FL-2501-V					0.1-1.5 L/min
46	FI161	Catalytic reactor outlet cooling gas Omega FL-2501-V					0.1-1.5 L/min
47	XR201	Ocean Optics:HR2000+CG Optical spectrometer; 74-UV collimating lens					
48	TRI202	Thermocouple	-200… +1250	+20… +50	<10	1 to 1.2	-
49	TC203	Temperature control via tracing. (1) cool to manageable temperature <200°C & (2) prevent condensation >100°C. Req. may need adjustment.	-200… +1250	+20… +50	<10	1 to 1.2	-
50	PRI204	Pressure sensor					
51	DPRI205	Pressure difference sensor AE-PP+M-10.0-0002B-B			0-2	0.01-1	
52	MFC Instr.	Power supply/readout unit, Type E-7210; Flowbus connectivity(unit from older setup, ** see photograph; to connect unit with existing flow bus circuit.	<50	Ambient	-	-	-
53	Enclosures	Plasma & catalytic reactor enclosures					

		(To keep reactors in continuously ventilated volume, total air flow through lab ventilation dilute CO conc. Below TLV)					
54	Calib. Gases	Calibration gas bottles of appropriate composition for GC calibration					
55 **56**	TR211 to TR-N	Four N-type Thermocouples	-200… +1250	-200… +1250			
57	FLT2 & FLT3	Whatman FP050/1 Filter holder with 50 mm paper filter					
58	SS-MWG	Solid-state MW generator assembled out of generator module and power supply. It is swappable between both reactors					
59	SRF	Surfatron plasma generator					
60	TST1	Lauda Thermostat RE304 Ethylene Glycol solution coolant					
61	CMP2	KNF SC 920 (Pressure regulation)					
62	CMP3	KNF N838.3 KT.18 (Compressor to feed gas chromatograph with sample gas)					
63	TT230, TT309	Two thermocouples	-200… +1250	-20…+20			
64	FT231, FT310	Flowswitch depends on TST1/TST2					~ 1 L/min
65	V250	Pneumatic ball valve					
66	V251	Pneumatic ball valve					
67	V252	Membrane valve, manual (to choke CPM3 to reduce flow)		ambient		VACUUM-ATM	
68	V253	Pneumatic ball valve					
69	PRI301	Pressure sensor ~ 0.75 – 1.5 bara				0.75 – 1.5	
70	TTR302	Thermal Camera, FLIR A645 SC(Image processing required)					
71	TR303	Thermocouple, 0.5 mm diameter (Tmeas. Below catalytic bed but has to remain outside MW field)	-200… +1250	0 to 1000			
72	TC304/ TRI304	Controls tracing embedded in reactor 0.5 mm(To prevent condensation of moisture)	-200… +1250	0 to 200			
73	TC305	Temperature control on tracing	-200… +1250				
74	V311	Pneumatic ball valve			Ambient	<8	

75	V312	Ball valve, manual				
76	V313	Ball valve, manual				
77	V314	Pneumatic ball valve				
78	V315	Pneumatic ball valve				
79	CND	Condensor(To condense bulk of moisture out of gas stream to avoid condensation in ventilation)				
80	ITR	Impedance transformer, SAIREM Magic-t transformet with E-bend waveguide	<50	Ambient		
81	MRA	Microwave reactor assembly consists of split shell waveguide, sairem MW circuitry elements, quartz tube.	0 to 1000	0 to 1000	<2	ATM+
82	TST2	Lauda RE620 (Ethylene glycol solution coolant)				
83	GWB1	Both 1 & 2 are Gas wash bottles(CaO added as adsorption agent)	Ambient	Ambient	VACUUM-ATM	VACUUM-ATM
84	GWB2	To dewater sample gas, custom designed at 30 mbara	Ambient	Ambient	VACUUM-ATM	VACUUM-ATM
85	Mass Spectrometer	HIDEN Model No: HAS-223-001(for completeness systems parts are included below)				
86	CMP-SC	Compressor to mass spectrometer model no: Nxd561 100/240V				
87	PT420	Pressure sensor				
88	XT421	Ion detector				
89	V423	Bypass valve				
90	CMP-TM	Turbo-molecular pump				
91	STM	Static mixer				
92	FI401	F-111B-100-RAD-33-V	The purpose of these instruments is to add a carrier gas so that 1) It can be verified that the GC line has a positive flow and 2) so that the gas consumption by the MS can be reduced by adding a carrier gas to the stream into it.			
93	PC402	P-602CV-350A-RAD-33-V				
94	MFC403	F-201CV-200-RAD-22-V				
95	MFC404	F-201CV-200-RAD-22-V				
96	MFC405	F-201CV-200-RAD-22-V				
97	MFT406	F-101D-RAD-33-V				
98	V410	Pneumatic ball valve				
99	V413	Three-way ball valve; Modify to minimize dead volume sample bag connection				
100	CAP	Capillary to reduce pressure, while avoiding condensation				

		of moisture(also ref.to V415)	
101	Gas Chromat.	Varian CP4900 (Labview Interface available in EZ-Chrom)	
102	L001	Stainless Steel or copper piping Ø 6mm or Ø 1/4''	
103	L002	Copper piping Ø 6 mm or Ø 1/4''	
104	L003	Stainless steel, copper piping, PE or pneumatic tubing ~Ø6mm or Ø1/4''	
105	L004	Traced piping ~ Ø 6mm or Ø 1/4'', CO compatible (e.g. copper)	100-105 or 90-100
106	L005	Ø 6mm pneumatic tubing	
107	L006	Traced line, CO compatible, see TC203	100-105 or 50-60
108	L007	Rigid coax, UT-250A-TP-M17 (Avoid hexagonal connecting nut to prevent overtightening)	
109	L008	Piping ~ Ø 6mm or ~ Ø 1/4'', CO compatible (e.g. copper)	
110	L009	Traced line, CO compatible, see TC304	100-105
111	L010	Piping ~Ø 6mm, CO compatible (e.g. copper)	
112	L011	Silicone tube, hose connections to glassware and ethylene glycol compatible	
113	L012	6 mm stainless steel or copper	
114	L013	Any type of hosepipe Øi 10 mm suffices	
115	Computers	Various computers connected to KVM Switch	
116	i/o device(s)	National instruments devices for LabVIEW interfacing	Real-time embedded controller, cRIO, required due to unsupervised operation.
117	XT290	Door Switch	
118	FT291	Flow switch on interlock, SL5101(Interlock on ventilation failure)	
119	XT292	Microwave survey meter on interlock, Sairem, DFM M24DC 2450MHZ	
120	XT293	Magnetic position switch	
121	XT390	Door switch	
122	FT391	Flow switch on interlock, SL5101	
123	XT392	Microwave survey meter, ref. to XT292	

124	XT393	Magnetic position switch (To verify where SS-MWG is placed)			
125	XT380 -	Gas alarm sensors for CO, CO2,			
126	XT383	O2 and explosion limit resp.			
127	FNC	Tubular furnace, carbolite MTF 10/15/130		1000 max	
128	FNC-PS	Power supply of tubular furnace			
129	PRI350	Pressure sensor			0.075 – 1.5 bar
130	TR351	N-Type thermocouple	-200… +1250	600- 1000	
131	V415	5 Way valve			
132	LT142	Level verification to protect PMP1			
133	TC141	Tracing regulator			
134	TC300	Tracing regulator			

List of Publications

Curriculum Vitae

Acknowledgments

List of Publications

Publications:

1. **Lalit S. Gangurde**, Guido S.J. Sturm, Tushar J. Devadiga, A. I. Stankiewicz, Georgios Stefanidis, Complexity and challenges in non-contact high-temperature measurements in microwave-assisted catalytic reactors, Industrial and Engineering Chemistry Research, 56 (45), 13379–13391, 2017.

2. **Lalit S. Gangurde**, Guido S. J. Sturm, M. J. Valero-Romero, Reyes Mallada, Jesus Santamaria, Andrzej I. Stankiewicz, Georgios D. Stefanidis, Synthesis, characterization, and application of ruthenium-doped $SrTiO_3$ perovskite catalyst for microwave-assisted methane dry reforming, Chemical Engineering and Processing: Process Intensification, 127, 178-190, 2018.

3. Mangesh R. Avhad, **Lalit S. Gangurde**, Marcos Sánchez, Abderrahim Bouaid, José Aracil, Mercedes Martínez, Jorge M. Marchetti. Enhancing biodiesel production using green glycerol-enriched calcium oxide catalyst: An optimization study, Catalysis letters, 148 (4), 1169–1180, 2018.

Oral Presentations:

1. **Lalit S. Gangurde**, Guido Sturm, A. I. Stankiewicz, G.D. Stefanidis. "Complexity and challenges in non-contact high-temperature measurements in microwave-assisted catalytic reactors" at 16th International Conference on Microwave and High-Frequency Heating (AMPERE 2017), 18–21st September 2017, Delft University of Technology, Delft, The Netherlands. **ISBN for Book of abstract is 978-90-9030327-7**

2. **Lalit S. Gangurde,** Guido Sturm, A. I. Stankiewicz, Georgios D. Stefanidis. "Methane dry reforming by microwave heating" at 3rd Global Congress on Microwave Energy Applications, Cartagena (Spain), 25–29th July 2016. **ISBN for Book of abstract is 978-84-16325-21-4.**

3. **Lalit S. Gangurde,** Guido Sturm, A. I. Stankiewicz, G.D. Stefanidis. "Microwave-assisted methane reforming reactions" at 15th International Conference on Microwave and High-Frequency Heating (AMPERE 2015), 14–17th September 2015, Krakow University of Technology, Krakow, Poland. **ISBN for Book of abstract is 978-83-928784-4-5.**

4. **Lalit S. Gangurde,** Guido Sturm, A. I. Stankiewicz, G.D. Stefanidis. "New approach in microwave assisted reforming reactions" at Delft Process Technology Institute (DPTI) 2015 Annual Event, 5th June 2015, Den Haag, The Netherlands.

5. **Lalit S. Gangurde,** Guido Sturm, A. I. Stankiewicz, G.D. Stefanidis. "New approach in microwave-assisted reforming reactions" in Jubilee Symposium at Jagiellonian University, 28th April 2014, Krakow, Poland

Poster Presentations:

1. 5th European Process Intensification Conference, 27th Sept to 1th Oct 2015, Nice, France

2. 2nd Annual Event of the TU Delft Process Technology Institute, 7th Nov. 2014, SS Rotterdam, the Netherlands.

3. Netherlands Process Technology Symposium (NPS14), 3–5th Nov. 2014, Utrecht, the Netherlands.

4. 1st Delft Process Technology Institute (DPTI) Annual Event, 14th November 2013, Den Haag, the Netherlands.

Conferences attended

1. 4th TU Delft process technology annual event on 21st June 2016, Rotterdam, the Netherlands.

2. 3rd European Young Engineers Conference on 30th April 2014, Warsaw, Poland.

3. COMSOL Conference, 23–25 October 2013, Rotterdam. the Netherlands.

4. 9th European Congress of Chemical Engineering(ECCE9) on 21–25th April 2013, Den Haag, Netherlands

Doctoral Education Program

Discipline-related skills

1. Course: Chemical Product-Centric Process Design, 30 & 31st May 2017, TU Delft.

2. Course: Fundamentals and Practice of Process Intensification, 2–3 April 2014, Process and Energy Department, TU Delft.

3. Summer School: High Energy Processing Ultrasound and Microwave Technologies, 9–12 September 2015, Krakow University of Technology, Krakow Poland

4. Course: Gas-Phase Processing of Nanostructured Solids, 3–5 September 2013, ChemE Department, TU Delft.

5. Course: Computational Fluid Dynamics for Chemical Engineers, 8–12 July 2013, TU Delft.

6. Course: COMSOL Multiphysics Intensive Training, 13–14 May 2013, Zoetermeer, the Netherlands.

7. Workshop on crystalline materials, diffraction, and databases, 23rd March 2017, TU Delft.

8. Scientific Visit to ASML Company, 23rd October 2014, Veldhoven, the Netherlands.

9. A trip to the world leading steel production company TATA Steel, 15th March 2017, IJmuiden, The Netherlands.

Research-related skills

1. R1.A2 The informed researcher: Information and data skills, 14th & 28th March 2017, TU Delft.

Learning on the Job

2. Teaching assistant for WB3560 Process Technique II course in academic years 2012–13, 13–14 & 14–15 (including attending lectures, answering to students doubts, supervision, and checking of exams) 3ME, TU Delft.

3. Supervised a M.Sc. & a B.Sc. Student. (Including correcting thesis), 28th April to 14th Dec. 2016 and 15th April to 5th Sept 2017, P&E department, TU Delft.

4. Seminar 'Are you ready to publish? Understanding the publishing process' 5th February 2015, Science Centre, TU Delft, The Netherlands.

5. Writing the first journal article, 6th September 2017, Industrial and Engineering Chemistry Research Journal.

6. Oral Presentation addressed a major international audience in 15th International Conference on Microwave and High-Frequency Heating (AMPERE 2015), 14–17 September 2015, Krakow University of Technology, Krakow, Poland.

7. Oral Presentation addressed a major international audience in the 3rd Global Congress on Microwave Energy Applications (3GCMEA), 25–29 July 2016, Cartagena, Spain.

8. Oral presentation, addressed a small International Audience at Delft Process Technology Institute (DPTI) 2015 Annual Event, 5th June 2015, Den Haag, The Netherlands.

9. Oral Presentation, addressing a major international audience in Jubilee Symposium at Jagiellonian University, 28th April 2014, Krakow, Poland.

10. Poster presentation, the major international audience at Netherlands Process Symposium (NPS14), 3–5 November 2014, Utrecht, The Netherlands.

11. Poster presentation, small audience at 1st Delft Process Technology Institute (DPTI) Annual Event, 14th November 2013, Den Haag, The Netherlands.

12. Poster Presentation: the small audience at the 2nd Annual Event of DPTI, Rotterdam, 7th November 2014.

Transferable skills

1. C9. M1. Ph.D. Startup Course, 18, 21 & 28th June 2013, Art Centre Delft,

2. C8.M1. Communication, Coping-strategies & Awareness, 28th May & 4th June 2014, Industrial Design Department, TU Delft.

3. C11. M1. How to manage your research information, 9th & 15th May 2014, Library, TU Delft,

4. How to write a scientific paper (and Get It Published), 9th Jan 2017, Aula Building, TU Delft.

5. T1.B3 Writing a Dissertation (PROM-3), 2nd May to 13th June 2017, TPM, Room 'I, TU Delft.

6. C8.M5. How to become effective in a network conversation, 4th April 2014, Faculty of Technology, Policy and Management(TPM), TU Delft.

7. C8. M3. Self-management Strategies, 16th & 23rd April 2014, Library, TU Delft.

8. C9. M2. Time Management, 19th September & 30th October 2014, Library, TU Delft.

9. C13. M6. Self-presentation: Presenting yourself and your work, 12th June & 26th June 2013, Industrial Design, TU Delft.

10. C9. M4. How to keep motivated after your GO? Regain your flow! 7th & 14th April 2014, Library, TU Delft.

11. C13. M7. Lead a better (academic) life, 29th September 2014, Library, TU Delft.

12. C12. M6. Self-presentation 2 - storyline and presentation slides, 22nd & 29th June & 6th July 2016, Faculty of EEMSC & Library, TU Delft.

Curriculum Vitae

Lalit Sayaji Gangurde was born on 27th September 1988, in Ghodegaon, a small village in Malegaon, district Nasik of Maharashtra state, India. He completed his schooling from Ravalgaon English School, Ravalgaon, India. He finished his Junior and senior college studies from K.B.H. Jr. College Malegaon, India. In 2009, he graduated with Bachelors of science degree in chemistry from M.S.G. College Malegaon, India.

To acquire profound knowledge of catalysis and material science, in July 2009, he joined master's program in the Department of chemistry, University of Pune, Pune, India. He obtained his master's degree in April 2011 with specialization in inorganic chemistry. This master's program inspired him to get more insight into the exciting field of catalysis. So, after completing master's program, he started working as a Project Assistant in the heterogeneous catalysis Division, National Chemical Laboratory, Pune, India. He worked in NCL from 13th July 2011 to 9th November 2012 on the project entitled "Development of internal reforming catalysts for 500 W Solid Oxide Fuel Cell Stack." During this Project work, he learned various catalyst preparation methods to prepare various mixed metal oxide catalysts with different supports and active phases. He learned various characterization techniques to investigate physical and chemical properties of prepared materials. He was also involved in the performance evaluation of prepared catalysts for steam reforming of methane and water gas shift reactions. This experience has developed an interest in him to do further doctoral studies.

Since Dec. 2012, he started working as a Ph.D. researcher in Process and energy department of the Delft University of Technology, the Netherlands. His doctoral work is the part of a project entitled Towards Perfect Chemical Reactor, funded by European Research Council. His Ph.D. research dealt with the process intensification of microwave-assisted methane dry reforming process. This process converts two greenhouse gases, CH_4 and CO_2 into syngas (H_2 + CO) which can be used as a renewable source of energy. The results obtained in his research work have been published as research articles. The results have also been presented at various national and international conferences. Besides this, he has worked as a teaching assistant for Process technology course for bachelor's student. He has also supervised masters and bachelors project students. Currently, he has been appointed as a postdoctoral researcher in the Delaware Energy Institute (DEI) at the University of Delaware (USA) effective from October 1, 2018.

For More information: https://www.linkedin.com/in/lalit-gangurde-948b9560/
Email: lalitgangurde88@gmail.com

Acknowledgments

While writing the acknowledgments, my thought process is taking me to the flashback of my journey from sending my application for this Ph.D. position to at this moment, now writing this acknowledgment section. The one significant observation I have about myself is that the way I was thinking and seeing the world before starting Ph.D. and now while completing my Ph.D. This Journey has really been an unexpectedly long, filled with a lot of emotional ups and downs. Completion of a Ph.D. demands a lot of skills on the personal and professional level. When I joined, I knew very little about it, so this journey has taught me a lot of things. Even though I was a driver on this journey, but it could not have been possible to complete it without the tremendous support and motivation which I received from various people at different levels. This support acted as a fuel to drive myself safely through this long doctoral journey.

Firstly, I am thankful to my first Promoter Andrzej Stankiewicz for giving me an opportunity to become a part of this very interdisciplinary group at the Delft University of technology, the Netherlands. Starting from my first interaction with him until the end of Ph.D., He was always a great support, encouragement, and inspiration to carry out the research work. His suggestions and comments during various meeting and interactions helped me a lot to improve the quality of the research work. The research work done in this doctoral thesis has received funding from the European Research Council under the European Union's Seventh Framework Programme (FP7/2007-2013) / ERC grant agreement no. 267348. I am thankful to ERC for trusting on all the people involved in this project as the outcome of this research activities came out a bit late in terms of research articles.

I would like to thank with a lot of gratitude to my daily supervisor and second promotor Professor Georgios Stefanidis for helping me throughout my Ph.D. Journey. Even though the journey has been extended and stressful, he guided me to keep myself in the correct direction. He helped me to improve in various skills required to be a good researcher. He taught me to be calm and compose to face the unexpected challenges came during the experimental work or dealing with any other kind of stressful situations. He has helped me a lot to improve my scientific writing skills and guided me at a very minute level. He also gave me the necessary guidance to improve my presentation skills at various national and international conferences. I am very grateful for his significant contribution in improving and providing correct suggestions to write the quality research articles, conference abstracts and at the end for final Ph.D.thesis. Thank you, Georgios once again for everything you did for me.

Special thanks to Dr. Guido Sturm for helping me in designing the P&ID of my reactor setup. He has significantly contributed to designing and developing the custom designed microwave cavity for this work. Without his help, it would have been impossible to build a completely new

microwave reactor system. I have learned a lot of things from you Guido so thank you very much again for everything. I would like to thank Prof. Santamaria and Reyes Malada for allowing me to work at the University of Zaragoza, Spain for catalyst synthesis and characterization work. It was really pleasant and excellent learning experience to stay in Zaragoza and learn new things from experts in the microwave catalysis field. Thanks to Diego, Nuria, Marta and Hema for helping me in the Analytical Lab and other relevant work in Zaragoza University. I would also like to thank Prof. Jorge Gascon for allowing me to work in the Chemical Engineering department of TU Delft for catalyst synthesis and characterization purpose. Thank you very much, Maria Jose, for teaching me some more inside details of catalyst synthesis and characterization. You were always energetic and ready to help me in every possible way, I really appreciate everything you did for our collaborative work in terms of improving the quality of research results and writing it more correctly in a scientific language.

A special appreciation goes to all the technicians in the DEMO staff for helping and guiding me for all the technical aspects during the reactor development time phase. I would like to thank Michel van den Brink for helping me in the Analytical lab related problems, safety-related issues, correcting and approving my safety report. Aad beeloo and Rob Van den Boogaard for arranging the meetings to speed up the reactor construction work. Jaap van Raamt for ordering all the necessary materials and helping me to solve the reactor construction related problems. Martijn Karsten, who designed and constructed the electrical cabinet of the whole reactor set up and his help for all the electrical technical issues. Bas Overtoom and Gerard van de Sande for construction of reactor setup and minor modifications in the setup whenever it's needed. Lennart Middelplaats, who designed the Labview interface for reactor control system and helped me afterword’s also in some problems related to the reactor control system.

I would like to thank my Master’s project student Tushar Devadiga for his contribution to work with me in various technical challenges to start the operation of newly developed microwave reactor assembly. His contribution as a Masters student was really very helpful for me to plan my further research work. I would also like to thank my bachelor's student, Diederik S. van Roemburg, who worked on a comparative study of commercial catalysts. The results of his work are a significant contribution to my Ph.D. thesis. Leslie Van Leeuwen and Helma Duijndam-Nieuwpoort, Our group secretaries and most important persons in the group. Thank you very much for helping me in all the documental work and any other kind of small problems, doubts or issues from starting till the end of my Ph.D. time. Thank you Prof. Dr. P.V. Aravind for becoming the part of my go no go committee and assessment.

Joining as a Ph.D. student at TU Delft, gave me an opportunity to expand my friendship with more international colleagues in our process and energy department. My first office mates Iza Franssen, Maryum Khodadadian, and Daniel Irimia thanks for being such a sweet and helpful colleagues in my initial days. It was a great experience and learning to attend all our Intensified reaction and separation systems group meetings and to get to know about the research progress of all the people

working in the group. I would like to thanks to Rohit Kacker, Javier Fernandez, George Krintiras, Sergio Moreno, Fatemeh Anisi. Marloes Reus, Weiwei Li, Fatma Ibis, Rumen Georgiev for having interesting discussions during drinks and snacks session after these group meetings. I would like to thank Meng wang, Xuan Tao, Peng Yan, Uttiya Sengupta, Mahinder Ramdin, Nikolaos Chrysochoidis-Antsos, Metin Çelik, Tim Becker, Karsten Baumgarten for a nice time and fun activities during our P&E outings and short visits to different places. Thanks to some newly joined people in our group, Vinay Mahajan, Vikrant Verma, and Sathish Sanjeevi for coffee break conversations on life after Ph.D. topic. Thanks to my current office mates, Ali Poursaeidesfahani, Farnaz Eghbal Sarabi and Hirad Seyed Salehi for tolerating my all-time silent nature in the office. Thanks to Hakan Nigar for your help, suggestions, and discussion for some future simulation study possibilities with the results obtained in this work. I would also like to thank Hanaa for translating summary in Dutch. I would like to thank the graduate school for organizing a doctoral education program, and various interactive events among all the new Ph.D.'s in the TU Delft. The different courses organized by 3ME Graduate school in discipline-related skills, research-related skills, and transferable skills have really helped me to improve not only as a researcher but also on the personal and professional level.

Thank you, Jitendra Khairnar to provide me accommodation in the Netherlands. Jagdish Thibe for helping me financially whenever I needed. Bhaskar Patil, for introducing me to Ramerstraat friends. The stay at Ramaerstraat made me happy and engaged me in all kind of parties, social events, outing, box cricket matches, Ganesh Utsav, etc. Special thanks to Rajat Bharadwaj for the invitation to his marriage, it gave me a chance to meet your family and visit the most important touristic places in Delhi. You both Rajat and Rupali are always a great support to me at my time in Delft. Thanks to Purvil Khakharia for your help and support whenever I needed. Thanks to Sumit Sachdeva for being a very good friend and always ready to help me with the small doubts or problems in professional and personal life. Trinath for being such a nice friend, organizer, and guide on our trips. Thank you very much to all my dear friends in the Netherlands, Aditya thallam thattai, Hrishikesh Patel, Ajith-Vaishnavi, Shreyash-Gunjan, Navin-Mitwa, Vyankatesh Session, Vasudevan Lakshminarayanan, Sushil-Jaymala Gaikwad, Bhaskar-Mohini, Manas Manohar, Prathna Chandrasekaran, Edwin Gnanakumar, Jalindar Padwal, Ashwinikumar Sharma for nice dinners and exciting conversations. Thank you very much, Samir and Shruti Kulkarni for all the necessary support from providing me food and helping me to call home on my first day in the Netherlands. It was amazing to see Netherlands Marathi Mandal and Rashmin group, celebrating our own culture and festivals miles away from our native place even in the more elaborative way and giving the opportunity to meet some of the great people in various art forms. thanks for organizing all these events.

I think it could not have been possible for me to come to the Netherlands if I would not have got the opportunity to work as a project assistant in National Chemical Laboratory Pune, India. I would like to thank Dr.C.V.V Satyanarayana for giving me the opportunity to work under his guidance in his research group. I would like to thank the friends I made during my stay at NCL, and then they

became friends forever. Hanmant Gurav, Mangesh Avhad, Gajanan Kale, Reji NK, Aditya Dharanipragada, Narasimharao Kanna, Richa Bobade, Nishita Lucas, Dama Srikanth, Lakshmiprasad ane nenu, Chandan Das, Vineetha Lakshmi Das, Atul Nagpure, Swanand Patange, James Violet. Tushar Sakpal. Sonali Katkar for being such a lovely friend at NCL and Pune University, Pune. Thanks to all my Masters, Bachelors and Ravalgaon English school friends for always being with me and supporting me all the time. Special thanks to some of the very close friends from my school days, Prashant Lokhande, Pradip Jagdale, Swapnil Nikumbh, Swapnil Kulkarni, Umesh Nikam, and Kishor Patil for our entertaining conversations. Thanks to both my paternal uncles Chandrashekhar Jadhav and Vijay Jadhav for their tremendous support from childhood till date. Thanks to the Jadhav and Suryawanshi families for their love and affection gave to me.

Special thanks to Mangesh Avhad for always caring about me and always there for me to know about my research progress and helping me in every possible way. Your friendship is indeed unconditional. Thank you very much for offering me a co-authorship in your publication and having collaboration between the Netherlands and Norway. I would also like to thank Tejansh Chandole, your always there for me in all my personal and professional issues. Our conversations were always giving me positive energy and motivating me to do my best. I am fortunate to have a friend like you. Thanks to Avinash Bansode, Yogesh More, Abhijeet Chaudhari, Mayur More to share the various aspects of life.

I could not have existed without getting the unconditional love, affection, and care from my parents. I would like to pay special thanks to my father for his efforts to provide me all the necessary things to the best of his abilities since childhood till my college time and supporting me in every decision on personal and professional front. My mother for understanding me in every situation, her constant support and motivating words whenever I speak to her have boosted my confidence and inspired me to be realistic and nice to everyone I meet. My two pillar of strength and great support at any time are my both brothers Lakhan and Kishor Gangurde, without you guys I could not have thought to come to the Netherlands as you were always there to take care of our parents and support them and me in all the critical situations. Kishor, you came almost all the time to drop and receive me at the airport and always there for me irrespective of your own busy schedule and work. Lakhan, I know you're also going through a very tough time of your life, but still, you did not have any complaints, and you was always there with parents. I would like to thank also to Gayatri Kulkarni and her family for the warm welcome all the time I come to the home. Special thanks to Rohini More and her family to keep patience and faith in me. Thanks to all relatives for understanding me as I was absent almost for 6 years for all the most important life events of all my near and dear relatives.

Lalit Gangurde,
Delft, April 2018.

Propositions

Accompanying the thesis

Process Intensification of Microwave-Assisted Methane Dry Reforming

Lalit Sayaji Gangurde
Delft University of Technology

1. Reproducibility of temperature profiles in microwave heated heterogeneous catalytic systems is unachievable, since it is sensitive to many factors that vary under real reaction conditions.
2. The best way to evaluate the performance of microwave-heated catalytic reactions is to monitor microwave power consumption, product composition and temperature by both point sensors (e.g., optical fiber's or thermocouples) and thermal camera.
3. The limitations of carbon-based catalysts for microwave-assisted methane dry reforming can be overcome with the ruthenium doped $SrTiO_3$ perovskite catalyst (chapter 4).
4. Small, compact and optimized microwave reactors with improved hybrid catalytic systems would be able to provide higher CH_4 and CO_2 conversions as compared to large-scale carbon-based catalytic microwave reactors.
5. In order to be successful in what you do, control of your own thoughts, and motivation towards your work is much more important than money, time, and previous knowledge.
6. Freedom of research comes when you have authority, experience, and power to take your own decisions.
7. Political leaders and civilians of developing countries should only focus on development.
8. To avoid the consequences of personal data leakage from the social networking sites, one must limit their data feed to these sites.
9. Your own philosophy about life changes with every new experience.
10. Unawareness about the unpredictable nature of research success rate increases self-doubt and depression in Ph. D. researchers.

These propositions are considered opposable and defendable and as such has been approved by the promotor, Prof.dr.ir. A.I. Stankiewicz.

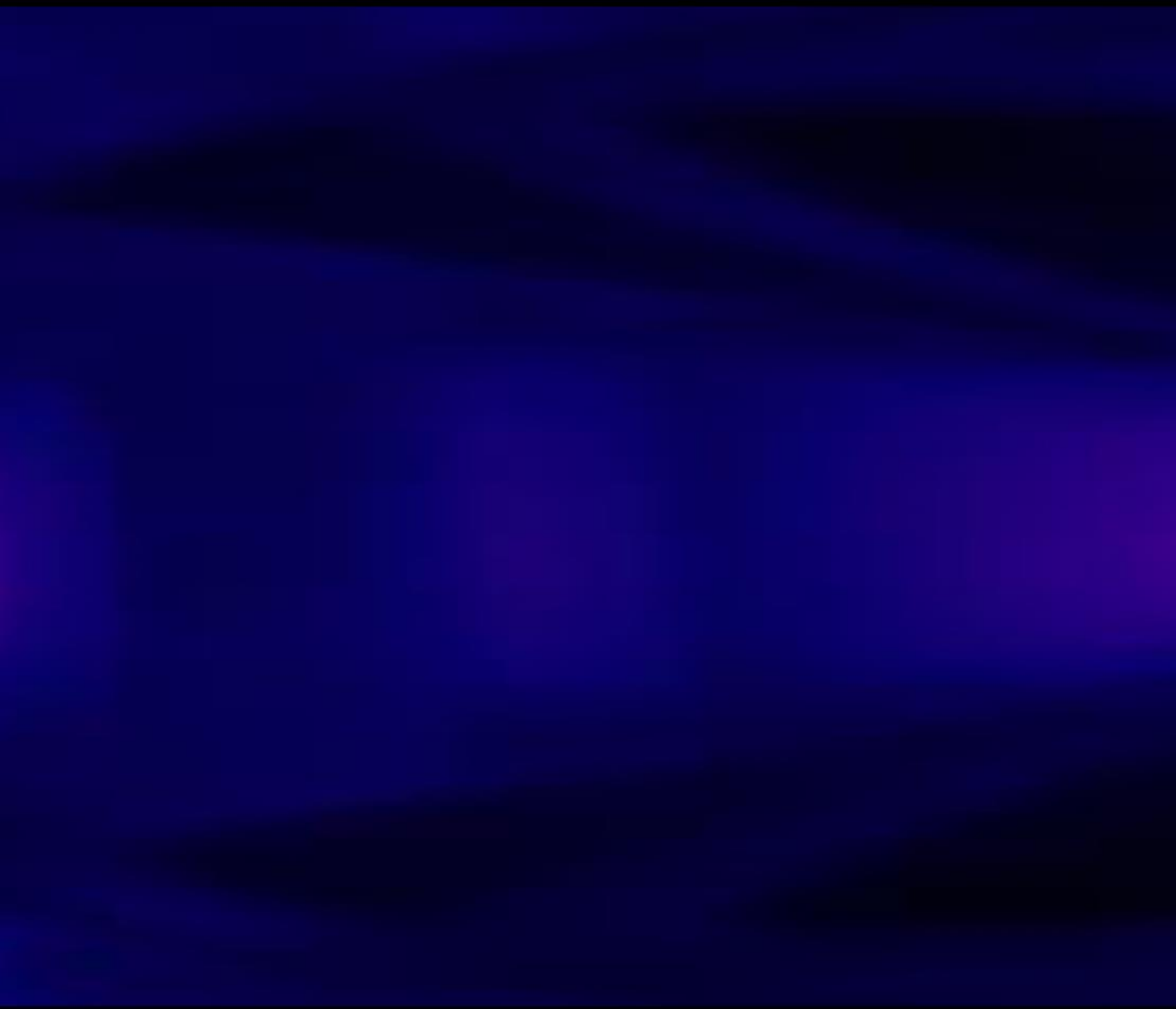

TU Delft

ISBN: 978-94-6375-229-9